

AD-A201 810

FIRST QUARTERLY REPORT

FOR THE PROJECT

"COMPOSITE CERAMIC SUPERCONDUCTING  
WIRES FOR ELECTRIC MOTOR APPLICATIONS"

PRIME CONTRACTOR

CERAMICS PROCESS SYSTEMS CORPORATION  
840 MEMORIAL DRIVE  
CAMBRIDGE, MASSACHUSETTS 02139

30 SEPTEMBER 1988

DTIC  
ELECTE  
NOV 02 1988  
S D  
A-H



**CERAMICS**  
PROCESS SYSTEMS

88 11 02 023

DISTRIBUTION STATEMENT A

Approved for public release;  
Distribution Unlimited

FIRST QUARTERLY REPORT

FOR THE PROJECT

"COMPOSITE CERAMIC SUPERCONDUCTING  
WIRES FOR ELECTRIC MOTOR APPLICATIONS"

PRIME CONTRACTOR

CERAMICS PROCESS SYSTEMS CORPORATION  
840 MEMORIAL DRIVE  
CAMBRIDGE, MASSACHUSETTS 02139

30 SEPTEMBER 1988

DARPA ORDER NO: -  
CONTRACT NO: N00014-88-C-0512  
CONTRACT EFFECTIVE DATE: 30 JUNE 1988  
CONTRACT EXPIRATION DATE: 31 MARCH 1991  
PRINCIPAL INVESTIGATOR: JOHN W. HALLORAN  
(617) 354-2020

Prepared for  
DEFENSE ADVANCED RESEARCH PROJECTS AGENCY  
1400 Wilson Boulevard  
Arlington, VA 22209

OFFICE OF NAVAL RESEARCH  
800 North Quincy Street  
Arlington, VA 22217-5000

APPROVED FOR PUBLIC RELEASE: DISTRIBUTION IS UNLIMITED

The views and conclusions contained in this document are those of the authors and should not be interpreted as necessarily representing the official policies, either expressed or implied, of the Defense Advanced Research Projects Agency or the U. S. Government.

DTIC  
SELECTED  
NOV 02 1988  
H

UNCLASSIFIED

SECURITY CLASSIFICATION OF THIS PAGE

REPORT DOCUMENTATION PAGE												
1a. REPORT SECURITY CLASSIFICATION UNCLASSIFIED		1b. RESTRICTIVE MARKINGS N/A										
2a. SECURITY CLASSIFICATION AUTHORITY N/A		3. DISTRIBUTION/AVAILABILITY OF REPORT Approved for public release, Distribution Unlimited										
2b. DECLASSIFICATION/DOWNGRADING SCHEDULE N/A												
4. PERFORMING ORGANIZATION REPORT NUMBER(S) N/A		5. MONITORING ORGANIZATION REPORT NUMBER(S) N/A										
6a. NAME OF PERFORMING ORGANIZATION Ceramics Process Systems Corporation		6b. OFFICE SYMBOL (if applicable) N/A	7a. NAME OF MONITORING ORGANIZATION Office of Naval Research									
6c. ADDRESS (City, State and ZIP Code) 840 Memorial Drive Cambridge, MA 02139		7b. ADDRESS (City, State and ZIP Code) 800 North Quincy Street Arlington, VA 22217-5000										
8a. NAME OF FUNDING/SPONSORING ORGANIZATION Defense Advanced Research Projects Agency		8b. OFFICE SYMBOL (if applicable) N/A	8. PROCUREMENT INSTRUMENT IDENTIFICATION NUMBER Contract N00014-88-C-0512									
6c. ADDRESS (City, State and ZIP Code) 1400 Wilson Boulevard Arlington, VA 22209		10. SOURCE OF FUNDING NOS. <table border="1"> <thead> <tr> <th>PROGRAM ELEMENT NO.</th> <th>PROJECT NO.</th> <th>TASK NO.</th> <th>WORK UNIT NO.</th> </tr> </thead> <tbody> <tr> <td> </td> <td> </td> <td> </td> <td> </td> </tr> </tbody> </table>			PROGRAM ELEMENT NO.	PROJECT NO.	TASK NO.	WORK UNIT NO.				
PROGRAM ELEMENT NO.	PROJECT NO.				TASK NO.	WORK UNIT NO.						
11. TITLE (Include Security Classification) Composite Ceramic Superconducting Wires...												
12. PERSONAL AUTHOR(S) John W. Halloran												
13a. TYPE OF REPORT Technical Report	13b. TIME COVERED FROM :6/30/88 to 9/30/88	14. DATE OF REPORT (Yr., Mo., Day) 88/9/30	15. PAGE COUNT 172									
16. SUPPLEMENTARY NOTES N/A												
17. COSATI CODES <table border="1"> <thead> <tr> <th>FIELD</th> <th>GROUP</th> <th>SUB. GR.</th> </tr> </thead> <tbody> <tr> <td> </td> <td> </td> <td> </td> </tr> </tbody> </table>		FIELD	GROUP	SUB. GR.				18. SUBJECT TERMS (Continue on reverse if necessary and identify by block number)  Superconductor, Ceramic, Motor				
FIELD	GROUP	SUB. GR.										
19. ABSTRACT (Continue on reverse if necessary and identify by block number)  SEE ATTACHED												
20. DISTRIBUTION/AVAILABILITY OF ABSTRACT UNCLASSIFIED/UNLIMITED <input checked="" type="checkbox"/> SAME AS RPT. <input type="checkbox"/> OTIC USERS <input type="checkbox"/>		21. ABSTRACT SECURITY CLASSIFICATION UNCLASSIFIED										
22a. NAME OF RESPONSIBLE INDIVIDUAL John W. Halloran		22b. TELEPHONE NUMBER (Include Area Code) 617-354-2020	22c. OFFICE SYMBOL N/A									

DD FORM 1473, 83 APR

EDITION OF 1 JAN 73 IS OBSOLETE.

UNCLASSIFIED

COMPOSITE CERAMIC SUPERCONDUCTING WIRES  
FOR ELECTRIC MOTOR APPLICATIONS

ABSTRACT

This is the First Quarterly Report of a program to produce practical htsc wires, and build a htsc electric motor using this wire. The htsc ceramic wire will be a flexible composite of many fine ceramic filaments clad with copper or aluminum. The three basic elements of this method are: 1) spinning polymer-containing "green" fibers; 2) sintering the fibers to make bare superconducting ceramic filaments; and 3) cladding the filaments with copper. Albany International Research Corporation (AIResCo) is working with CPS to improve the green fiber spinning process and bring it to pilot scale production. Emerson Motor Division (EMD) of Emerson Electric Company, will evaluate the composite wire and in define a set of realistic property requirements for practical htsc motors. The second task, to design and build htsc motors, will be undertaken by Emerson Motor Division. This report covers development activities during the period July through September, 1988, on the wire development task at CPS and AIResCo. The start of the Emerson subcontract was deferred until October 1, 1988.

During this Quarter, most of the fibers were prepared from a Rhone-Poulenc powder. This material was suitable for spinning and highly sinterable, but contained excess copper oxide. Much effort went to scaling up in-house powder production of highly phase pure  $\text{YBa}_2\text{Cu}_3\text{O}_7$  powder to production rates adequate to supply the development program. The influence of powder characteristics on fiber spinning and sintering is now being studied to optimize the powder for the wire manufacturing. → (JES) ←

Research at AIResCo has led to a method to melt spin green fiber. Melt spun fiber containing up to 50 volume percent powder has been made in continuous spools with lengths up to 0.25 kilometers, limited only by the small experimental batches. This melt spun fiber appears to have favorable binder burnout characteristics. We anticipate preparing continuous spools of  $\text{YBa}_2\text{Cu}_3\text{O}_7$  melt spun green fiber early in the next quarter to be the feedstock for the continuous sintering development.

Sintering and annealing experiments were conducted to establish a relationship between heat treatment and  $J_c$ , but critical current densities could not be simply correlated to zone sintering conditions because of scatter in the  $j_c$  data. Further observations were made on microstructure development, primarily for the CuO-excess Rhone-Poulenc powder. Preliminary results on a rapid oxygen intercalation anneal suggests that filaments may be successfully restored to the superconducting state by a 15 minute isothermal anneal at 525°C in oxygen.

A new cladding concept was developed, based upon a technique to treat the surfaces of  $\text{YBa}_2\text{Cu}_3\text{O}_7$  filaments so that they can be bonded to copper ribbons by a solder reflow process. The surface treatment presently involves a thin layer of silver on the  $\text{YBa}_2\text{Cu}_3\text{O}_7$  surface. Early ribbon coupon specimens were fabricated with the reflow method using a few  $\text{YBa}_2\text{Cu}_3\text{O}_7$  filaments or graphite fiber as a surrogate.

A data base of processing conditions and  $J_c$  was constructed. The highest critical current density determined for a  $\text{YBa}_2\text{Cu}_3\text{O}_7$  filament was 792 A/cm<sup>2</sup>. We have begun to examine the repeatability of  $j_c$  data, magnetic field effects, and of self field critical current density data.

COMPOSITE CERAMIC SUPERCONDUCTING WIRES FOR  
ELECTRIC MOTOR APPLICATIONS

ABSTRACT

This is the First Quarterly Report of a program to produce practical HTSC wires and build a HTSC electric motor using these wires. The HTSC ceramic wire will be a flexible composite of many fine ceramic filaments clad with copper or aluminum. The three basic elements of the wire manufacturing method are: 1) spinning polymer-containing "green" fibers; 2) sintering the fibers to make bare superconducting ceramic filaments; and 3) cladding the filaments. Albany International Research Corporation (AIResCo) is working with CPS to improve the green fiber spinning process and bring it to pilot scale production. Emerson Motor Division, of Emerson Electric Company, will evaluate the composite wire, define a set of realistic property requirements for practical HTSC motors, and subsequently design and build a "proof of concept" HTSC motor. This report covers development activities during the period July through September, 1988, on the wire development task at CPS and AIResCo. The initiation of the Emerson subcontract was deferred until October 1, 1988.

During this Quarter, most of the fibers were prepared using Rhone-Poulenc powder. This material was suitable for spinning and highly sinterable, but contained excess copper oxide. Much effort went to scaling up in-house powder production of highly phase pure  $\text{YBa}_2\text{Cu}_3\text{O}_{7-\delta}$  powder. Current production rates are adequate to supply the development program. The influence of powder characteristics on fiber spinning and sintering is now being studied so that the powder can be optimized to meet the needs of wire manufacturing.

Research at AIResCo has led to development of a method to melt spin green fiber. Melt spun fiber containing up to 50 volume percent powder has been made in continuous spools with lengths up to 0.25 kilometers, limited only by the small experimental batches. This melt spun fiber appears to have favorable binder burnout characteristics. It is anticipated that continuous spools of  $\text{YBa}_2\text{Cu}_3\text{O}_{7-\delta}$  melt spun green fiber prepared at AIResCo will be available early in the next Quarter for use as the feedstock for the continuous sintering development.

Sintering and annealing experiments were conducted to establish a relationship between heat treatment and  $J_c$ , but critical current densities could not be simply correlated to zone sintering conditions because of scatter in the  $J_c$  data. Further observations were made on microstructure development, primarily for the CuO-excess Rhone-Poulenc powder. Preliminary results on a rapid oxygen intercalation anneal suggest that filaments may be successfully restored to the superconducting state following a 15 minute isothermal anneal at 525°C.

A new cladding concept was developed, based upon a technique to treat the surfaces of  $\text{YBa}_2\text{Cu}_3\text{O}_{7-\delta}$  filaments so that they can be bonded to copper ribbons using a solder reflow process. The surface treatment presently involves a thin layer of silver on the  $\text{YBa}_2\text{Cu}_3\text{O}_{7-\delta}$  surface. Early ribbon specimens were fabricated with the reflow method using a few  $\text{YBa}_2\text{Cu}_3\text{O}_{7-\delta}$  filaments or graphite fiber as a surrogate.

A database of processing conditions and  $J_c$  was constructed. The highest critical current density determined for a  $\text{YBa}_2\text{Cu}_3\text{O}_{7-\delta}$  filament was  $792 \text{ A/cm}^2$ . Examination of the repeatability of  $J_c$  data, magnetic field effects, and self field critical current density data has begun.



Accession For	
NTIS GRA&I	<input checked="" type="checkbox"/>
DTIC TAB	<input type="checkbox"/>
Unannounced	<input type="checkbox"/>
Justification	
By	
Distribution/	
Availability Codes	
Avail and/or	
Dist	Special
A-1	

## TABLE OF CONTENTS

### LIST OF FIGURES

### LIST OF TABLES

SECTION 1:	GENERAL INTRODUCTION . . . . .	1
1.1	Program Overview . . . . .	1
1.2	Composite Wire Design Philosophy . . . . .	3
1.3	Program Schedule . . . . .	10
SECTION 2:	WIRE FABRICATION . . . . .	22
2.1	Introduction and General Comments . . . . .	22
2.2	Fiber Preparation . . . . .	26
2.2.1	Introduction . . . . .	26
2.2.2	Dry spinning developments. . . . .	27
2.2.3	Melt spun fiber fabrication. . . . .	29
2.3	Heat Treatment of Fibers . . . . .	44
2.3.1	Introduction. . . . .	44
2.3.2	Sintering of $\text{YBa}_2\text{Cu}_3\text{O}_{7-x}$ Fibers . . . . .	45
2.3.3	Oxygen intercalation studies. . . . .	52
2.3.4	Sintering conditions, microstructure, and $J_c$ . . . . .	54
2.3.5	Quantitative stereology of microstructure development . . . . .	74
2.3.6	Continuous laboratory scale sintering furnace . . . . .	86
2.4	Filament Cladding and Wire Fabrication . . . . .	87
2.4.1	Introduction. . . . .	87
2.4.2	Outline of the reflow bonding process . . . . .	88
2.4.3	Preliminary experiments on silver metallization . . . . .	91
2.4.4	Binder burnout, sintering, and annealing. . . . .	93
2.4.7	Fabrication of ribbon conductors. . . . .	99
2.4.8	Metal cladding by electrodeposition . . . . .	107
2.5	Electrical and Magnetic Characterization . . . . .	108
2.5.1	Introduction. . . . .	108
2.5.2	Specimen preparation. . . . .	108
2.5.3	Critical temperature. . . . .	109
2.5.4	Critical current in zero applied magnetic field . . . . .	111
2.5.4	Self Field Effects. . . . .	117
2.5.5	Critical current density in a magnetic field. . . . .	119
2.5.6	Reproducibility of critical current density data. . . . .	121
2.6	Summary . . . . .	127
SECTION 3:	HIGH TEMPERATURE SUPERCONDUCTING MOTOR DESIGN AND FABRICATION . . . . .	130
SECTION 4:	GENERAL DISCUSSION AND SUMMARY . . . . .	132
APPENDIX 1:	SUMMARY OF FINAL REPORT OF ONR CONTRACT NUMBER N00014-87-C- 0789 . . . . .	135

## LIST OF FIGURES

Figure 1.1.1	Schematic of the Flexible Ribbon Conductor Concept Illustrating an Array of Fine Superconductor Filaments in a Normal Metal Cladding. . . . .	5
Figure 1.1.2	Gantt Chart for Program Tasks. . . . .	21
Figure 2.2.1	TGA of Candidate Polymers in Nitrogen. . . . .	32
Figure 2.2.2	TGA of Candidate Polymers in Air. . . . .	33
Figure 2.2.3	Modified Die Assembly. . . . .	37
Figure 2.2.4A	Micrograph of 3498-54-1, 50 vol% BaTiO <sub>3</sub> in EVA. . . . .	41
Figure 2.2.4B	Micrograph of 3498-61-1, 50 vol% BaTiO <sub>3</sub> in HDPE. . . . .	42
Figure 2.2.5	Sintered Barium Titanate Filament. . . . .	43
Figure 2.3.1	Typical Temperature-Time Profile for Zone Sintering. . . . .	47
Figure 2.3.2A	Polished and Etched Microstructure of a YBa <sub>2</sub> Cu <sub>3</sub> O <sub>7-δ</sub> Filament Zone Sintered at 966°C for Four Passes, with 14 Minutes at Temperature. . . . .	57
Figure 2.3.2B	Polished and Etched Microstructure of a YBa <sub>2</sub> Cu <sub>3</sub> O <sub>7-δ</sub> Filament Zone Sintered at 966°C for Ten Passes, with 35 Minutes at Temperature. . . . .	58
Figure 2.3.3A	YBa <sub>2</sub> Cu <sub>3</sub> O <sub>7-δ</sub> Filament Sintered Isothermally for 28 Minutes at 966°C. . . . .	59
Figure 2.3.3B	YBa <sub>2</sub> Cu <sub>3</sub> O <sub>7-δ</sub> Filament Zone Sintered for 8 Passes at 966°C, with 28 Minutes at Temperature. . . . .	60
Figure 2.3.4A	Fracture Surface of YBa <sub>2</sub> Cu <sub>3</sub> O <sub>7-δ</sub> Filament after 2 Zone Passes at 970°C. . . . .	62
Figure 2.3.4B	Fracture Surface of YBa <sub>2</sub> Cu <sub>3</sub> O <sub>7-δ</sub> Filament after 6 Zone Passes at 970°C. . . . .	63
Figure 2.3.4C	Fracture Surface of YBa <sub>2</sub> Cu <sub>3</sub> O <sub>7-δ</sub> Filament after 10 Zone Passes at 970°C. . . . .	64
Figure 2.3.5	Critical Current Density at Liquid Nitrogen Temperature in Self Field versus Number of Zone Passes at 970°C. . . . .	65
Figure 2.3.6A	YBa <sub>2</sub> Cu <sub>3</sub> O <sub>7-δ</sub> Filament Zone Sintered at 950°C for 2 Passes. . . . .	67
Figure 2.3.6B	YBa <sub>2</sub> Cu <sub>3</sub> O <sub>7-δ</sub> Filament Zone Sintered at 950°C for 6 Passes. . . . .	68
Figure 2.3.6C	YBa <sub>2</sub> Cu <sub>3</sub> O <sub>7-δ</sub> Filament Zone Sintered at 950°C for 10 Passes. . . . .	69
Figure 2.3.7A	Microstructure of YBa <sub>2</sub> Cu <sub>3</sub> O <sub>7-δ</sub> Filament Sintered 14 hours at 925°C. . . . .	72
Figure 2.3.7B	Microstructure of YBa <sub>2</sub> Cu <sub>3</sub> O <sub>7-δ</sub> Filament Zone Sintered at 925°C for 8 Passes, Followed by a 16 Hour Isothermal Hold. . . . .	73
Figure 2.3.8	Average Aspect Ratio versus Average Grain Width for YBa <sub>2</sub> Cu <sub>3</sub> O <sub>7-δ</sub> Filaments Sintered at 935 and 950°C. . . . .	76
Figure 2.3.9	Grain Length Distributions For YBa <sub>2</sub> Cu <sub>3</sub> O <sub>7-δ</sub> Filaments Zone Sintered at 950°C for 2, 4, 6, 8, and 10 Passes. Each Pass Corresponds to 3.5 Minutes at Temperature. . . . .	78
Figure 2.3.10	Grain Length Distributions for YBa <sub>2</sub> Cu <sub>3</sub> O <sub>7-δ</sub> Filaments Zone Sintered at 935°C for 4, 8, and 12 Passes. Each Pass Corresponds to 3.5 Minutes at Temperature. . . . .	79

LIST OF FIGURES (Continued)

Figure 2.3.11A	Average Grain Width versus Number of Zone Passes and Time at Temperature for $\text{YBa}_2\text{Cu}_3\text{O}_{7-\delta}$ Filaments Sintered at 935°C. . . . .	80
Figure 2.3.11B	Average Grain Length versus Number of Passes for $\text{YBa}_2\text{Cu}_3\text{O}_{7-\delta}$ Filaments Sintered at 935°C. . . . .	81
Figure 2.3.12	Grain Size Distributions in Isothermally Sintered $\text{YBa}_2\text{Cu}_3\text{O}_{7-\delta}$ Filaments. . . . .	82
Figure 2.3.13	Critical Current Density versus Average Grain Length for $\text{YBa}_2\text{Cu}_3\text{O}_{7-\delta}$ Filaments Sintered Under a Variety of Conditions. . . . .	84
Figure 2.3.14	Critical Current Density versus Number of Repeated Passes for $\text{YBa}_2\text{Cu}_3\text{O}_{7-\delta}$ Filaments Zone Sintered at 935°C. . . . .	85
Figure 2.4.1	Flexible Ribbon Conductor Fabricated by Solder Reflow Bonding to Copper Strips. . . . .	89
Figure 2.4.2	Fracture Surface of $\text{YBa}_2\text{Cu}_3\text{O}_{7-\delta}$ Filament with Silver Coating Sintered at 955°C. . . . .	92
Figure 2.4.3	Cross-Section of Silver Coated Filament Zone Sintered at 925°C. . . . .	94
Figure 2.4.10	Assembly of Composite using Copper Channel. . . . .	105
Figure 2.4.11	Set-up For Continuous Production of FRC with Surrogate Filament. . . . .	106
Figure 2.5.1	Proposed Instrumentation for Resistive Measurement of Critical Temperature of Superconducting Fibers. . . . .	110
Figure 2.5.2	V-I Data from a Typical $J_c$ Test. . . . .	114
Figure 2.5.3	Voltage-Current Raw Data for Two $\text{YBa}_2\text{Cu}_3\text{O}_{7-\delta}$ Filaments, Illustrating Method of Determining Critical Current. . . . .	116
Figure 2.5.4	A) $J_c$ versus $H_{\text{applied}}$ for a $\text{YBa}_2\text{Cu}_3\text{O}_{7-\delta}$ Filament, B) Calculated Weak Link $J_c$ versus $H_a$ Relationship from Peterson and Ekin. . . . .	120
Figure 2.5.5	V-I Data for Five Nominally Identical Filaments. . . . .	124

## LIST OF TABLES

TABLE 1.1	QUARTERLY WORK STATEMENT COMPOSITE CERAMIC SUPERCONDUCTING WIRES FOR ELECTRIC MOTOR APPLICATIONS . . .	12
TABLE 2.2.1	CANDIDATE POLYMERS FOR MELT SPINNING . . . . .	31
TABLE 2.2.2	CSI MIXER-EXTRUDER MATRIX OF EXPERIMENTS . . . . .	34
TABLE 2.2.3	SUMMARY OF TRI-COMPONENT BLEND EXPERIMENTS . . . . .	38
TABLE 2.2.4	MECHANICAL TEST DATA ON VARIOUS FIBERS . . . . .	39
TABLE 2.3.1	TRANSPORT CRITICAL CURRENT DENSITIES AT 77 K Corrected Results of Previously Reported Fibers . . . . .	49
TABLE 2.3.2	TRANSPORT CRITICAL CURRENT DENSITIES AT 77 K Effect of Oxygen Annealing Time . . . . .	53
TABLE 2.3.3	TRANSPORT CRITICAL CURRENT DENSITIES AT 77 K Effect of Number of Passes Through Hot Zone/Time at Sintering Temperature 970°C, 5.6 cm/min, 1 h O <sub>2</sub> anneal . . . . .	61
TABLE 2.3.4	TRANSPORT CRITICAL CURRENT DENSITIES AT 77 K Effect of Number of Passes Through Furnace on Critical Current for Sintered Newly-Spun Fibers 950°C, 5.5 cm/min Sled Speed, 60 min O <sub>2</sub> Anneal . . . . .	70
TABLE 2.3.5	TRANSPORT CRITICAL CURRENT DENSITIES AT 77 K Effect of Number of Passes 935°C, 5.5 cm/min Sled Speed, 60 min O <sub>2</sub> Anneal . . . . .	70
TABLE 2.3.6	TRANSPORT CRITICAL CURRENT DENSITIES AT 77 K Isothermal Holds for 30 min, 60 min O <sub>2</sub> Anneal . . . . .	71
TABLE 2.3.7	GRAIN SIZE DATA FOR SINTERED FILAMENTS . . . . .	75
TABLE 2.5.1	TABLE OF J <sub>c</sub> VALUES AS MEASURED USING A 200 ms CURRENT PULSE VERSUS USING A STEPPED (DC) CURRENT SOURCE . . . . .	112
TABLE 2.5.2	CRITICAL CURRENT VARIATION FOUR ZONE PASSES AT 935°C . . .	123

COMPOSITE CERAMIC SUPERCONDUCTING WIRES FOR  
ELECTRIC MOTOR APPLICATIONS

JOHN W. HALLORAN  
PRINCIPAL INVESTIGATOR  
CERAMICS PROCESS SYSTEMS CORPORATION  
CAMBRIDGE, MASSACHUSETTS

SECTION I

GENERAL INTRODUCTION

1.1 Program Overview

This is the First Quarterly Report of a program to develop superconducting (SC) electric motors from the recently discovered ceramic superconductors. This program involves two main tasks: to produce useable quantities of practical high temperature superconductor (HTSC) wire, and to design and build a HTSC electric motor using this wire. As prime contractor, Ceramics Process Systems Corporation (CPS) is responsible for program management. The task of developing HTSC wire will be undertaken by a CPS affiliate company, CPS Superconductor Corporation (CPSS). The current approach being pursued to fabricate HTSC ceramic wire is to create a flexible composite of many fine ceramic filaments clad with copper or aluminum. The three basic elements of this method: 1) spinning polymer-containing "green" fibers, 2) sintering the fibers to make bare superconducting ceramic filaments, and, 3) cladding the filaments, were developed in a previous

program that began in August 1987<sup>1</sup>. The present program significantly extends this effort. Albany International Research Corporation (AIResCo) is working with CPSS to improve the green fiber spinning process and bring it to pilot scale production. The sintering and cladding operations will be significantly improved and combined to allow production of continuous lengths of composite ceramic wire. A major emphasis will be placed on improving the engineering properties of the composite HTSC wire, both in terms of its critical current in applied magnetic fields,  $J_c(H)$ , and for properties related to the manufacture and performance of motor windings. Emerson Motor Division (EMD) of Emerson Electric Company, will work closely with CPSS in evaluating the composite wire and in defining a set of realistic property requirements for practical HTSC motors.

The second task, to design and build HTSC motors, will be undertaken by EMD as a subcontractor to CPS. EMD does not propose a specific design for a HTSC motor at this time, largely because the relevant properties of the new HTSC materials, in wire form, have simply not yet been defined well enough to justify a detailed motor design. Rather, one of their first objectives is to define how a superconducting motor should be designed, so that it respects the unique properties of the HTSC ceramics, and fulfills performance criteria for target applications appropriate to SC motors operating in a liquid nitrogen cryogenic environment.

This report covers development activities during the period July through September, 1988. Most of this work was performed before the actual

---

<sup>1</sup> "Composite Ceramic Superconducting Filaments for Superconducting Cable," ONR Contract N00014-87-C-0789, Final Report 12 July 1988. A brief summary of this report is included here as Appendix I.

contract was received, under ONR authorization to proceed "at risk." CPS chose to begin activities on the wire development task at CPSS and AIResCo, but to defer the start of the EMD subcontract until October 1, 1988. Consequently, this report will only present progress in the wire manufacture development task. This is discussed in Section 2. Section 3 will present the initial development plans for HTSC motor design and fabrication.

## 1.2 Composite Wire Design Philosophy

The strategy for producing practical wires from HTSC ceramics centers around the use of fine ceramic filaments in a normal metal matrix. In this regard, it is similar to traditional low temperature superconductor multi-filamentary conductor designs. However, the motivating factors influencing the use of fine ceramic filaments is different. Low temperature superconductors favor fine filaments primarily to promote stability against flux jumps, and to minimize AC losses<sup>2</sup>. A recent analysis by Collings<sup>3</sup> has shown that for  $\text{YBa}_2\text{Cu}_3\text{O}_{7-\delta}$  at liquid nitrogen temperature, even macroscopically large filaments are intrinsically stable against flux jumps, so fine filaments are not required for thermal or electrical reasons, unless AC losses are a concern. However, in the case of HTSC materials, fine ceramic filaments are necessary for mechanical reasons, permitting the brittle ceramics to be used like conventional flexible wires. The CPSS design incorporates an array of

---

<sup>2</sup> E.W. Collings, Applied Superconductivity, The Metallurgy and Physics of Titanium Alloys, 2, Applications, Plenum Press, NY, 1986

<sup>3</sup> E.W. Collings, "Design Considerations for High  $T_c$  Ceramic Superconductors," presented at the MRS International Meeting, Tokyo, May 30, 1988, to be published in Cryogenics

fine ceramic filaments located at the mechanical neutral axis of a composite ribbon. A schematic of a flexible ribbon conductor is shown in Figure 1.1.1.

The bending radius that can be tolerated by the composite ribbon before damage occurs depends upon the filament diameter. Using simple beam theory, the minimum radius of curvature,  $R$ , which the filament of diameter  $D$  can withstand is related to the maximum tolerable tensile stress,  $S_m$ , and Young's modulus  $E$  by the simple relation:

$$R = ED/2S_m$$

that illustrates how flexibility demands fine diameter filaments. Tensile stresses generated upon flexure can also be partially compensated for by any compressive pre-stress that might be exerted on the ceramic filaments by the metal cladding. The thermal expansion difference between  $YBa_2Cu_3O_{7-\delta}$  and the metal matrix can be used to generate a desirable axial compressive stress in the  $YBa_2Cu_3O_{7-\delta}$  filament,  $S_r$ , that can be approximated by:

$$S_r = E(a_{sc} - a_m)(T_d - T_o)$$

where  $a$  is the thermal expansion coefficient for the metal and the superconductor,  $T_d$  is the temperature that the metal cladding is deposited, and  $T_o$  is the operating temperature, which is room temperature for handling and winding, and liquid nitrogen temperature for use. This compressive stress can be significant, since a copper cladding can generate 75 psi/°C and aluminum can create 110 psi/°C. With a 300°C cladding deposition temperature, a copper clad filament will experience more than 20,000 psi axial compressive stress at room temperature, and almost 40,000 psi at liquid nitrogen temperature.

The stabilizer ratio, or the volume ratio of normal metal to superconductor, is a major design parameter for practical superconductor

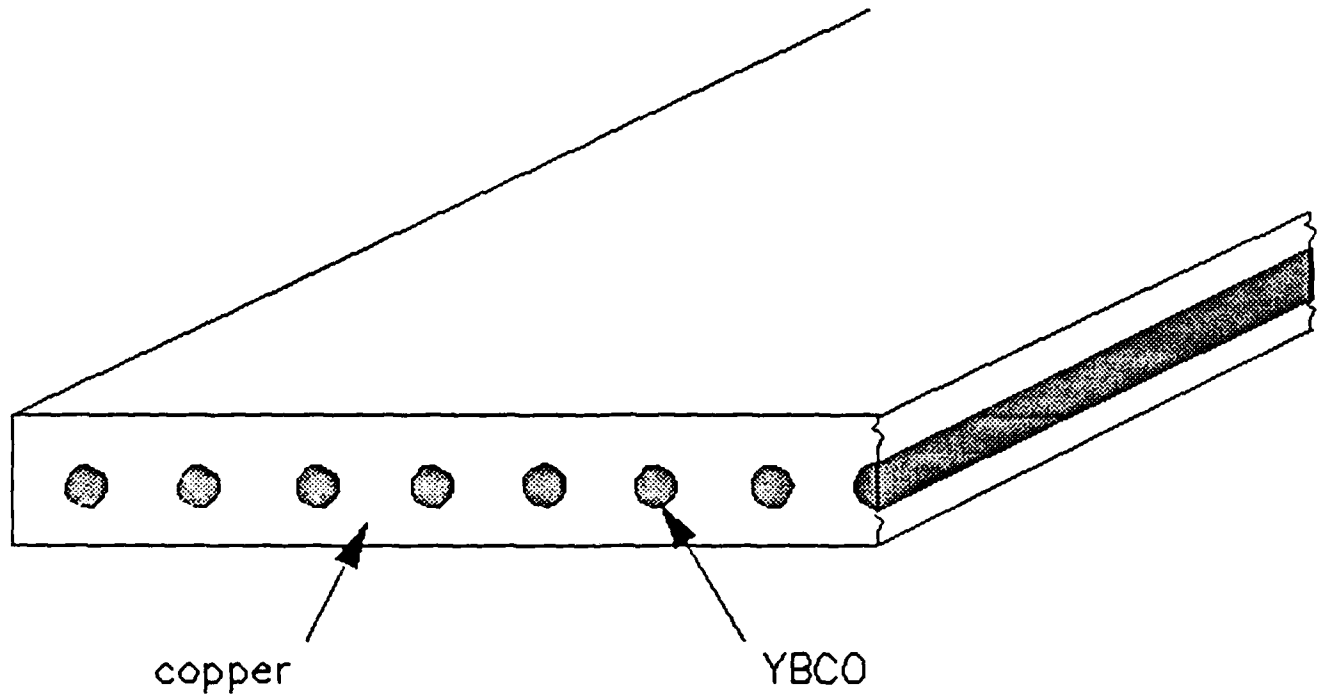


Figure 1.1.1 Schematic of the Flexible Ribbon Conductor Concept Illustrating an Array of Fine Superconductor Filaments in a Normal Metal Cladding.

wires. The stabilizer ratio must be large enough to provide for current shunting and stabilization without being so large that the net current density is diluted. In the case of the ribbon conductor, the stabilizing metal acts as a barrier to hermetically isolate the HTSC ceramic from the environment and is also the matrix for mechanical support. The cladding metal reinforces the ceramic by bearing some fraction of the tensile loads, and is the medium that applies the compressive pre-stress to the ceramic filament. For the ribbon conductor shown in Figure 1.1.1, with filaments of diameter  $D$  and center-to-center spacing  $W$ , in a ribbon of thickness,  $t$ , the metal/superconductor stabilizer ratio,  $SR$  is:

$$SR = 4tW/\pi D^2 - 1$$

The practical handling of the ribbon may also play a role in specifying  $SR$  for the ribbon conductor. If very tight bending radii are specified, very fine filament diameters may be required. This in turn may require a higher  $SR$  to prevent the ribbon thickness from becoming too small to handle conveniently as a single ribbon wire. It may be necessary to adopt tows of fine ribbons with individual wires bound sufficiently loosely such that each wire is able to respond independently to flexure.

The mechanical behavior of the ribbon conductor is of great interest and is being analyzed in some detail, though the task is not presently complete. For illustration, however, a few approximate relations might suffice to provide a simple model. For example, consider simple tensile loading of the composite ribbon conductor bearing a load,  $P$ . Neglecting multi-axial effects, one can simply equate the axial tensile strain in the superconductor and the metal cladding. This allows one to express the tensile stress experienced by the superconductor filament,  $S_{sc}$ , in terms of the

applied tensile load,  $P$ , the compressive pre-stress,  $S_r$ , the filament diameter, the stabilizer ratio, and the elastic modulus ratio

$e = E_{SC}/E_{metal}$  as:

$$S_{sc} = (4P/\pi D^2)e/(e+SR) - S_r$$

The difference between this filament tensile stress and the stress that would be experienced by an unclad filament bearing the same tensile load can be defined as the reinforcement ratio,  $f_R$ , given by:

$$f_R = e/(SR+e) - S_r/(4P/\pi D^2)$$

The significance of the compressive pre-stress term in this expression indicates the desirability of applying the cladding at as high a temperature as possible. In the case of  $YBa_2Cu_3O_{7-\delta}$ , the cladding would be applied to a sintered filament that had already received an oxygen intercalation anneal. The upper limit on the cladding temperature is likely to be determined by the temperature at which oxygen loss kinetics become significant.

As stated earlier, the design presently being considered is based on preparing bare superconducting filaments that are subsequently clad with metal in a separate step at temperatures below the oxygen intercalation anneal temperature. This is primarily motivated by the need to anneal  $YBa_2Cu_3O_{7-\delta}$  after sintering to restore the superconducting orthorhombic phase, and secondarily to permit the use of base metals such as aluminum or copper, that are chemically reactive with  $YBa_2Cu_3O_{7-\delta}$  at high temperature. A further advantage of bare filament sintering is that the sintering heat treatment can be optimized for the  $YBa_2Cu_3O_{7-\delta}$  ceramic, since it is being treated in isolation. This contrasts with a cofiring approach, where the ceramic is sintered along with the metal cladding; the heat treatment schedule being some compromise between what optimizes the ceramic and what is best for the

metallization. To a degree, post-anneal cladding is necessitated by the properties of  $\text{YBa}_2\text{Cu}_3\text{O}_{7-\delta}$  in particular, not HTSC ceramics in general. If a new material were to be discovered that is compatible with base metals at sintering temperature, cladding would probably be done differently.

The concept of a tailored amount of compressive pre-stress introduces the need to consider factors other than simple mechanical properties that might be enhanced or degraded by this residual stress. It is well established in low temperature superconductors that mechanical strain decreases the upper critical field and degrades critical current<sup>4</sup>, and if the high temperature superconductors behave similarly, excessive pre-stress may be detrimental. In addition, these twinned perovskite-based ceramic superconductors might experience domain effects similar to those which lead to aging phenomena in ferroelectric ceramics, which is known to be accelerated by mechanical stress<sup>5</sup>. On the other hand, some evidence<sup>6</sup> suggest that compressive stress can increase the critical temperature of  $\text{YBa}_2\text{Cu}_3\text{O}_{7-\delta}$ . Moreover, a compressive stress field may be beneficial if it suppresses microcracking in  $\text{YBa}_2\text{Cu}_3\text{O}_{7-\delta}$ . In many polycrystalline ceramics including  $\text{YBa}_2\text{Cu}_3\text{O}_{7-\delta}$ , a large thermal expansion anisotropy will promote spontaneous microcracking if the grains are larger than some critical size. A compressive strain field can suppress microcracking, since microcracking is dilational.

---

<sup>4</sup> J.W. Ekin, "Mechanical Properties and Strain Effects in Superconductors," Chapter 7, in Superconductor Materials Science, Metallurgy, Fabrication, and Applications, eds., S. Foner and B. Schwartz (1981) pp. 455-509

<sup>5</sup> G.H. Haertling, "Piezoelectric and Electro-Optic Ceramics," Chapter 3 in Ceramic Materials for Electronics, R.C. Buchanan, ed., Marcel Dekker, Inc. NY, 1986

<sup>6</sup> Y. Nishi, N. Ninomiya, and S. Tokunaga, J. Materials Science Letters, 7 (1988) pp. 361-362

The final feature of the design is to produce the superconductor filaments by sintering green fibers spun from  $\text{YBa}_2\text{Cu}_3\text{O}_{7-\delta}$  powder. The fiber method was chosen because it naturally produces continuous fiber that can be many kilometers long, and because it can be easily implemented as a large scale manufacturing operation using conventional textile spinning machinery. The chosen fiber preparation method uses a dope consisting of HTSC powder and appropriate polymer resins. This method is believed to have advantages over alternative fiber forming methods such as sol-gel or precursor techniques; one advantage is simplicity. It is a challenge to prepare a high quality  $\text{YBa}_2\text{Cu}_3\text{O}_{7-\delta}$  powder; the difficulties of synthesizing the necessary precursors, alkoxides, etc., and preparing them into a tractable form for spinning and heat treating only adds to the challenge. Heat treatment of the powder-derived fibers involves only the microstructural processes of densification and grain growth, since the  $\text{YBa}_2\text{Cu}_3\text{O}_{7-\delta}$  compound is already present. Precursor-derived fibers undergo a variety of chemical reactions during sintering, leading to  $\text{YBa}_2\text{Cu}_3\text{O}_{7-\delta}$  phase formation occurring simultaneously with the physical reactions associated with microstructure development. Such a process would be inherently more difficult to control. Another advantage to the use of powder-derived fibers is that green particle orientation can be developed using well established methods that would provide an identifiable mechanism for grain orientation. Finally, the chemical syntheses for precursor methods might require extensive modification to be applied to another composition, while powder-derived fibers can easily be prepared from virtually any powder. Consequently, the fiber technology developed for  $\text{YBa}_2\text{Cu}_3\text{O}_{7-\delta}$  can be readily adapted to other HTSC materials. CPSS develops (and tests) new spinning formulations and methods using barium titanate before

attempting them with the more costly  $\text{YBa}_2\text{Cu}_3\text{O}_{7-\delta}$ . Essentially the same fiber spinning methods have been applied to a number of  $\text{YBa}_2\text{Cu}_3\text{O}_{7-\delta}$  powders with a variety of particle sizes, as well as preparation of fibers from  $\text{YBa}_2\text{Cu}_3\text{O}_{7-\delta}/\text{Ag}$  powder composites.

### 1.3 Program Schedule

This program has a very aggressive schedule in which the wire manufacturing process to produce continuous composite ceramic wire on a laboratory scale is to be developed by the end of the first year. This process will be improved and expanded to pilot plant scale by the end of the second year. Effort during the third year will focus on optimizing the process and supplying HTSC wire to support the experimental motor program. The HTSC motor tasks emphasize application studies and design work during the first year, wire testing and evaluation during the second year, and experimental motor fabrication and testing during the third year. The nature of the wire manufacturing process is sequential; HTSC powder production must be scaled-up before continuous green fiber can be spun, continuous green fiber is needed to develop the continuous sintering process, and a continuous cladding process must be available before long sintered filaments can be handled. Moreover, test motors obviously cannot be wound before wire is available. To overcome these difficulties and accelerate progress, the program is organized to accomplish much of the development activities in parallel. This is done by simulating continuous processes through careful design of discrete experiments, and employing "surrogates" to allow downstream processes to be developed before their feedstock is available from upstream processes. For example, larger scale fiber spinning experiments are executed

using barium titanate powder instead of the less readily available (and more expensive)  $\text{YBa}_2\text{Cu}_3\text{O}_{7-\delta}$  powder. Spinning dopes and methods developed for the "white fiber" are then transferred, with modification if necessary, to make "black fiber" using  $\text{YBa}_2\text{Cu}_3\text{O}_{7-\delta}$ . Currently, sintering and cladding experiments are done on short lengths of  $\text{YBa}_2\text{Cu}_3\text{O}_{7-\delta}$  filament, with particular emphasis on determining necessary heat treatments and surface treatments to improve  $J_c$  or to metallize the  $\text{YBa}_2\text{Cu}_3\text{O}_{7-\delta}$  surface. Meanwhile, graphite fibers or metal wires are used as surrogates for  $\text{YBa}_2\text{Cu}_3\text{O}_{7-\delta}$  filament to investigate the mechanical aspects of the cladding process.

The detailed schedule of activities for each task and subtask are listed in Table 1.1 for each Quarterly Report Period. Figure 1.1.2 displays much of the same information as a Gantt chart showing the more important tasks. CPSS emphasizes that this statement of work reflects current plans, and is expected to be revised as the research progresses.

TABLE 1.1

QUARTERLY WORK STATEMENT  
COMPOSITE CERAMIC SUPERCONDUCTING WIRES FOR  
ELECTRIC MOTOR APPLICATIONS

FIRST REPORT PERIOD: THIRD QUARTER 1988

TASK I: COMPOSITE WIRE MANUFACTURING

SUBTASK IA) POWDER PRODUCTION

- 1) Supply consistent quality powder for fiber spinning at rate of at least 2 kilograms per month
- 2) Determine optimum particle size distribution and surface area for fiber spinning and sintering
- 3) Continuing improvement of powder production

SUBTASK IB) GREEN FIBER DEVELOPMENT

- 1) Supply continuous green fiber from laboratory apparatus to support sintering activities
- 2) Define and optimize laboratory-scale dry spinning conditions
- 3) Define green fiber requirements for handling and spooling
- 4) Develop procedures to characterize green textures by X-ray diffraction, and begin study of texture as a function of spinning conditions, fiber stretching, and powder characteristics
- 5) Begin development of melt spinning process at AIResCo
- 6) Deliver sample spools of green fiber to DARPA

SUBTASK IC) FIBER SINTERING AND MICROSTRUCTURE DEVELOPMENT

- 1) Begin study of density, grain size, and texture as a function of temperature zones and residence times for directional recrystallization
- 2) Define continuous fiber sintering parameters (zone temperatures, fiber velocity, zone passes for microstructure development and oxygen annealing)
- 3) Correlate green texture with sintered texture

SUBTASK ID) FILAMENT CLADDING DEVELOPMENT

- 1) Define mechanical and electrical requirements of filament cladding
- 2) Screen a variety of aqueous and non-aqueous plating baths for electrodeposition onto bare or premetallized sintered ceramic
- 3) Clad short lengths of filament by electroplating on a bench-scale
- 4) Obtain solder-clad copper foil and define processing parameters for mechanical cladding
- 5) Begin to set up continuous reel-to-reel cladding facility using a surrogate fiber

TASK II: CHARACTERIZATION

- 1) Electrical and magnetic properties
  - a) Determine resistance vs. temperature for sintered filaments
  - b) Determine critical current density at liquid nitrogen temperature on sintered filaments as a function of magnetic field
- 2) Mechanical and physical properties
  - a) Determine tensile strength of green, fired, and early specimens of clad filaments

TASK III: MOTOR DESIGN AND CONSTRUCTION

No activities during this period

TABLE 1.1 (con't)

SECOND REPORT PERIOD: FOURTH QUARTER 1988

TASK I: COMPOSITE WIRE MANUFACTURING

## SUBTASK IA) POWDER PRODUCTION

- 1) Supply improved powder for fiber spinning at CPS and AIResCo at rate of at least 4 kilograms per month
- 2) Continue to define optimum particle size distribution and surface area for fiber spinning and sintering
- 3) Continuing improvement of powder production

## SUBTASK IB) GREEN FIBER DEVELOPMENT

- 1) Supply continuous green fiber from AIResCo to support sintering activities
- 2) Define and optimize spinning conditions, primarily at the AIResCo facility
- 3) Define advanced spinning concepts at AIResCo
- 4) Continue to characterize green textures as a function of spinning conditions, fiber stretching, and powder characteristics
- 5) Define binder burnout conditions for melt spun candidate polymers

## SUBTASK IC) FIBER SINTERING AND MICROSTRUCTURE DEVELOPMENT

- 1) Continue directional recrystallization process development
- 2) Achieve continuous fiber sintering and annealing, and develop procedures for handling sintered filament
- 3) Correlate sintered filament texture with critical current

## SUBTASK ID) FILAMENT CLADDING DEVELOPMENT

- 1) Select cladding process for further development, either electroplating or mechanical cladding
- 2) Continue development of continuous cladding facility using surrogate filament

TASK II: CHARACTERIZATION

- 1) Electrical and magnetic properties
  - a) Determine resistance vs. temperature for sintered filaments and early clad wires
  - b) Determine critical current density at liquid nitrogen temperature on sintered filaments and clad wires as a function of magnetic field, and correlate with microstructure
- 2) Mechanical and physical properties
  - a) Determine tensile strength of green, fired, and clad filaments

TASK III: MOTOR DESIGN AND CONSTRUCTION

- 1) Assign motor design engineer and mechanical engineer to project on full time basis
- 2) Conduct detailed literature research on superconductive motors and mechanical systems that can operate at liquid nitrogen temperature
- 3) Begin Application Study - Engage consultants to evaluate motor technologies that are potential candidates for HTSC
- 4) Define initial wire property targets for design database
- 5) Engage consultant to study and report on physical properties, effect of environment, test requirements and test methods for HTSC conductors

TABLE 1.1 (con't)

THIRD REPORT PERIOD: FIRST QUARTER 1989

TASK I: COMPOSITE WIRE MANUFACTURING

## SUBTASK IA) POWDER PRODUCTION

- 1) Supply consistent powder for fiber spinning at CPS and AIResCo
- 2) Continue study of effects of surface area, particle shape, particle size distribution on fiber spinning and sintering

## SUBTASK IB) GREEN FIBER DEVELOPMENT

- 1) Supply continuous green fiber dry-spun at AIResCo to support sintering activities
- 2) Continue green texture studies on CPS and AIResCo green fiber, using both shear texturing and magnetic orientation
- 3) Begin refining first generation dry spinning dope and/or developing second generation dry spinning dope for process improvement at AIResCo

## SUBTASK IC) FIBER SINTERING AND MICROSTRUCTURE DEVELOPMENT

- 1) Initiate detailed study of effect of microstructural and textural parameters on 77 K critical current
- 2) Continue development and upgrade laboratory scale continuous sintering furnace

## SUBTASK ID) FILAMENT CLADDING DEVELOPMENT

- 1) Incorporate sintered fiber in continuous cladding facility to prepare short lengths of complete wire
- 2) Deliver short lengths of complete wire to EMD for preliminary evaluation
- 3) Deliver short length samples of complete wire to DARPA

TASK II: CHARACTERIZATION

- 1) Determine critical current of wire samples in presence of magnetic field and relate to wire microstructure and processing
- 2) Define the effect of handling and mechanical loading on critical current of wire to determine damage thresholds

TASK III: MOTOR DESIGN AND CONSTRUCTION

- 1) Continue literature research on superconductive motors and mechanical systems that can operate at liquid nitrogen temperature
- 2) Continue Application Study of military and civilian applications for HTSC motors, identify all motor applications and markets
- 3) Determine maximum mechanical stresses of wires wound under various manufacturing processes
- 4) Update wire property targets for design database
- 5) Continue study of physical properties, effect of environment, test requirements and test methods for HTSC conductors

## TABLE 1.1 (con't)

FOURTH REPORT PERIOD: SECOND QUARTER 1989

TASK I: COMPOSITE WIRE MANUFACTURING

## SUBTASK IA) POWDER PRODUCTION

- 1) Supply consistent powder for fiber spinning at CPS and AIResCo
- 2) Continue study of effects of surface area, particle shape, particle size distribution on fiber spinning and sintering

## SUBTASK IB) GREEN FIBER DEVELOPMENT

- 1) Supply continuous green fiber dry-spun at AIResCo to support sintering activities
- 2) Continue green texture studies on CPS and AIResCo green fiber, using both shear texturing and magnetic orientation
- 3) Deliver spools of oriented green fiber to DARPA
- 4) Evaluate second generation dry spinning dope for process improvement at AIResCo
- 5) Begin design of pilot scale spinning facility at CPS

## SUBTASK IC) FIBER SINTERING AND MICROSTRUCTURE DEVELOPMENT

- 1) Continue study of effect of microstructural and textural parameters on critical current as a function of temperature and magnetic field
- 2) Continue development and upgrade laboratory scale continuous sintering furnace
- 3) Process improvement in laboratory scale continuous sintering
- 4) Begin design of pilot scale sintering facility

## SUBTASK ID) FILAMENT CLADDING DEVELOPMENT

- 1) Continue development and upgrading of continuous cladding facility
- 2) Combine laboratory scale sintering furnace with continuous cladding facility to prepare semi-continuous lengths of complete wire
- 3) Deliver short lengths of improved wire to EMD for evaluation of physical and electrical properties

TASK II: CHARACTERIZATION

- 1) Continue examination of critical current of wire samples in presence of magnetic field and relate to wire microstructure and processing
- 2) Determine tensile properties of complete wire samples
- 3) Continue to define the effect of handling and mechanical loading on critical current of wire

TASK III: MOTOR DESIGN AND CONSTRUCTION

- 1) Initiate in-depth study of most promising applications of HTSC motors identified in applications study
- 2) Design and build wire testing equipment for mechanical and electrical properties; test equipment to be designed to evaluate properties at 77 K in static and time varying magnetic fields with variable applied mechanical stress
- 3) Initiate research on termination of superconductor wire
- 4) Initiate discussions with wire insulating companies to develop insulation systems; convey mechanical, thermal and chemical limitations of superconductor wire
- 5) Develop bearing system that can operate in 77 K ambient

TABLE 1.1 (con't)

FIFTH REPORT PERIOD: THIRD QUARTER 1989

TASK I: COMPOSITE WIRE MANUFACTURING

## SUBTASK IA) POWDER PRODUCTION

- 1) Supply consistent powder for fiber spinning at CPS and AIResCo
- 2) Continue study of effects of surface area, particle shape, particle size distribution on fiber spinning and sintering

## SUBTASK IB) GREEN FIBER DEVELOPMENT

- 1) Supply standard textured green fiber to CPS for wire production and special fibers for experiments
- 2) Continue green texture studies, to optimize process
- 3) Begin installation of pilot scale spinning facility at CPS

## SUBTASK IC) FIBER SINTERING AND MICROSTRUCTURE DEVELOPMENT

- 1) Continue study of effect of microstructural and textural parameters on critical current as a function of temperature and magnetic field
- 2) Begin acquisition of pilot scale continuous sintering furnace
- 3) Process improvement in laboratory scale continuous sintering

## SUBTASK ID) FILAMENT CLADDING DEVELOPMENT

- 1) Continue development and upgrading of continuous cladding facility
- 2) Upgrade laboratory scale sintering furnace and continuous cladding facility to produce continuous lengths of complete wire
- 3) Deliver spools of complete wire to EMD for evaluation of physical and electrical properties
- 4) Begin optimization of electrical and physical properties of wire

TASK II: CHARACTERIZATION

- 1) Continue examination of critical current of wire samples in presence of magnetic field and relate to wire microstructure and processing
- 2) Determine effect of wire length on wire properties
- 3) Continue to define the effect of handling and mechanical loading on critical current of wire

TASK III: MOTOR DESIGN AND CONSTRUCTION

- 1) Finalize design of initial proof-of-principle motor to be built and evaluated
- 2) Determine manufacturing requirements imposed on the wire based on the design being considered
- 3) Perform initial tests on short lengths of wire supplied by CPS. Evaluate bending radii
- 4) Design cryogenic system for initial motor; design and build 77 K test stand
- 5) Develop and begin testing of termination methods for SC wire
- 6) Evaluate recommended insulation systems with wire samples

TABLE 1.1 (con't)

SIXTH REPORT PERIOD: FOURTH QUARTER 1989

TASK I: COMPOSITE WIRE MANUFACTURING

## SUBTASK IA) POWDER PRODUCTION

- 1) Supply optimized powder for fiber spinning at CPS and AIResCo
- 2) Scale up powder production to produce at least 20 kg optimized powder per month

## SUBTASK IB) GREEN FIBER DEVELOPMENT

- 1) Supply standard textured green fiber to CPS for wire production and special fibers for experiments
- 2) Continue process optimization
- 3) Continue installation of pilot scale spinning facility at CPS

## SUBTASK IC) FIBER SINTERING AND MICROSTRUCTURE DEVELOPMENT

- 1) Continue study of effect of microstructural and textural parameters on critical current as a function of temperature and magnetic field
- 2) Begin installation of pilot scale continuous sintering furnace
- 3) Continue process optimization in laboratory scale continuous sintering

## SUBTASK ID) FILAMENT CLADDING DEVELOPMENT

- 1) Continue development and upgrading of continuous cladding facility
- 2) Deliver spools of improved wire to EMD for physical and electrical properties evaluation
- 3) Continue optimization of electrical and physical properties of wire
- 4) Supply wire to EMD to support experimental motor building

TASK II: CHARACTERIZATION

- 1) Continue examination of critical current of wire samples in presence of magnetic field and relate to wire microstructure and processing
- 2) Examination of wire samples from experimental motors to identify performance limiting problems
- 3) Mechanical and electrical properties of continuous wire lengths

TASK III: MOTOR DESIGN AND CONSTRUCTION

- 1) Begin fabricating parts for initial proof-of-principle motor
- 2) Continue development of bearing system
- 3) Continue termination methods testing
- 4) Obtain insulating system on short lengths of wire
- 5) Continue building of test stand
- 6) Initiate study of advanced HTSC motor design

TABLE 1.1 (con't)

SEVENTH REPORT PERIOD: FIRST QUARTER 1990

TASK I: COMPOSITE WIRE MANUFACTURING

## SUBTASK IA) POWDER PRODUCTION

- 1) Supply optimized powder for fiber spinning at CPS and AIResCo

## SUBTASK IB) GREEN FIBER DEVELOPMENT

- 1) Supply standard textured green fiber to CPS for wire production and special fibers for experiments
- 2) Begin operation and de-bugging of CPS pilot scale dry spinning facility

## SUBTASK IC) FIBER SINTERING AND MICROSTRUCTURE DEVELOPMENT

- 1) Continue study of effect of microstructural and textural parameters on critical current as a function of temperature and magnetic field
- 2) Begin operation and de-bugging of pilot scale continuous sintering furnace
- 3) Continue process optimization in laboratory scale continuous sintering

## SUBTASK ID) FILAMENT CLADDING DEVELOPMENT

- 1) Combine continuous cladding facility with continuous sintering facility
- 2) Continue to deliver spools of experimental wire to EMD for physical and electrical properties evaluation
- 3) Continue optimization of electrical and physical properties of wire
- 4) Supply wire to EMD to support experimental motor building

TASK II: CHARACTERIZATION

- 1) Continue examination of critical current of wire samples in presence of magnetic field and relate to wire microstructure and processing
- 2) Examination of wire samples from experimental motors to identify performance limiting problems
- 3) Mechanical and electrical properties of continuous wire lengths

TASK III: MOTOR DESIGN AND CONSTRUCTION

- 1) Insulate spools of wire
- 2) Evaluate physical and mechanical properties of insulated wire
- 3) Perform collette tests on insulated SC wire; determine endurance to vibratory forces and degree of physical restraint and/or isolation required; continue studies of effects of magnetic fields
- 4) Continue fabrication proof-of-principle motor parts
- 5) Continue advanced motor design studies

TABLE 1.1 (con't)

EIGHTH REPORT PERIOD: SECOND QUARTER 1990

TASK I: COMPOSITE WIRE MANUFACTURING

## SUBTASK IA) POWDER PRODUCTION

- 1) Supply optimized powder for fiber spinning at CPS and AIResCo

## SUBTASK IB) GREEN FIBER DEVELOPMENT

- 1) Supply standard textured green fiber for wire production from CPS pilot scale dry spinning facility

## SUBTASK IC and ID) FIBER SINTERING AND CLADDING

- 1) Begin process optimization for pilot scale continuous sintering and cladding facility
- 2) Define effects of manufacturing parameters on critical current and physical properties of wire
- 3) Deliver spools of wire from the CPS pilot plant to EMD for building prototype motors
- 4) Deliver spools of experimental wire to EMD for physical and electrical properties evaluation
- 5) Continue optimization of electrical and physical properties of wire

TASK II: CHARACTERIZATION

- 1) Continue examination of critical current of wire samples in presence of magnetic field and relate to wire microstructure and processing
- 2) Examination of wire samples from experimental motors to identify performance limiting problems
- 3) Mechanical and electrical properties of continuous wire

TASK III: MOTOR DESIGN AND CONSTRUCTION

- 1) Assemble proof-of principle HTSC motor and begin evaluation of electrical performance, stability, and efficiency
- 2) Continue coilette testing
- 3) Continue advanced motor design

TABLE 1.1 (con't)

NINTH, TENTH, AND ELEVENTH REPORT PERIODS:  
THIRD QUARTER 1990 THROUGH FIRST QUARTER 1991

TASK I: WIRE MANUFACTURE

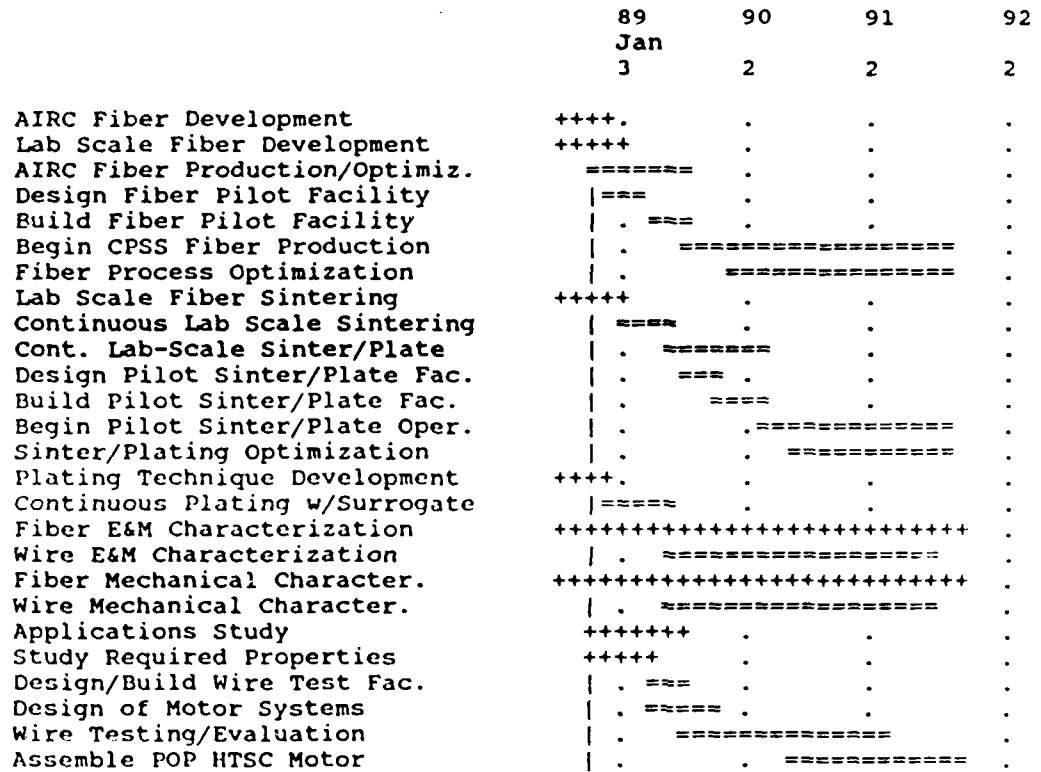
- 1) Continue manufacturing development, upgrade facilities, identify and install process controls to improve yields
- 2) Identify property-limiting faults in wire from prototype motors to improve wire quality
- 3) Manufacture second generation composite wire in response to needs of prototype motors

TASK II: CHARACTERIZATION

- 1) Detailed examination of tensile properties, damage tolerance, delayed failure, and environmental degradation of composite wires
- 2) Continued characterization of transport properties as related to structure and processing.

TASK III: MOTOR DESIGN AND CONSTRUCTION

- 1) Finalize testing of proof-of-principle motor, modify and redesign as indicated by initial results
- 2) Finalize and report on properties, insulation, termination, and results of initial motor testing
- 3) Recommend design for further evaluation of HTSC motor program; provide complete design analysis of each design
- 4) Begin fabrication of functional models of motors of original design, and/or proof-of-principle models of advanced designs
- 5) Continue development of improved insulation termination and winding techniques; evaluate improved wire



-----  
 === Task - Slack time (==---), or  
 +++ Started task Resource delay (---==)

Figure 1.1.2 Gantt Chart for Program Tasks.

## SECTION 2

## WIRE FABRICATION

ZONGYI CHEN, JOHN HALLORAN, JAMES HODGE, LORI JO KLEMPNER,  
MATTHEW NEAL, MARK PARISH, VIREN PATHARI, AND RAYSHA PICERNO  
CPS SUPERCONDUCTOR CORPORATION

GEORGE BAKIS, DANA EAGLES, WESLEY ISHIDA, AND STEPHEN TIERNAN  
ALBANY INTERNATIONAL RESEARCH CORPORATION

## 2.1 Introduction and General Comments

This section presents results of activities aimed at wire manufacturing, including work performed at CPSS and AResCo. It is organized so that each of the major tasks is reported as a subsection. This reflects the breakdown of the current development activities since the powder synthesis, green fiber spinning, heat treatment, and metal cladding processes are now being developed separately. It must be emphasized, however, that the entire wire process is sequential, and the capability in each step affects all of the others. The output of one step is the feedstock for the next, so "downstream" effects are quite direct. Process capability in one step also places constraints on the preceding steps, so that there is also a strong "upstream" influence. This development program is organized in an attempt to maximize opportunity for parallel development. CPSS attempts to use simulations, surrogates, and substitutes to allow each step to progress as rapidly as possible, without being bottlenecked by the current level of development in the preceding step. With adequate communication, this approach should be adequate for the first several quarters of this program when all processes are at the bench top scale.

During the first half of 1989, emphasis will be on combining these elements into a laboratory scale, continuous wire forming process. The continuous wire forming process naturally separates into a "front end" or green fiber, and a "back end" or sintered filament segments that can be

conducted independently. This separation reflects the handling characteristics of the material. The flexible green fiber is easy to handle, and can be conveniently stored in multi-kilometer lengths on a spool, either as a monofilament or a woven array of several green fibers. The powder preparation and green fiber processing can be accomplished separately from the subsequent steps. In contrast, once the fiber is removed from the spool and fed into the sintering furnace, the material becomes difficult to handle until it is completely clad with metal. It does not seem practical to spool the bare filaments after sintering, as they are too fragile for such handling. The cladding step must immediately follow the heat treatment, preferably accepting the continuous filaments while they are still on the furnace belt. The goal of the cladding operation incorporates a process that connects to the exit end of the continuous sintering furnace and clads the filament array with the reinforcing metal, producing a composite ribbon conductor suitable for spooling.

Simultaneous to the development of the process to render the  $\text{YBa}_2\text{Cu}_3\text{O}_{7-\delta}$  into the form of continuous composite ribbons, there are sets of tasks more related to the materials science of the superconductor. These are aimed at characterizing and enhancing the properties of the material, with most emphasis on improving the transport critical current density. Much of the program is set up as a feedback loop, where processing conditions are evaluated as to their influence on transport critical current. This becomes most noticeable in the heat treatment and cladding tasks, where most of the effort is aimed at evaluating the critical current density of experimental filaments. CPSS seeks to optimize critical current empirically by attempting strategies such as producing microstructural texture and "benign" grain boundaries. A grain boundary is benign if it does not create a weak link. The hypothesis that a sufficiently low angle grain boundary could be benign if it has no compositional segregation or contaminants will be tested. Fibers

will ultimately be prepared from phase pure powders or from powders containing a controlled sintering aid. To date, most work used commercial  $\text{YBa}_2\text{Cu}_3\text{O}_{7-\delta}$  powders having an excess of copper oxide that leads to an optically visible  $\text{CuO}$  phase between the grains. Currently, phase pure  $\text{YBa}_2\text{Cu}_3\text{O}_{7-\delta}$  powder is being produced at CPSS in quantities sufficient to make fibers.

Two methods are being explored to obtain microstructural texture. One method exploits the tremendous elongational flow accompanying fiber spinning that will orient all the platy particles to create a "green" microstructural texture. At present, platy-particle  $\text{YBa}_2\text{Cu}_3\text{O}_{7-\delta}$  powder has not been produced in quantities sufficient to spin fiber, and therefore green textured fiber has not been evaluated. The second method being explored to induce texture is an attempt to exploit the anisotropy of grain growth during sintering. Exposing the material to axial temperature gradients has been attempted in order to induce directional recrystallization. In practice, the filaments have been passed repeatedly through the hot zone of a tube furnace, a process CPSS refers to as multiple zone sintering.

Transport critical current ( $J_c$ ) is the property on which most activity is focussed, since the reliability of the data is so consequential. During this Quarter a problem was uncovered and corrected with the  $J_c$  measurement technique. In addition, great concerns have been raised about the meaning of critical current in a weak-link material, about self-field effects in the filaments, and about the statistical variation of measured  $J_c$  in "identically" treated specimens.

The starting  $\text{YBa}_2\text{Cu}_3\text{O}_{7-\delta}$  powder is critically important. There is significant activity at CPSS to produce high quality  $\text{YBa}_2\text{Cu}_3\text{O}_{7-\delta}$  powder in sufficient amounts to support the development program. CPSS has chosen to prepare a highly phase pure product with less than 1% impurity phase detectable by x-ray diffraction. Though producing large quantities of consistent material has proved difficult, material is now being prepared in

quantities adequate for current program needs. By fabricating trial fibers and examining their sintering behavior and electrical characteristics, optimal particle size and powder characteristics are being determined. This work is not complete and will be addressed in the next Quarterly Report.

The powder requirements for this program are stringent. With heat treatments based on very rapid sintering, the powder must be highly sinterable. Phase purity is very important for two reasons: Contaminant phases such as barium cuprate can interfere with the rheology of the fiber spinning dope, and the very brief heat treatments leave no time for decomposition of residual barium carbonate. Note that residual reactants and impurity phases are evidence of poor control of the powder manufacturing process. It is pointless to base a multi-step development program on non-reproducible  $\text{YBa}_2\text{Cu}_3\text{O}_{7-\delta}$  feedstock.

In addition to CPSS's  $\text{YBa}_2\text{Cu}_3\text{O}_{7-\delta}$  production efforts, a number of commercially available powders have been evaluated for phase purity and sinterability. Most of the  $\text{YBa}_2\text{Cu}_3\text{O}_{7-\delta}$  specimens described in this report were prepared from a single lot of commercial powder obtained from Rhone-Poulenc<sup>7</sup>. This particular powder lot was reasonably satisfactory in that it could be easily spun into highly sinterable fibers. The powder consisted of greater than 90 wt%  $\text{YBa}_2\text{Cu}_3\text{O}_{7-\delta}$ , containing 5-10 wt% barium cuprate and approximately 2 wt% CuO as determined by semi-quantitative X-ray diffraction analysis. The surface area was 1.8 m<sup>2</sup>/gm, with median particle size of 2.5 μm. The excess CuO was present as inclusions and intergranular phases in sintered specimens. It probably accounts for the excellent sinterability of this powder, functioning as a liquid-phase sintering aid. An attempt was made to obtain more Rhone-Poulenc powder for further experimentation, but the manufacturer was unable to fill the order.

---

<sup>7</sup> Superamic-Y123, Lot SU14146CI, Rhone-Poulenc, Inc., Monmouth Junction, NJ

Several other powders have been evaluated. Samples from Superconductive Components, Inc.<sup>8</sup> have to date been unsuitable. An early sample, containing only about 50%  $\text{YBa}_2\text{Cu}_3\text{O}_{7-\delta}$  phase, with the balance being residual reactants and intermediate phases, was not sinterable. A recent sample was essentially phase pure  $\text{YBa}_2\text{Cu}_3\text{O}_{7-\delta}$ , but was also too coarse to sinter. Two samples of powder from HiTc Superconco<sup>9</sup> contained only a few percent barium cuprate and a trace of barium carbonate, but again were too coarse to be sinterable. A sample of W.R. Grace powder<sup>10</sup>, nominally phase pure, was also not sinterable due to its very large particle size.

## 2.2 Fiber Preparation

### 2.2.1 Introduction

The primary activities during this Quarter concentrated on the production of experimental quantities of  $\text{YBa}_2\text{Cu}_3\text{O}_{7-\delta}$  green fibers using the dry spinning method, the examination of binder burnout and related processes, and the initial exploration of melt spinning as an alternative fiber spinning process. The melt spinning work was executed at AIResCo using their existing facilities with necessary modifications. Much of the material presented in this Section originated in periodic reports submitted to CPSS by the AIResCo co-authors of this Section, and has been incorporated into this report without specific attribution.

The capability to produce green fiber by both dry spinning and melt spinning has been developed. Trial fiber samples can be routinely generated using  $\text{YBa}_2\text{Cu}_3\text{O}_{7-\delta}$  dry spinning dopes. These dry spun fibers are spun

---

<sup>8</sup> Superconductive Components, Inc., Columbus, Ohio. The early lot was SS-ACS "first batch 87." The recent lot was SS-ACS-88 "March 1988"

<sup>9</sup> HiTc Superconco, Inc., Lambertville, NJ. Grade SC5-F6.5, lot 033188 and grade SC5-P, lot 031688

<sup>10</sup> Davidson Chemical Division, W. R. Grace, Chattanooga, TN, lot 14666-33-340

continuously, but are collected discontinuously in 30-100 cm lengths. The diameters of the dry spun fibers can be adjusted between 20-400  $\mu\text{m}$ . Recent melt spinning techniques have been used to produce continuous lengths up to 0.25 km, using barium titanate. Of particular significance is the ability to melt spin at solids loadings as high as 50 vol% (a requirement for subsequent processing).

### 2.2.2 Dry spinning developments

In the previous DARPA/ONR contract CPS developed a method to prepare  $\text{YBa}_2\text{Cu}_3\text{O}_{7-\delta}$  green fibers based on a dry spinning process. The formulations, "spin dopes," consisted of a suspension of  $\text{YBa}_2\text{Cu}_3\text{O}_{7-\delta}$  powder in an appropriately viscoelastic polymer solution. Successful dopes could be dry spun to produce flexible 20-200  $\mu\text{m}$  green fibers. These formulations allowed solids loadings of up to 55 vol% ceramic in the green fiber.

The dry spinning dopes were formulated with acrylic resins capable of clean burnout at temperatures as low as 500°C. Two successful polymers employed included a  $10^6$  molecular weight acrylic (for high fiber strength), and a lower molecular weight acrylic with hydroxyl functionality cross-linked with a melamine-formaldehyde agent. The extent of the cross-linking reaction dominated the rheology and "spinnability" of the dope. The dope formulations also included a plasticizer, a toluene/methylethylketone/xylene solvent mixture, and sorbitan trioleate (a dispersant for the ceramic powder). These materials were typically mixed with 75-80 wt%  $\text{YBa}_2\text{Cu}_3\text{O}_{7-\delta}$  powder and agitated until the cross-linking reaction rendered the material "spinnable." The development of the dry spinning dope formulations and process is documented in detail elsewhere<sup>11</sup>.

---

<sup>11</sup> "Composite Ceramic Superconducting Filaments for Superconducting Cable," ONR Contract N00014-87-C-0789, Final Report, 12 July 1988 .

Experimental quantities of dry spun fibers were produced in a simple laboratory scale apparatus. The spinning process is essentially continuous, although the collection of the spun fiber is in 30-100 cm lengths. The laboratory scale dry spinning apparatus includes a dope delivery system (in most cases, a simple syringe-type glue dispenser), a spinnerette, a drying column, and a take-up reel. After compounding, the dope is loaded into a 30 ml syringe fitted with an air piston. The air piston forces dope (at a uniform rate) through the dispenser tip-spinnerette. The extruded dope emerges into the upper part of the drying column and experiences significant elongation under the force of its weight until the fiber is dry. The resulting fiber diameter depends upon dope rheology, spinnerette size, and the solvent evaporation rate determined by drying air temperature and velocity. The more recent dry spinning work uses a two stage drying column where the upper stage has a faster air flow at a relatively low temperature (to prevent solvent vapor accumulation in the early stage of drying) and the lower stage has a slower flow of higher temperature air (to drive off the remaining solvent).

Despite these achievements, the dry spinning processing method has several drawbacks. For example, a commercial scale operation would need a solvent recovery system to collect the organic solvents driven off during fiber drying. The current formulation relies on a crosslinking mechanism to modify the rheology of the ceramic-polymer spinning solution, introducing additional sensitive variables of mixing time and aging effects. Also, during drying the fibers have such a low tensile strength that spin line breakage occurs easily, making it difficult to dry spin monofilaments continuously. This problem could be overcome by spinning multifilamentary tows, but that may introduce subsequent problems in the sintering and cladding operations.

### 2.2.3 Melt spun fiber fabrication

A melt spinning process avoids many of the problems associated with dry spinning. In melt spinning, a thermoplastic polymer is melted, extruded through a spinnerette, and drawn in a cooling column. Tractability is obtained through the viscosity-temperature relation of a thermoplastic melt, rather than the more complex viscosity-solvent content relation of a polymer solution. Melt spinning is common in textile fiber applications, while dry spinning is used only for polymers that cannot be melt processed. Originally this technique was not considered since it requires unique equipment not available at CPS. The capabilities of AIResCo are being used in the current program to evaluate the melt spinning processes. During the first Quarter, a program was undertaken to explore the possibility of developing a melt spinning process capable of handling  $\text{YBa}_2\text{Cu}_3\text{O}_{7-x}$  solids loadings of up to 50 vol%, that could be successfully burnt out, and would produce high quality sintered filaments. The tasks involve examining candidate linear polymers and developing processing methods using existing melt spinning equipment.

Three critical criteria were defined for green fiber fabrication:

1) complete burnout of the polymer system below  $500^\circ\text{C}$ , 2) non-reactivity of the polymer with the ceramic powder, and 3) shape retention of the ceramic fiber upon binder burnout. To meet the first two criteria, the candidate polymer systems could not contain any elemental nitrogen or chlorine and had to burn without charring. To meet the shape retention criterion, polymers with different burnoff temperatures, crosslinkable polymers, and formulations with different ceramic loadings needed to be evaluated.

Thermoplastic polymers chosen for the initial study are listed in Table 2.2.1. All of these polymers were believed to offer complete burnability. However, polyethylene can be crosslinked and polyether-ether ketone (PEEK) has a considerably higher melting point; properties believed to

offer advantages in fiber shape retention. A thermoplastic grade of polymethylmethacrylate was included for comparison with the dry spun process.

Thermal Gravimetric Analysis (TGA) of candidate polymers was performed both in nitrogen and air. The results are presented in Figures 2.2.1 and 2.2.2. This data was collected to create a baseline for comparison with solids filled polymer samples. The burnout temperature for a particular polymer is almost always greater in nitrogen (due to the absence of oxygen). Polyethylene and polypropylene are susceptible to oxidative degradation at tertiary hydrogen sites in the polymer chain. Polypropylene has more tertiary hydrogen sites than polyethylene, and is therefore more susceptible to this type of degradation. In oxidative degradation, free radicals are generated that react with oxygen and eventually lead to polymer chain degradation. All the candidate polymers, except the PEEK systems, had satisfactory burnout characteristics.

Initial work at AIResCo focused on determining the extrudability of various ceramic/polymer compositions utilizing three solids loading levels: 10, 30, and 50 vol%. A CSI mixing extruder<sup>12</sup> was employed for these experiments (data are summarized in Table 2.2.2). Fiber samples from successful runs were delivered to CPSS for binder burnout studies. The most uniform fibers (and easily processable compositions) were achieved using polypropylene carbonate. However, upon spooling, these fibers were slightly tacky, and therefore adhered to one another. Attempts at making 50 vol% ceramic loaded compositions were unsuccessful using these simple polymer systems and the CSI mixing extruder, although the extrudability of the 30 vol% filled systems suggested that higher loadings might be attainable using a conventional screw extruder. This type of extruder requires larger batch sizes, and therefore, greater amounts of powder

---

<sup>12</sup> Custom Scientific Instruments, Inc., 13 Wing Drive, Cedar Knolls, New Jersey 07927

TABLE 2.2.1  
CANDIDATE POLYMERS FOR MELT SPINNING

<u>POLYMER</u>	<u>MELTING POINT (°C)</u>	<u>DENSITY (g/cc)</u>	<u>TENSILE STRENGTH (lb/in<sup>2</sup>)</u>	<u>% ELONGATION AT BREAK</u>
Polyoxy-methylene	85	1.41	$8.80 \times 10^3$	50
High Density Polyethylene (HDPE)	131	0.948	$6.50 \times 10^3$	530
Polypropylene (PP)	165	0.903	$5.00 \times 10^3$	11
Ethylene Vinyl Acetate (EVA)	204	0.94	$2.90 \times 10^3$	750
Polymethyl-methacrylate (PMMA)	71	1.18	$10.2 \times 10^3$	4
Polypropylene-carbonate (PPC)	40	1.26	$5.00 \times 10^3$	9-160
Polyether-ether ketone (PEEK)	243	1.32	$13.3 \times 10^3$	4

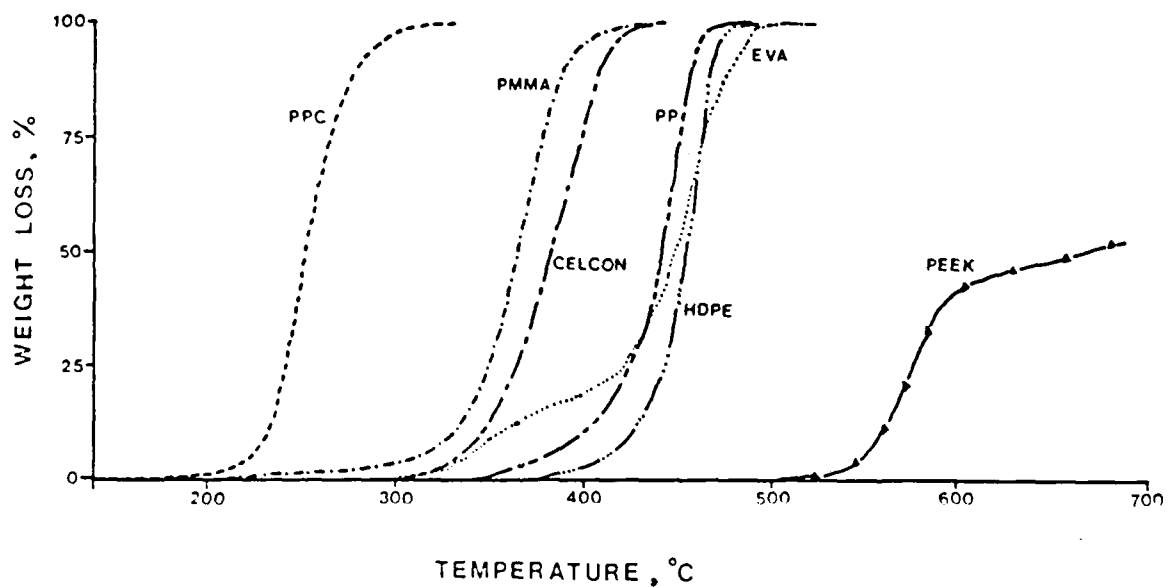


Figure 2.2.1 TGA of Candidate Polymers in Nitrogen.

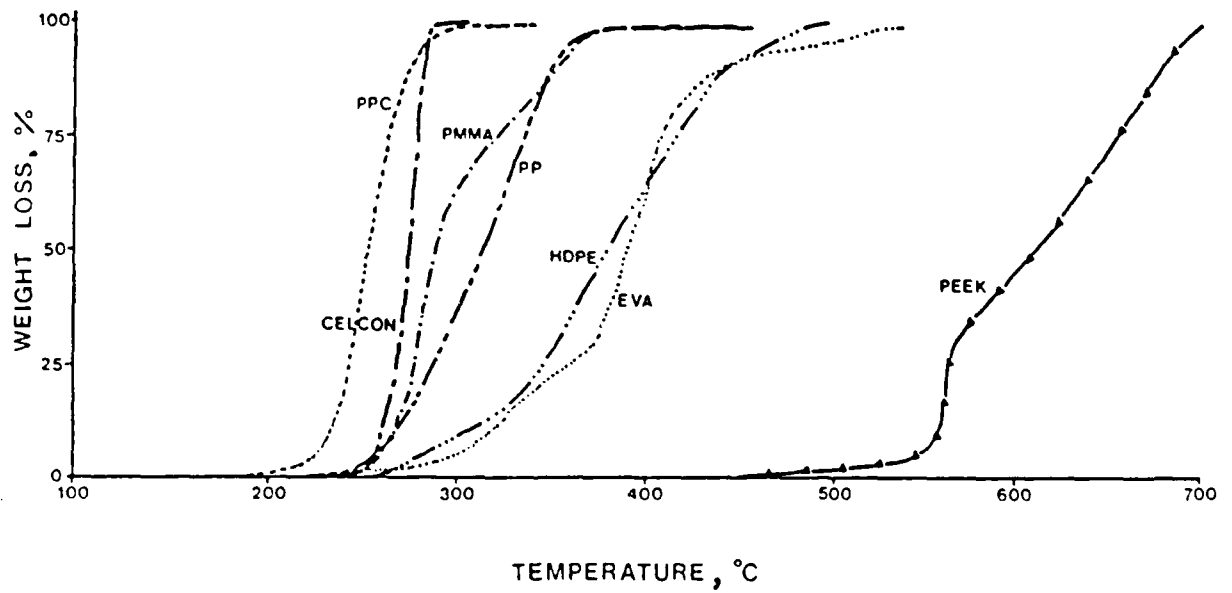


Figure 2.2.2 TGA of Candidate Polymers in Air.

TABLE 2.2.2

## CSI MIXER-EXTRUDER MATRIX OF EXPERIMENTS

<u>POLYMER</u>	<u>YBa<sub>2</sub>Cu<sub>3</sub>O<sub>7-δ</sub> VOL %</u>	<u>RESULT</u>
HDPE	10	Spun sample 3498-4-1
HDPE	30	Spun sample 3498-5-4
HDPE	50	Not extrudable on CSI.
PP	10	Spun sample 3498-9-3
PP	30	Spun sample 3498-11-1
Celcon	10	Spun sample 3498-12-3
Celcon	30	Spun sample 3498-21-1
PMMA	30	Not extrudable on CSI.
PPC	10	Spun sample 3498-23-1
PPC	30	Spun sample 3498-24-1
PPC	50	Not extrudable on CSI.

than was available at the time. Consequently, barium titanate<sup>13</sup> was used as a surrogate powder for higher solids loading experiments.

Subsequent efforts at AIResCo focused on fabricating a 50 vol% BaTiO<sub>3</sub> fiber using conventional melt extrusion. Polymers that were extrudable at the levels of 10 and 30 vol% YBa<sub>2</sub>Cu<sub>3</sub>O<sub>7-δ</sub> in the CSI trials were chosen for scale-up to conventional extrusion equipment. Preparation of samples involved the added step of vacuum drying the blend at room temperature to remove any volatiles. The extruder was fitted with a special mixing head screw that offers greater shearing and better mixing than conventional screws. Samples of 50 vol% BaTiO<sub>3</sub> prepared with HDPE or PPC showed loss of flow during extrusion. Changing the process conditions did not result in steady flow of

<sup>13</sup> TICON-HPB, a barium titanate powder with specific surface area 2.9 m<sup>2</sup>/gm, median particle size 1.2 μm. TAM Ceramics, Inc., Niagara Falls, NY

the extrudate. Upon disassembly of the system, it was noted that caking on the screw had caused the loss of flow.

After these two unsuccessful spin attempts with simple powder-polymer systems, a third component was introduced into the blend, acting as a processing aid (lubricant). Prior experience with filled polymer systems containing waxes, at both AIResCo and CPSS, suggested wax as a viable processing aid. To obtain maximum benefit from the lubricant, blends were prepared by melt compounding the ceramic, wax, and polymer prior to extrusion in a sigma blade mixer with jacketed oil heating capability.

The first tri-component blend consisted of 50.1 vol% BaTiO<sub>3</sub> in polypropylene and paraffin wax. Samples were made by two different procedures to determine if the method of component introduction would influence the compounding properties. The first method involved heating the ceramic to the desired temperature, adding wax, and then gradually adding polypropylene while mixing. The second method consisted of melting the wax, then gradually mixing in the ceramic. Upon completion, both samples had a similar paste-like appearance.

The two BaTiO<sub>3</sub>/PP/wax blends were extruded using a one inch diameter barrel extruder to fabricate fiber using a 25 mil die. The fibers produced from these blends were extremely brittle and discontinuous due to unsteady flow of extrudate through the die. Throughout these spin trials, it was noted that melt pressure at the die block steadily increased. Both samples were processed similarly, suggesting that the method of component introduction into the batch mixer does not affect fiber processing.

To obtain flexible fiber and steadier melt pressures, a blend with a 2:1 weight ratio of wax to polypropylene was prepared. Extrusion of this blend resulted in a brittle sample that could not be drawn. During this run melt pressure was considerably lower than with the previous samples and it

appeared to remain steady, suggesting the need for higher wax loading to improve processability.

Due to the brittleness of fiber produced from the wax blends, a lower MW lubricant was substituted for wax as the third component. Additionally, the die assembly of the extruder was modified to streamline the flow of material. Figure 2.2.3 illustrates the modified assembly designed to minimize shear gradients that cause flow separation. Extrusion of the new blend sample resulted in a continuous fiber which was flexible while hot, but brittle upon cooling. During processing, the new blend showed no evidence of flow channel plugging in the extruder as seen with the wax and two component blends.

Since the flexibility requirement appeared to be solved with the switch of lubricants, the next step involved evaluation of different polymers to determine their effect on processing and drawability. Table 2.2.3 summarizes the tri-component blend results. Blends made with polypropylene were too stiff for this particular application. For future experiments, a more suitable grade of polypropylene will be selected from the wide variety of polymer materials available.

The two most successful samples (see Table 2.2.3) were 3498-54-1, made with ethylene vinyl acetate copolymer (EVA) and 3498-61-1, made with high density polyethylene (HDPE). Both are adequately strong and can be easily handled, although the EVA fiber is much more elastomeric. Both fiber samples were drawn subsequent to extrusion, however, because of the nature of the polymer, the HDPE fibers show a greater degree of alignment in the extrusion direction, resulting in an oriented fiber.

Crystallinity in polymers is influenced by stress, both during crystallization and afterwards. This is the basis of the drawing process by which the mechanical properties of fibers are enhanced. By stretching the fibers, more of the molecular segments are induced to align in the direction

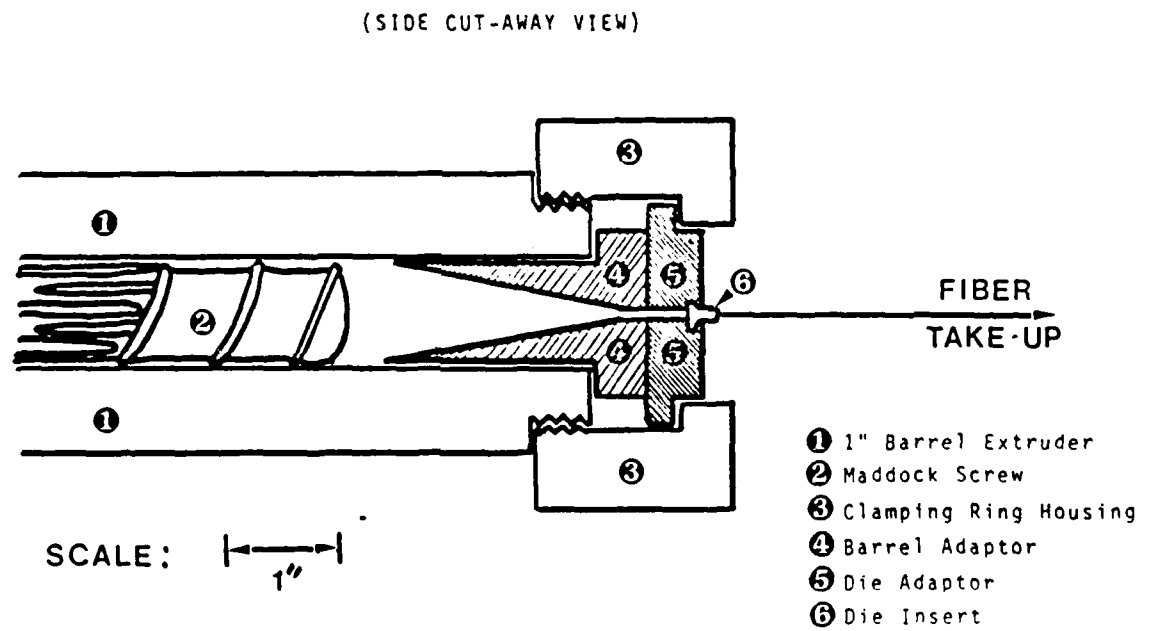


Figure 2.2.3 Modified Die Assembly.

TABLE 2.2.3

## SUMMARY OF TRI-COMPONENT BLEND EXPERIMENTS

<u>POLYMER</u>	<u>SAMPLE #</u>	<u>VOLUME % BaTiO<sub>3</sub></u>	<u>COMMENTS</u>
PP	3498-36-1	50	3:1 PP/wax. Spun into brittle fiber.
PP	3498-42-1	50	1:2 PP/wax. Spun into brittle fiber.
PP	3498-43-1	50	3:1 PP/lub Spun into brittle fiber.
PP	3498-48-1	25	1:2 PP/lub Spun into flexible fiber which could not be drawn.
PP	3498-49-1	40	2:1 PP/lub Spun drawable fibers that were more flexible than 43-1 but less flexible than 48-1.
EVA	3498-50-1	34	1:1 EVA/ lub Spun fibers that were extremely flexible, drawable and windable. These fibers had a lot of stretch.
EVA	3498-54-1	50	2:1 EVA/ lub Spun fibers that were very flexible, drawable, windable and stretchable. When wound on a spool the fiber did not stick to itself like PPC fibers.
PMMA	-----	34	1:1 PMMA/lub. Sample was not extrudable.
Celcon	-----	--	Blend could not be compounded on the sigma blade mixer.
HDPE	3498-59-1	34	1:1 HDPE/lub Spun fibers that drew unevenly. Fiber surface was rough due to trapped water not removed in vacuum drying.
HDPE	3498-60-1	34	1:1 HDPE/lub Spun flexible fiber that could be drawn. Fiber surface had non-uniformities upon visual inspection.
HDPE	3498-61-1	46	2:1 HDPE/lub. Spun fibers that were very flexible and drawable. Fiber surface was very uniform.

TABLE 2.2.4

## MECHANICAL TEST DATA ON VARIOUS FIBERS

SAMPLE #	POLYMER	VOLUME % POLYMER/OIL/BaTiO <sub>3</sub>		DENIER	AVG. DIAMETER (MICRONS)	TENSILE STRENGTH AT BREAK <sup>2</sup> 10 <sup>3</sup> x(lb/in <sup>2</sup> )	TENSILE MODULUS 10 <sup>4</sup> x(lb/in <sup>2</sup> )	% ELONGATION AT BREAK
3498-59-1	HDPE	30	/36/ 34	5750	584	0.540	3.6	10
3498-60-1	HDPE	30	/36/ 34	320	140	2.4	3.1	380
3498-61-1	HDPE	40	/14/ 46	200	112	3.2	12.0	27
3498-50-1	EVA	32	/34/ 34	720	203	0.820	0.7	410
3498-54-1	EVA	32	/17/ 51	2820	356	1.10	4.3	9.8
----	NYLON	-----		--	--	9.0	25 - 30	100
----	GRAPHITE	-----		--	--	5500	3000	0.6
----	NEXTEL 440 (Alumina Fiber)	-----		--	--	200 - 300	3000	<1.0

of the applied stress. Table 2.2.4 summarizes mechanical test data on both HDPE and EVA fiber samples. Also included for comparison is data on nylon, graphite and Nextel 440 ceramic fibers. Considering this limited database, HDPE fiber samples appear to become more oriented as they are drawn to thinner fiber diameters than the EVA samples, which do not seem to show the same effect.

Micrographs of the green fibers are presented in Figures 2.2.4A and 2.2.4B. The microstructure of an EVA fiber (Figure 2.2.4A) looks similar to that of dry spun fibers, with the ceramic particles embedded in a featureless polymer matrix. There is no visual evidence that the fiber had been drawn to 410% elongation. The HDPE fiber microstructure (Figure 2.2.4B) has obvious signs of drawing. This fiber consists of taffy-like polymer strings connecting the ceramic particles. After binder burnout, the solids packing reflects the green microstructure. The EVA specimen has more uniform particle packing, while the HDPE specimen shows gaps between particles that are remnants of the stringy green structure. In spite of these differences, the EVA and HDPE barium titanate filaments are visually identical after sintering. This microstructure is exemplified in Figure 2.2.5, showing the as-fired surface of a barium titanate fiber made from EVA, after two zone passes at a peak temperature of 1375°C. Both fiber systems appear readily sinterable into high density ceramic filaments. The same behavior is anticipated for  $\text{YBa}_2\text{Cu}_3\text{O}_{7-\delta}$  fibers.

Binder burnout studies are in progress to determine the effect of thermal binder removal on the phase purity of  $\text{YBa}_2\text{Cu}_3\text{O}_{7-\delta}$ . Preliminary experiments had indicated that slow binder burnout treatments, especially in oxygen lean environments, could create secondary phases in the  $\text{YBa}_2\text{Cu}_3\text{O}_{7-\delta}$ , apparently by reduction of the copper or carbonation of the barium. It is not known if these reactions also occur during the rapid binder burnout conditions

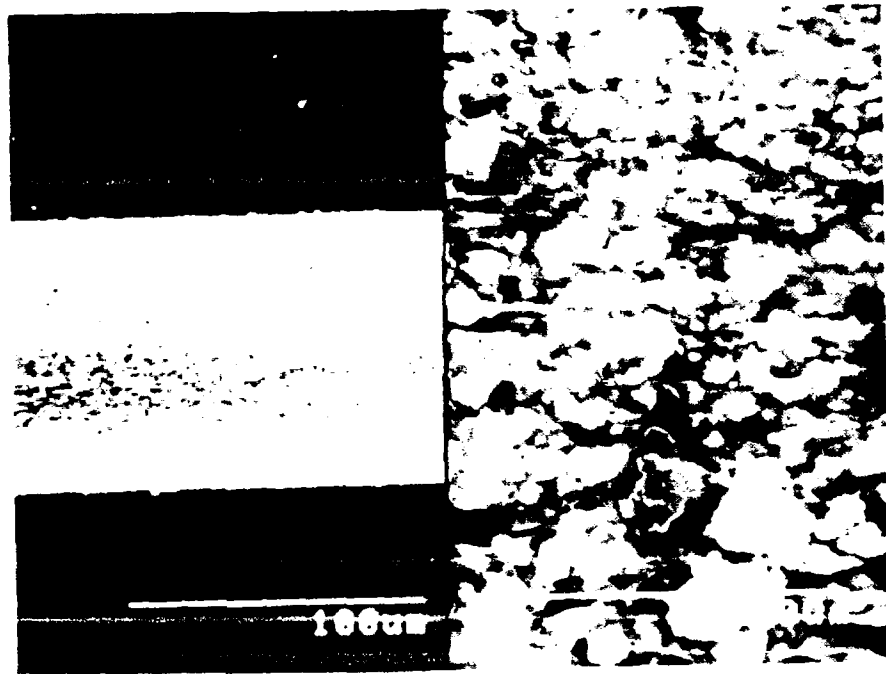


Figure 2.2.4A Micrograph of 3498-54-1, 50 vol% BaTiO<sub>3</sub> in EVA.

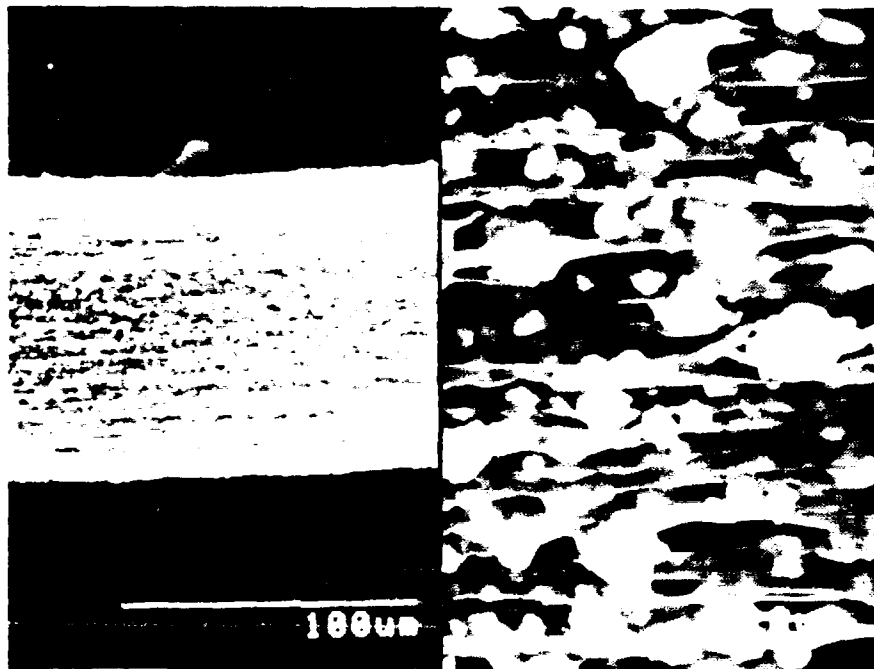


Figure 2.2.4B      Micrograph of 3498-61-1, 50 vol% BaTiO<sub>3</sub> in HDPE.

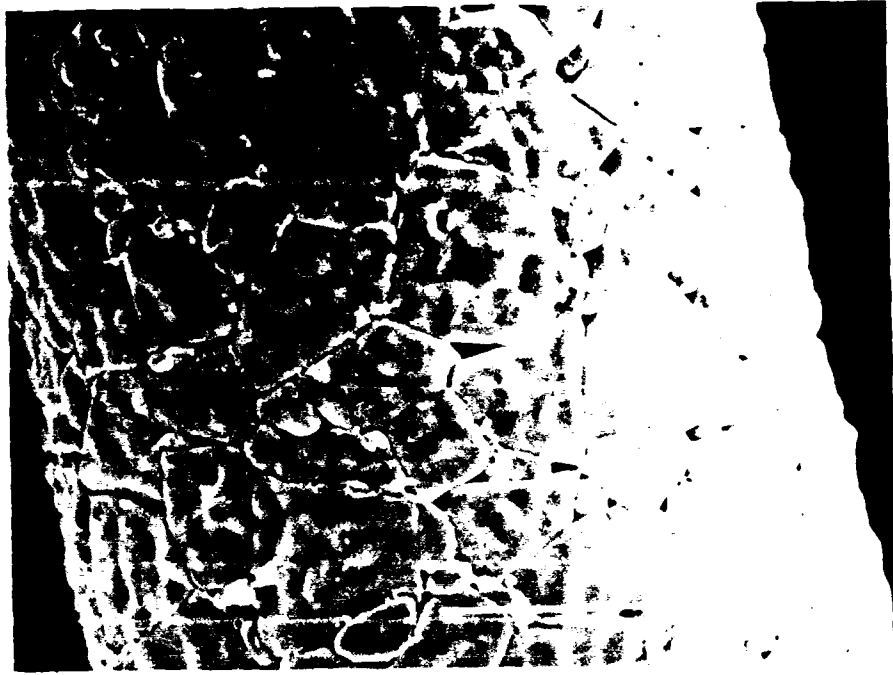


Figure 2.2.5 Sintered Barium Titanate Filament.

of zone sintering, or if they have deleterious effects on the behavior of the sintered filaments.

A choice between the use of the initial dry spinning method or the new melt spinning process will be made during the coming Quarter. Melt spinning looks very promising, but to date there has been no experience with this process in making highly loaded  $\text{YBa}_2\text{Cu}_3\text{O}_{7-\delta}$  fiber. Future work will focus on melt spin fabrication of 50 vol%  $\text{YBa}_2\text{Cu}_3\text{O}_{7-\delta}$  fibers. If the melt spun filaments are equivalent (or superior) to the dry spun product, it is anticipated that all green fiber activities will shift to melt spinning.

### 2.3 Heat Treatment of Fibers

#### 2.3.1 Introduction

Practical manufacture of  $\text{YBa}_2\text{Cu}_3\text{O}_{7-\delta}$  wire by a fiber process requires continuous sintering, annealing, and cladding. The process must ultimately be capable of producing many kilometers of wire per day, implying a residence time in the sintering furnace of no more than a few minutes. This requires very rapid sintering. Most  $\text{YBa}_2\text{Cu}_3\text{O}_{7-\delta}$  fiber sintering work to this point has been performed under conditions that yield high density after approximately five minutes of residence time at temperature. This restriction on residence time leads to a need for excellent sinterability in the  $\text{YBa}_2\text{Cu}_3\text{O}_{7-\delta}$  powder.

A side benefit of rapid sintering is that it relaxes constraints on setter materials. Rapidly sintered fibers seem to have no time to react with these materials. Fibers routinely supported on alumina substrates or alumina fiber mats show no evidence of reaction. Preliminary experiments have shown compatibility during zone sintering between  $\text{YBa}_2\text{Cu}_3\text{O}_{7-\delta}$  fibers and yttria-stabilized zirconia, chromel and alumel alloys, and Nextel alumina-silica-boria woven fabric. Note that the superconductor will react strongly with these materials during prolonged exposure to sintering temperature.

The purpose of the present heat treatment activity is to examine the microstructure and critical current of filaments sintered under conditions simulating a continuous multi-zone sintering furnace. Sintering heat treatments are currently conducted by moving the  $\text{YBa}_2\text{Cu}_3\text{O}_{7-\delta}$  filaments in and out of the hot zone of a tube furnace, so that they are repeatedly heated and cooled at a rate of approximately  $300^\circ\text{C}/\text{min}$ . This process is termed "multiple zone sintering." It was originally explored as a method to induce texture by directional recrystallization, initially without success, but is now being pursued because preliminary work suggested improvements in critical current associated with repeated zone passes.

The experimental design for sintering and annealing is essentially a feedback loop, where a heat treatment/powder characteristic condition is chosen, a number of short filament specimens are prepared, and the transport  $J_c$  is determined. The intent is to enhance  $J_c$  empirically, with interesting samples extensively characterized so that the critical current density can be related to microstructure. At present characterization is accomplished primarily by examination of fracture surfaces and polished sections by SEM, and by optical metallography. Other techniques are accomplished with outside collaboration. Professor Lagerlof of Case Western Reserve University is currently examining sintered filaments by various transmission electron microscopy (TEM) methods. Scanning Auger Microscopy (SAM) experiments are planned in collaboration with Dr. D. Kroeger at Oak Ridge National Laboratory.

### 2.3.2 Sintering of $\text{YBa}_2\text{Cu}_3\text{O}_{7-\delta}$ Fibers

Experiments performed under the previous contract<sup>14</sup> and the first two Quarters of this contract are aimed at simulating the manufacturing heat treatment process of continuous lengths of fiber rapidly passing through a

---

<sup>14</sup> "Composite Ceramic Superconducting Filaments for Superconducting Cable," ONR Contract N00014-87-C-0789, Final Report 12 July 1988

multi-zone furnace. To achieve this, short lengths (approximately 6 inches long) of green fiber and a simple existing laboratory furnace are being employed. The fibers are placed on an alumina substrate setter that is passed through the horizontal tube furnace at a controlled speed. The alumina substrate rests upon a low thermal mass sled made of rigid alumina fiberboard attached to a slender alumina push rod. The rod is attached to a motorized positioning-track apparatus that moves the sled in and out of the hot zone at controlled rates of between 4 and 150 cm/min. The hot zone of the peak temperature is 4 cm wide and fairly uniform between approximately linear  $7^{\circ}\text{C}/\text{cm}$  thermal gradients.

As the fibers are passed through the furnace, they are heated to the peak temperature in 4 to 8 min, remain at peak temperature for 1 to 2 min, and then cool at the same rate they were heated. An example of a typical heating profile is shown in Figure 2.3.1. The minimum temperature between successive passes is always below  $800^{\circ}\text{C}$ , but varies depending on when the drive mechanism is reversed. After sintering, samples are annealed in a separate furnace.

Variables that are being examined include various physical powder characteristics, including powder chemical and phase purity, green fiber formulation and physical characteristics, atmosphere control, time in the hot zone, heating and cooling rates, number of passes, and peak sintering temperature, as well as the annealing conditions including time, peak and minimum temperatures, atmosphere, and heating and cooling rates.

Sintering experiments have concentrated on several areas, including: constant time in the hot zone with varying number of passes, peak temperatures and sample velocities through the furnace; preheating schedules and atmospheres; varying number of passes at different peak temperatures keeping the velocity constant; and, varying the peak temperature with constant velocities and number of passes. Also, various annealing times and

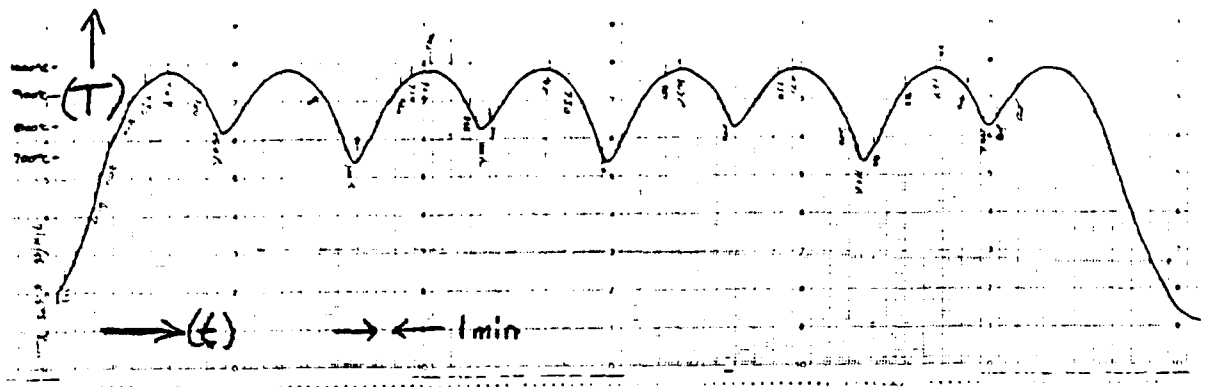


Figure 2.3.1 Typical Temperature-Time Profile for Zone Sintering.

temperatures were studied. Results were assessed by evaluation of the sintered microstructure and transport critical current density in self field. Most results are for 100-400  $\mu\text{m}$  diameter fibers dry spun using Rhone-Poulenc powder. These experimental fibers are larger than the 25-50  $\mu\text{m}$  filaments preferred for the composite wire, but are easier to handle for metallographic analysis and bare filament electrical measurements.

Smaller diameter green fibers can be directly passed into the hot furnace in air, with binder burnout occurring during the rapid heating (about 300°C/min). However, green fibers larger than about 200  $\mu\text{m}$  diameter tend to combust if heated this rapidly in air. This can be avoided if the green fibers are preheated above the binder decomposition temperature in an oxygen-lean atmosphere. All of the fibers used in the sintering experiments reported in this period were subjected to an initial preheat for binder burnout in a nitrogen rich atmosphere, by heating to 500°C at a rate of 5-10°C/min, and then cooling for storage at room temperature until the zone sintering experiments.

#### Correction of previous work

During this first Quarter a problem was discovered with the previous technique used for measuring transport critical current. This problem, its origin, and an improved measuring technique are discussed in Section 2.5. Fortunately, most of the filament specimens could be re-measured, to restore the integrity of the database. Table 2.3.1 presents the corrected critical current values obtained with a new DC measurement technique for the zone sintering conditions and specimens discussed in the previous report<sup>15</sup>. The absolute values are more than an factor of ten lower than the previous erroneous numbers, but still show the trends reported

---

<sup>15</sup> "Composite Ceramic Superconducting Filaments for Superconducting Cable," ONR Contract N00014-87-C-0789, Final Report 12 July 1988

TABLE 2.3.1

TRANSPORT CRITICAL CURRENT DENSITIES AT 77 K  
Corrected Results of Previously Reported Fibers

SPECIMEN NUMBER	TEMP (°C)	PASSES	SPEED (cm/min)	CRITICAL CURRENT (A/cm <sup>2</sup> )
24994C2	940	4	5.6	150 ± 5
24994D2	928	4	5.6	25 ± 5
24994B1	957	8	11	120 ± 10
24996A1	957	4	5.6	28 ± 5
24996A2	957	4	5.6	24 ± 5
24994E1	980	4	5.4	2 ± 1
24994E2	980	4	5.4	2 ± 1
24994F1	1208			15 ± 1
24994F2	1208			6 ± 1
24996F1	925	8	11	3 ± 1
28732B1	938	8	11	140 ± 10
28732D1	975	8	11	78 ± 5
28732D2	975	8	11	67 ± 5
28758B	960	4	5.4	58 ± 5
28757E1	940	6	5.8	32 ± 5
28737B	944	10	13.6	13 ± 1
24996C1	990	4	5.4	57 ± 10
24996C2	990	4	5.4	78 ± 10
28732E	988	8	11	12 ± 5
28737A1	960	10	13.6	2 ± 1
28737A2	960	10	13.6	0
28757G2	940	4	11.4	26 ± 10
28758A	940	8	11.2	30 ± 10
28764C	960	8	14.6	58 ± 10

NRT - no resistive transition observed

previously, where critical current varies systematically with number of zone sintering passes.

In previous work, some of the best results were found for samples heated to 966°C with eight passes through the hot zone at a rate of approximately 5.5 cm/min. This set of conditions was the basis for further tests in this Quarter, with an experimental sintering matrix built around these conditions. Several minor changes were made in the heat treatment procedures including the introduction of a new sled-drive mechanism to allow more consistent control of sled speed. Additionally, a longer sled was made to prepare longer sintered filaments, and a more controlled method for nitrogen atmosphere preheating was adopted, that appeared to effect filament properties and sintering behavior.

The most important change in the heat treatment procedure may have been the method that the temperature was measured. The prior work (included in Table 2.3.1) controlled temperature via a set point outside of the furnace tube, and reported a peak hot zone temperature inside the tube using a thermocouple suspended near the center of the tube. This monitoring thermocouple was withdrawn before the sled was moved into the hot zone. Consequently, small changes in the position of the thermocouple bead either due to the angle of the alumina sheath or to the position of the bead could result in a difference of measured temperature of 10°C or greater. Currently the thermocouple rests on top of the substrate directly next to the fibers on the sled. A fine diameter type K thermocouple of a small thermal mass is now used in order to more closely match the changing temperature response time of the very thin fibers. This seemingly trivial change in fact required

substantial work in order to be able to correlate the new results with the old data.<sup>16</sup>

Most of the differences in temperature measuring technique are related to the dynamic thermal environment of the zone sintering experiments. During these experiments the small black  $\text{YBa}_2\text{Cu}_3\text{O}_{7-\delta}$  fibers, the white alumina substrate, and the fine diameter thermocouple are all being introduced simultaneously into a cylindrical radiating cavity. It is likely that the radiant heat transfer is different for the  $\text{YBa}_2\text{Cu}_3\text{O}_{7-\delta}$  fibers, the substrate, and the thermocouple, since each has a quite different emissivity and view factor. The response time for the thermocouple to reach an equilibrium temperature in the sintering temperature range is several seconds; the finer diameter fibers probably respond to temperature changes in less time. In practice the temperature as measured by the thermocouple apparently never reaches the actual equilibrium temperature that the top of the sled is exposed to because of the relatively high speed of the moving sled through the hot zone. The fibers themselves may not have time to heat to the equilibrium temperature, though they get within a few degrees of it, and exposure to furnace heat appears to be consistent from experiment to experiment. In any event, all temperatures reported in the rest of this report reflect these changes of technique.

An issue of green fiber storage has begun to be examined as there seems to be some time-dependent degradation of the green fibers. Previously, 20-50 cm lengths of green fibers were stored by being attached at their ends to an identifying card, and allowed to hang freely, exposed to ambient air. The fibers are prepared in batches that last several weeks, with fibers being gradually used for heat treatment experiments throughout that period. After

---

<sup>16</sup> The sintering behavior characteristic of a particular temperature measured by the old fixed thermocouple method is reproduced by at about 20°C higher reading on the new traveling thermocouple. Consequently, data in this report cannot be directly compared with the previous work.

evidence showed that the green storage procedure might affect the sintered fiber behavior, storage of green fiber is currently done in a dry-air desiccator. Older ambient-stored fiber data was combined with the spinning and sintering date information, to permit future correlation. It was found that "fresh" fiber stored in a desiccator yielded sintered filaments with much improved critical current densities. Much of the recent data on filaments for older, air-stored "stale" green fibers has been rejected.

With the new configurations and procedures in place, initial experiments were performed to reproduce microstructures and results of earlier work. Of particular interest were attempts to reproduce previous data, that showed intriguing correlations between critical current density and zone sintering treatments. Once confident that the heat treatment procedure was reproducing microstructures of the earlier work, effort was concentrated on the continuing study of heat treatment effects on microstructure and transport properties.

### 2.3.3 Oxygen intercalation studies

Previously most effort was focussed on examining high temperature sintering conditions. Oxygen intercalation was accomplished with a separate anneal, in which a batch of as-sintered filaments were loaded into a cold furnace, heated to 500-520°C, held overnight, then furnace-cooled. Of course the proposed manufacturing method requires continuous sintering, with oxygen intercalation occurring during a controlled anneal. For practical manufacturing, total residence time in the annealing section of the furnace must be less than an hour. Transformation kinetics data<sup>17</sup> for  $\text{YBa}_2\text{Cu}_3\text{O}_{7-\delta}$  show a "nose" in the time-temperature-transformation (TTT) curve, indicating that

---

<sup>17</sup> D. Shi, and D.W. Capone II, "Kinetic Processes of the Orthorhombic to Tetragonal Phase Transition," in High-Temperature Superconductors II, D.W. Capone II, et al., eds., Materials Research Society, Pittsburgh, PA, 1988, pp. 175-178

isothermal anneals as short a 15 min might be adequate to oxidize the material into the superconducting orthorhombic state. During this Quarter, a series of experiments have begun to determine empirically the minimum isothermal annealing time required for oxygen intercalation. These results will be used to guide future controlled-cooling transformation heat treatments.

In one particular experiment, several fibers were sintered simultaneously using conditions that had previously produced good results (eight passes through the furnace heated to 965°C at a sled speed of approximately 5.5 cm/min). Subsequently these sintered filaments were divided into five groups that were placed in a box furnace preheated to 525°C and filled with flowing oxygen. One set of samples was removed after 15 min, the next after 30 min, then 60, 120, and 240 min. All samples were superconducting, with modest but measurable transport critical currents. These specimens were prepared from "stale" green fiber, which may account for the low values of  $J_c$ . There were no apparent differences in their microstructures. The critical current densities are shown in Table 2.3.2.

TABLE 2.3.2

TRANSPORT CRITICAL CURRENT DENSITIES AT 77 K  
Effect of Oxygen Annealing Time

SPECIMEN NUMBER	TEMP (°C)	PASSES	SPEED (cm/min)	FILAMENT DIAMETER (μm)	CRITICAL CURRENT (A/cm <sup>2</sup> )	DWELL TIME O <sub>2</sub> ANNEAL (min)
00663A	965	8	5.5	405	50 ± 1	15
00663B	965	8	5.5	387	61 ± 1	30
00663C	965	8	5.5	335	63 ± 1	60
00663D	965	8	5.5	347	51 ± 1	120
00663E	965	8	5.5	372	32 ± 1	240

Note that even a 15 min oxygen anneal at 525°C suffices to restore a measurable transport current density. These data seem to display a slight trend suggestive of an optimum oxygen annealing time around 60 min. This

trend is consistent with work performed in other laboratories, but the annealing time of around one hour is less than that observed elsewhere. This is due to the small dimensions of the filaments (100-200  $\mu\text{m}$ ), which reduce diffusion distances. These data are too preliminary for a conclusion at this time, but they indicate that an oxygen anneal of between 15 min to 2 h soak time at 500°C is sufficient to achieve superconductivity in the CPSS filaments. This isothermal experiment will be repeated periodically, using filaments sintered to yield higher critical current densities. At the point where the sintering treatment has been optimized, oxygen intercalation experiments under continuous cooling conditions will be initiated.

An annealing experiment, similar to that just described, was performed using an air atmosphere instead of oxygen. The results were not conclusive, but indicated that samples annealed in air for times of less than 60 min at 525°C had no resistive transition and exhibited no evidence of a Meissner effect (as indicated by the "float test"). Filaments annealed in air at 525°C for 120-240 min did display a Meissner effect, and often had a measurable transport critical current density ranging up to 140 A/cm<sup>2</sup>. The filaments made under the previous contract, which possessed the transport  $J_c$  data shown in Table 2.3.1, were annealed in air for 15 h. The present results indicate that an oxygen anneal can dramatically reduce the overall processing time.

#### 2.3.4 Sintering conditions, microstructure, and $J_c$

A set of experiments was undertaken to investigate the effects of the number of passes through the hot zone, total time in the hot zone, and the sintering temperature on microstructure and transport critical current densities. With all other conditions held constant, the number of passes was varied from 2 to 10, which changed the total time in the hot zone from 7 to

35 min.<sup>18</sup> These conditions produced samples with grain size increasing with number of passes through the hot zone. The grain growth appears to be a result of secondary recrystallization, which proceeds gradually with repeated zone passes. Filaments exposed to a few passes have occasional large secondary grains isolated in a finer grain matrix. With repeated passes, and increased time at temperature, the secondary recrystallization becomes more extensive. This can be illustrated in optical micrographs of filaments sintered at 966°C where the large secondary grains are clearly visible in sharp contrast in an over-etched fine grained matrix. Figure 2.3.2A is a filament after 4 passes (or 14 min), showing secondary grains in a matrix of residual fine grains. After the 35 min exposure corresponding to 10 passes, the microstructure consists entirely of secondary grains (Figure 2.3.2B).

Previous results had suggested that the multiple zone sintering method promoted grain growth as compared with isothermal holds for the same time at temperature. More recent observations do not support this. Figures 2.3.3A and B compare the microstructures of filaments that experienced 28 min at 966°C either as one isothermal hold (Figure 2.3.3A) or as eight standard zone passes (Figure 2.3.3B). In this case the microstructures are similar. This issue is currently being addressed in more detail.

Another series of samples (listed in Table 2.3.3) examines the effect of number of passes (and thus the total time) through the hot zone at a slightly higher temperature, 970°C. Figures 2.3.4A, B, and C show the optical micrographs for filaments after 2, 6, and 10 zone passes, respectively. The average grain size increased with number of passes, as expected. The critical

---

<sup>18</sup> For these non-isothermal zone sintering experiments, time at temperature is defined as time above the 890°C liquidus temperature in these copper oxide-rich materials. Time at temperature depends upon sled speed. At the standard 5.5 cm/min sled speed, each pass corresponds to 3.5 minutes "at temperature". Note that this definition differs slightly from what was used in previous reports<sup>1</sup>, which defined time at temperature above 900°C, so that each standard pass took 2.6 minutes.

current densities decrease with the number of passes and total time in the hot zone, as displayed in Figure 2.3.5. This might indicate a direct effect of zone sintering time or grain size on  $J_c$ , or may reflect the completeness of the oxygen anneal. Perhaps the higher  $J_c$  of the specimen that received two zone passes is related to oxygen diffusion enhanced by higher porosity or finer grain size. The possibility of adjusting the oxygen anneal times with sintered density and grain size will be investigated in more depth in the next project Quarter.

The results reported to this point have been experiments conducted with green fibers that had been stored in air. Newly spun fibers stored in a dry-air desiccator were found to produce sintered fibers with typical critical current densities in the range of hundreds of A/cm<sup>2</sup>. After examining the database, it was noted that green fibers that were exposed to laboratory (ambient) atmosphere for extended periods of time typically produced sintered filaments with  $J_c$  in the range of tens of A/cm<sup>2</sup>. Most of the results of these "stale" fibers have been rejected, and all subsequent work was, and will be, with "fresh" green fiber that has been stored in a desiccator following the spinning process.

One of the CPSS cladding processes (see Section 4) requires cofiring of  $\text{YBa}_2\text{Cu}_3\text{O}_{7-\delta}$  fibers coated with a silver alloy dope. Cofiring temperatures must be kept below eutectic points, so a series of fibers were sintered at reduced temperature to establish the microstructures and  $J_c$ 's of bare filaments produced at cladding temperatures. The first experiments examined filaments sintered at 950°C for between two and ten standard passes. As expected, sintering was slower at this lower temperature, requiring up to eight passes to achieve high density. The fracture surfaces of filaments



Figure 2.3.2A Polished and Etched Microstructure of a  $\text{YBa}_2\text{Cu}_3\text{O}_{7.5}$  Filament Zone Sintered at  $966^\circ\text{C}$  for Four Passes, with 14 Minutes at Temperature.

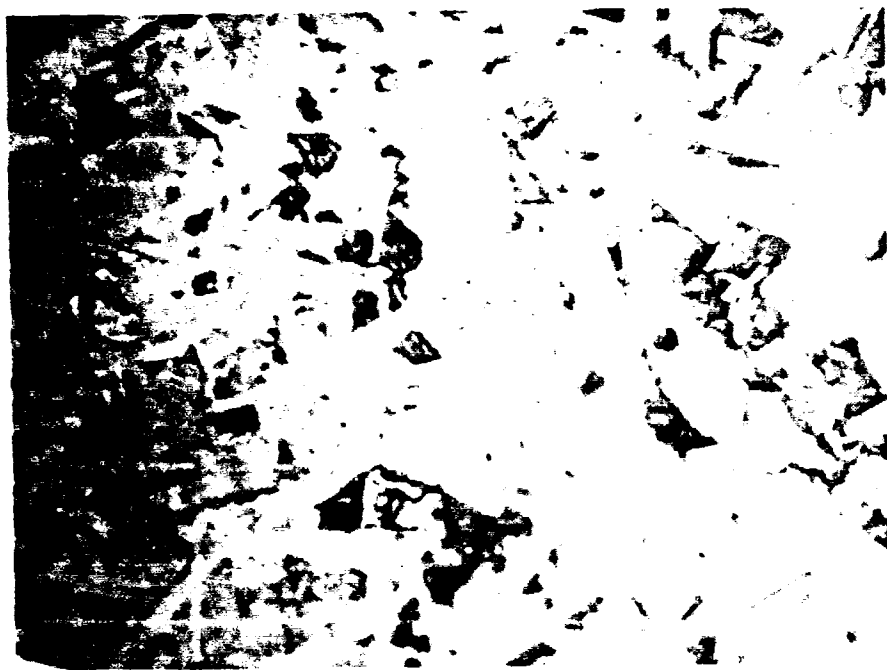


Figure 2.3.2B

Polished and Etched Microstructure of a  $\text{YBa}_2\text{Cu}_3\text{O}_{7.6}$  Filament Zone Sintered at  $966^\circ\text{C}$  for Ten Passes, with 35 Minutes at Temperature.

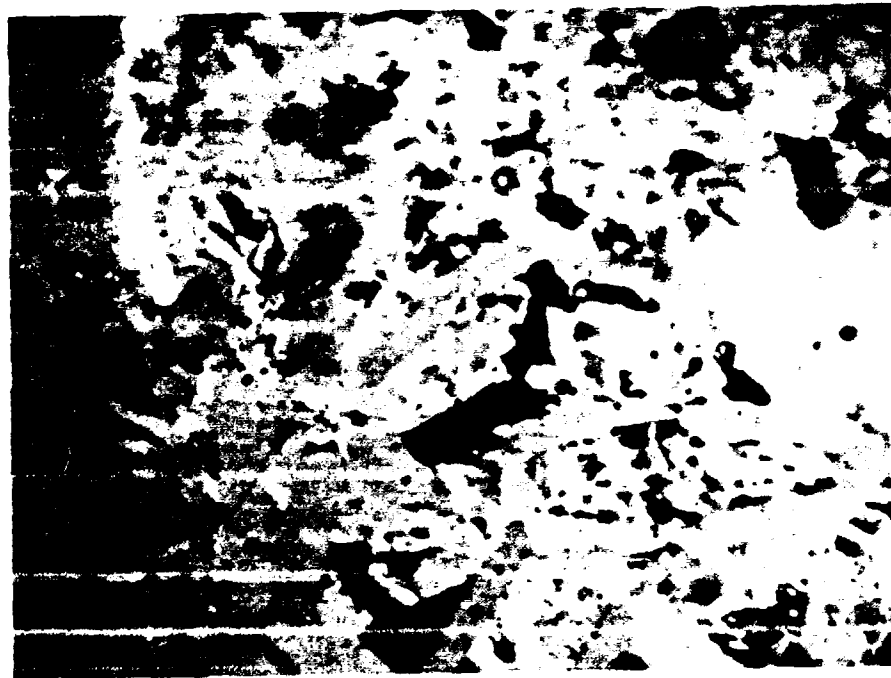


Figure 2.3.3A  $\text{YBa}_2\text{Cu}_3\text{O}_{7-x}$  Filament Sintered Isothermally for 28 Minutes at  $966^\circ\text{C}$ .

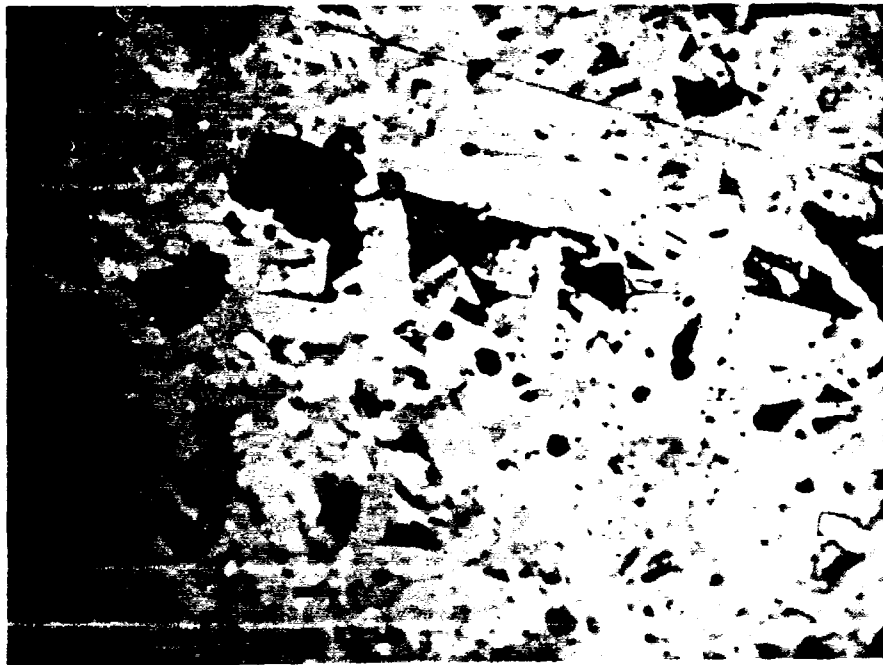


Figure 2.3.3B  $\text{YBa}_2\text{Cu}_3\text{O}_{7-x}$  Filament Zone Sintered for 8 Passes at  $966^\circ\text{C}$ , with 28 Minutes at Temperature.

TABLE 2.3.3

TRANSPORT CRITICAL CURRENT DENSITIES AT 77 K  
Effect of Number of Passes  
Through Hot Zone/Time at Sintering Temperature  
970°C, 5.6 cm/min, 1 h O<sub>2</sub> anneal

SPECIMEN NUMBER	PASSES	FIBER DIAMETER ( $\mu\text{m}$ )	CRITICAL CURRENT (A/cm <sup>2</sup> )
01103A	10	242	5 $\pm$ 1
01103B	8	221	8 $\pm$ 1
01103C	6	237	11 $\pm$ 1
01103C2		178	12 $\pm$ 1
01103D	4	242	22 $\pm$ 1
01103E	2	201	44 $\pm$ 1
01103E2		149	161 $\pm$ 1



Figure 2.3.4A      Fracture Surface of  $\text{YBa}_2\text{Cu}_3\text{O}_{7-\delta}$  Filament after 2 Zone Passes at  $970^\circ\text{C}$ .



Figure 2.3.4B Fracture Surface of  $\text{YBa}_2\text{Cu}_3\text{O}_{7-x}$  Filament after 6 Zone Passes at  $970^\circ\text{C}$ .



Figure 2.3.4C Fracture Surface of  $\text{YBa}_2\text{Cu}_3\text{O}_{7-x}$  Filament after 10 Zone Passes at  $970^\circ\text{C}$ .

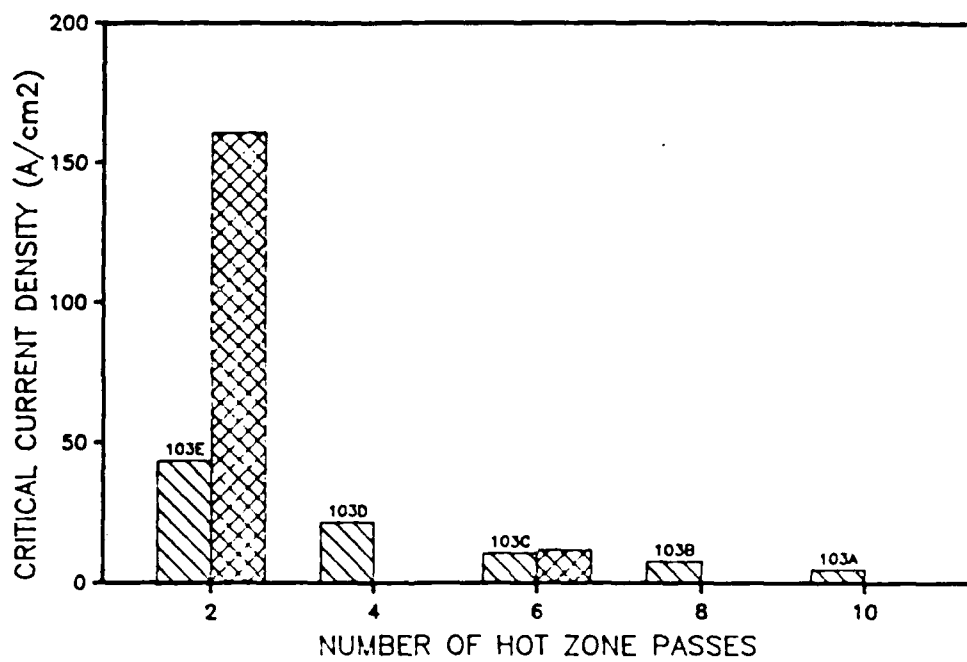


Figure 2.3.5 Critical Current Density at Liquid Nitrogen Temperature in Self Field versus Number of Zone Passes at 970°C.

exposed to 2, 6, and 10 passes appear in Figures 2.3.6A, B, and C, respectively. Both Figures 2.3.6A and B indicate open porosity. The eight and ten pass filaments were much less porous, as shown by Figure 2.3.6C.

The transport critical current densities of these 950°C specimens were as high as 405 A/cm<sup>2</sup>. The larger value seems to be associated with the use of fresh green fiber. Table 2.3.4 compares  $J_c$  for specimens exposed the various zone passes. There is a weak trend for lower  $J_c$  for the 8 and 10 pass specimens. Recall that these were the most dense filaments, which might have less efficient oxygen intercalation during the 60 min anneal. It is not possible at this time to clearly separate the effect of microstructure from the influence of the heat treatments themselves.

The highest critical current densities observed during this period were produced in the second series of lower temperature sintering experiments. Fresh fibers were sintered at 935°C for between 4 and 12 passes at the standard speed, followed by a 60 min anneal at 525°C. In this series the sled was loaded with enough fibers to produce up to five filaments suitable for  $J_c$  measurement. Microstructural development of these specimens are discussed in detail in Section 2.3.5. Table 2.3.5 presents the critical current densities. The values of  $J_c$  for certain specimens are higher, but scatter in the data is striking. This issue is discussed in detail in Section 2.5.5.

Most attention to date has been directed at brief sintering treatments that simulate a short residence time in a continuous furnace. Moreover, treatments based upon the idea of multiple zone sintering have been and are being pursued. A few experiments have been done to examine isothermal sintering and zone/isothermal hybrid treatments. Much longer sintering holds have also been examined to assess if rapid sintering was too short to obtain higher  $J_c$  values. The longer treatments have not yet produced better current densities, but the experiments do offer some interesting microstructural development behavior.

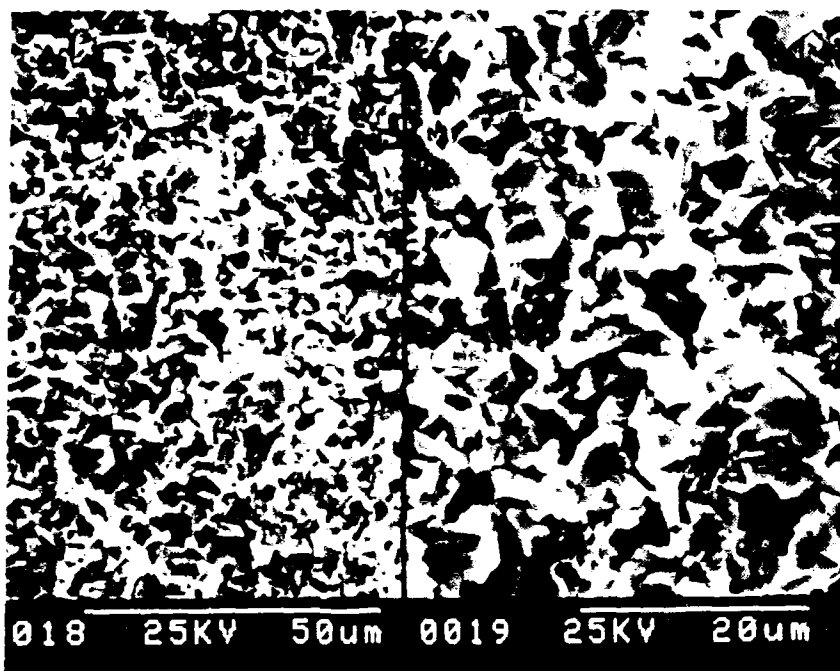


Figure 2.3.6A      YBa<sub>2</sub>Cu<sub>3</sub>O<sub>7-x</sub> Filament Zone Sintered at 950°C for  
2 Passes.

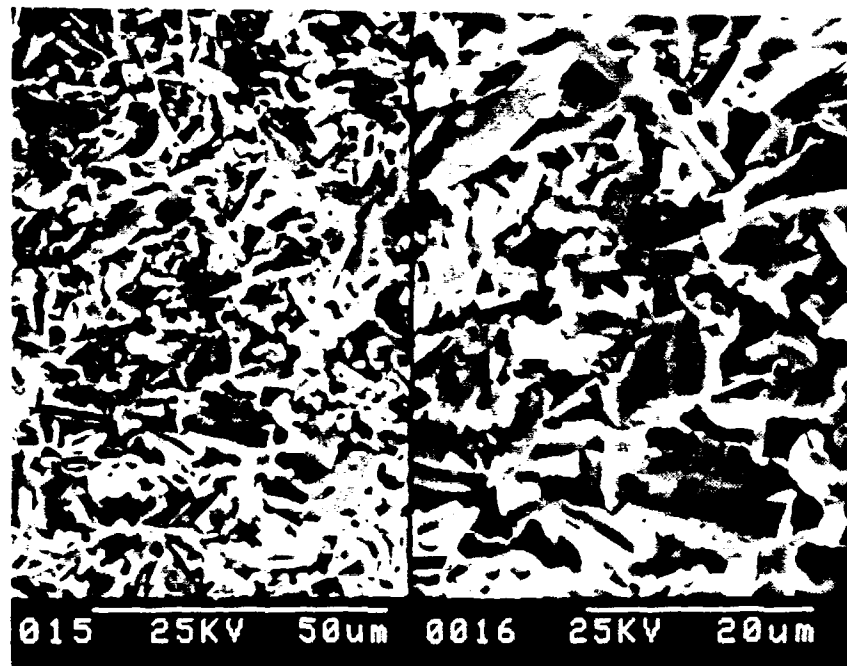


Figure 2.3.6B  $\text{YBa}_2\text{Cu}_3\text{O}_{7-x}$  Filament Zone Sintered at  $950^\circ\text{C}$  for 6 Passes.

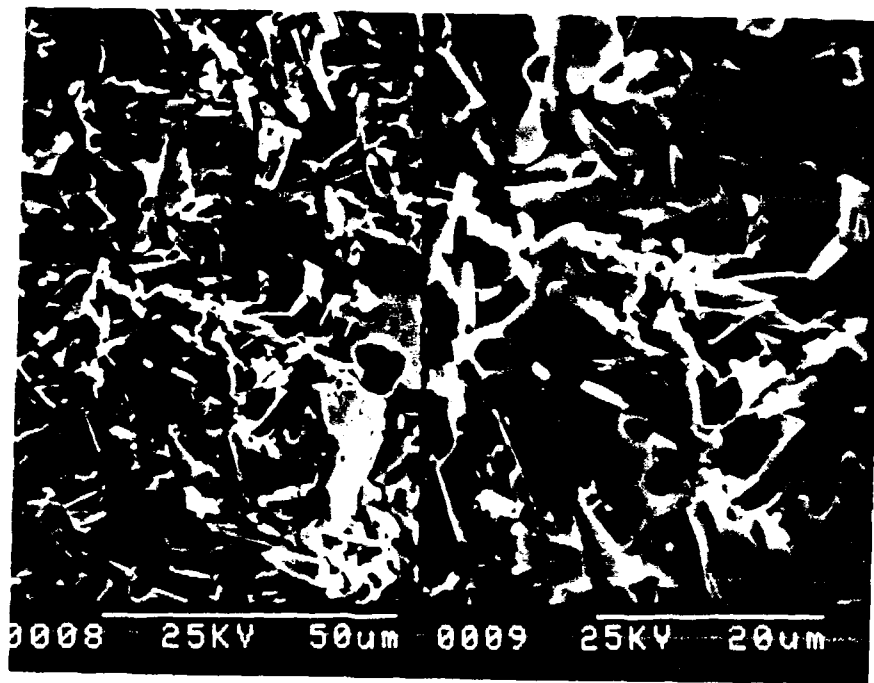


Figure 2.3.6C  $\text{YBa}_2\text{Cu}_3\text{O}_{7-\delta}$  Filament Zone Sintered at 950°C for 10 Passes.

TABLE 2.3.4

TRANSPORT CRITICAL CURRENT DENSITIES AT 77 K  
 Effect of Number of Passes Through Furnace on Critical Current  
 for Sintered Newly-Spun Fibers  
 950°C, 5.5 cm/min Sled Speed, 60 min O<sub>2</sub> Anneal

SPECIMEN NUMBER	PASSES	FIBER DIAMETER ( $\mu\text{m}$ )	CRITICAL CURRENT (A/cm <sup>2</sup> )
01147F	2	196	364 $\pm$ 10
01147D1	4	192	405 $\pm$ 2
01147E	6	178	352 $\pm$ 2
01147H	8	237	150 $\pm$ 2
01147G	10	207	217 $\pm$ 2

TABLE 2.3.5

TRANSPORT CRITICAL CURRENT DENSITIES AT 77 K  
 Effect of Number of Passes  
 935°C, 5.5 cm/min Sled Speed, 60 min O<sub>2</sub> Anneal

SPECIMEN NUMBER	PASSES	FIBER DIAMETER ( $\mu\text{m}$ )	CRITICAL CURRENT (A/cm <sup>2</sup> )
01153A	12	209	169 $\pm$ 2
01153A2		224	533 $\pm$ 2
01153A3		228	294 $\pm$ 2
01153B2	8	221	679 $\pm$ 2
01153C2	4	235	600 $\pm$ 2
01153C3		216	792 $\pm$ 2
01153C4		279	475 $\pm$ 2
01153C5		252	581 $\pm$ 2
01153C6		231	263 $\pm$ 2

Three filaments were prepared with 30 min isothermal sintering treatments at 935, 945, and 965°C. The critical current densities, presented in Table 2.3.6, are in the lower range of the "fresh" green fiber results. These can be compared with zone sintered filaments at similar time and temperature. The 935°C/30 min isothermal specimen can be roughly compared with the eight-pass specimen at the same temperature, that had a total time of

TABLE 2.3.6

TRANSPORT CRITICAL CURRENT DENSITIES AT 77 K  
Isothermal Holds for 30 min, 60 min O<sub>2</sub> Anneal

SPECIMEN NUMBER	TEMP (°C)	FIBER DIAMETER ( $\mu\text{m}$ )	CRITICAL CURRENT (A/cm <sup>2</sup> )
01153D3	935	207	170 $\pm$ 2
01153E	945	183	125 $\pm$ 2
01153F2	965	199	284 $\pm$ 2

28 min at high temperature. In this particular case, the zone sintered specimen had a larger critical current density. However, this does not seem to be true for another roughly comparable pair, the 945°C/30 min isothermal specimen and the 8 pass/28 min 950°C specimen that had roughly the same critical current density. Unfortunately the 965° isothermal specimen cannot be compared with the older zone sintered samples made from "stale" green fibers. This area will be examined more closely in the next Quarter.

Experiments involving multi-hour isothermal holds were undertaken to determine if critical current could be enhanced. Filaments were sintered as long as 16 h at the low temperature of 925°C, but to date these long term sintered filaments have displayed only modest  $J_c$  values around 50 A/cm<sup>2</sup>. Considerable grain growth occurs during the long holds. Some results indicate that previous zone sintering history may influence the microstructural development occurring during a long subsequent isothermal hold. Results are rather incomplete at this time, but can be illustrated by Figures 2.3.7A and B. A simple 14 h isothermal hold at 925°C produced the microstructure shown in Figure 2.3.7A, which exhibits copious grain growth with extensive pore entrapment. Contrast this with Figure 2.3.7B, which was exposed to eight zone passes followed by a 16 h isothermal hold. This specimen has a significantly finer grain size and much less pore entrapment. The initial



Figure 2.3.7A      Microstructure of YBa<sub>2</sub>Cu<sub>3</sub>O<sub>7-x</sub> Filament Sintered  
14 hours at 925°C.



Figure 2.3.7B Microstructure of YBa<sub>2</sub>Cu<sub>3</sub>O<sub>7-δ</sub> Filament Zone Sintered at 925°C for 8 Passes, Followed by a 16 Hour Isothermal Hold.

zone passes seem to have altered the path of microstructure development during subsequent grain growth.

### 2.3.5 Quantitative stereology of microstructure development

Polished and etched surfaces of selected filaments were examined in detail to determine the grain "widths," "lengths" and aspect ratios. Width and length were determined by measuring the shortest and longest dimensions in the platy-shaped grains. No attempt was made to introduce a stereological correction to account for the orientation of the grains with the plane of polish, so these data must be viewed as only proportional to the true grain shapes. Two artifacts of the polishing and etching can distort the results. First,  $\text{YBa}_2\text{Cu}_3\text{O}_{7-\delta}$  is prone to pull-outs, and a platy grain with its largest face nearly parallel to the plane of the polished surface tends to be lost as a pull-out. Thus the large equiaxed grains, that would be expected for grains with their basal planes parallel to the plane of polish, are very rarely observed. Nearly all of the visible grains show up as rectangular features intersecting the plane of polish, representing those grains intersecting the polish plane at an angle to their basal planes. A second artifact is created by the etchant that over-etches and obscures the finer grains. To compensate for this, the area fraction of obscured fine grains are lumped together as the less-than-1  $\mu\text{m}$  fraction. These fine grains visible in SEM fractographs are in fact the "primary" grains, i.e., those grains originating as powder particles. The larger grains are "secondary" grains resulting from a secondary recrystallization process (or in other terminology, discontinuous grain growth). The observations reported in this section essentially document the progress of the secondary recrystallization. Recall that these fibers were prepared from the Rhone-Poulenc powder, which contained excess copper oxide. The microstructure development reflects liquid phase sintering.

Seventeen filaments were selected for analysis. These were taken from three series prepared with fresh green fiber: series 01147, zone sintered at 950°C for 2 to 10 passes; series 01153A,B,C, zone sintered at 935°C for 4 to 12 passes; and series 01153D,E,F, that received a 28 min isothermal hold. The average width, length, and aspect ratios of these filaments are collected in Table 2.3.7, along with the critical current density and an estimate of the area fraction of over-etched fine primary grains. What follows is a presentation of actual distribution data as well as correlations using the combined data set.

TABLE 2.3.7

## GRAIN SIZE DATA FOR SINTERED FILAMENTS

SPECMN NUMBER	TEMP (°C)	PASS (#)	FIBER		AVERAGE	AVERAGE	ASPECT RATIO ave. ( $\sigma$ )	ESTIMATE PERCENT PRIMARY GRAINS
			DIAM ( $\mu\text{m}$ )	$J_c$ ( $\text{A}/\text{cm}^2$ )	GRAIN WIDTH ( $\mu\text{m}$ ) ( $\sigma$ )	GRAIN LENGTH ( $\mu\text{m}$ ) ( $\sigma$ )		
01147F	950	2	196	364±10	Too Fine to Measure		100	
01147D	950	4	192	405±2	0.98(0.45)	4.58(3.90)	4.62(3.08)	30
01147E	950	6	178	352±2	1.02(0.44)	3.90(3.28)	3.97(2.58)	10
01147H	950	8	237	150±2	1.38(0.89)	6.40(5.92)	4.61(2.38)	5
01147G	950	10	207	217±2	1.23(0.83)	6.11(4.74)	5.03(2.52)	<5
01153A	935	12	209	169±2	2.10(1.61)	7.71(6.77)	3.68(2.17)	10
01153A2			224	533±2				
01153A3			228	294±2				
01153B2	935	8	221	679±2	1.15(0.50)	5.57(4.22)	5.09(3.20)	10
01153C2	935	4	235	600±2	0.82(0.40)	4.56(3.58)	5.32(3.07)	30
01153C3			216	792±2				
01153C4			279	475±2				
01153C5			252	581±2				
01153C6			231	263±2				
01153D3	935	1 30 m	207	170±2	1.40(0.60)	6.92(3.90)	5.13(2.32)	15
01153E2	945	1 28 m	183	125±2	2.17(1.82)	8.88(9.57)	4.55(2.19)	5
01153F2	965	1 28 m	199	284±2	2.13(1.55)	8.27(7.51)	4.21(2.47)	5

Figure 2.3.8 displays the combined data for all filaments, showing the average aspect ratio versus the average grain width. It appears that the aspect ratio scatters around 4-5, independent of the grain width, indicating

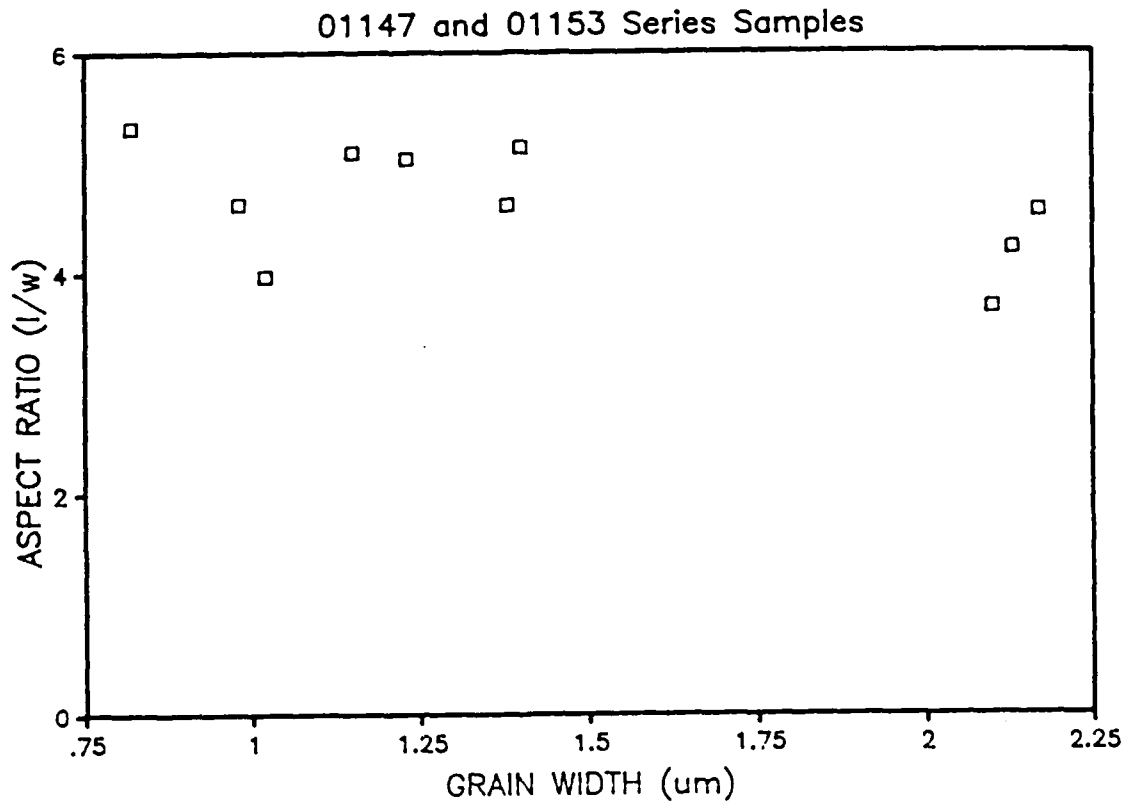


Figure 2.3.8

Average Aspect Ratio versus Average Grain Width for  $\text{YBa}_2\text{Cu}_3\text{O}_{7-\delta}$  Filaments Sintered at 935 and 950°C.

that the shape of the grains do not change as the microstructures develop.  $\text{YBa}_2\text{Cu}_3\text{O}_{7-\delta}$  appears to display a well-defined habit in the presence of a CuO-rich liquid phase.

Grain growth at  $950^\circ\text{C}$  is illustrated by Figure 2.3.9, as a sequence of histograms displaying the grain length distributions after 2, 4, 6, 8, and 10 repeated passes through the hot zone. Each pass corresponds to 3.5 min at temperature. The sample is relatively porous after two and four passes, but dense after six passes. Notice the less-than-1  $\mu\text{m}$  category, which corresponds to the finer primary grains. After two passes, the fine primary grain matrix occupies the entire structure. Upon further repeated passes, the fraction of primary matrix gradually diminishes, vanishing after ten passes. The population of larger secondary grains increases in proportion, with the mode gradually moving to larger grain sizes.

A similar development occurs at  $935^\circ\text{C}$ , shown in Figure 2.3.10. The sub-micron categories are truncated from these histograms, so only the population distributions of secondary grains are displayed. The maximum grain length, and number of larger grains increases with repeated passes. The progression of average grain sizes with time upon repeated passes is displayed in Figure 2.3.11A showing average grain width as a function of number of passes and time at temperature, and Figure 2.3.11B that shows the behavior of the average grain length. The size of the error bars show the standard deviation.

Figure 2.3.12 compares the grain size distributions in filaments sintered isothermally for thirty minutes at 935, 945, and  $965^\circ\text{C}$ . The most frequently occurring grain lengths are 4-6  $\mu\text{m}$  for all three temperatures, but the population of grains larger than 16  $\mu\text{m}$  is greater at higher temperature. One can compare the grain size distributions for zone sintered and isothermally sintered specimens using the  $935^\circ\text{C}$  histogram of Figure 2.3.12 and

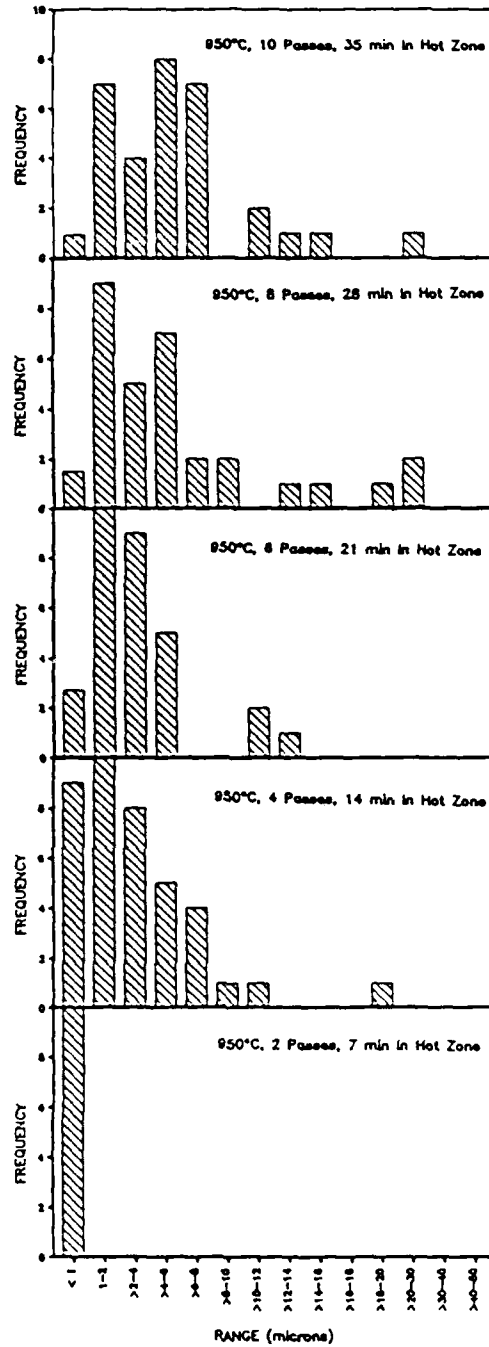


Figure 2.3.9

Grain Length Distributions For  $\text{YBa}_2\text{Cu}_3\text{O}_{7-\delta}$  Filaments Zone Sintered at  $950^\circ\text{C}$  for 2, 4, 6, 8, and 10 Passes. Each Pass Corresponds to 3.5 Minutes at Temperature.

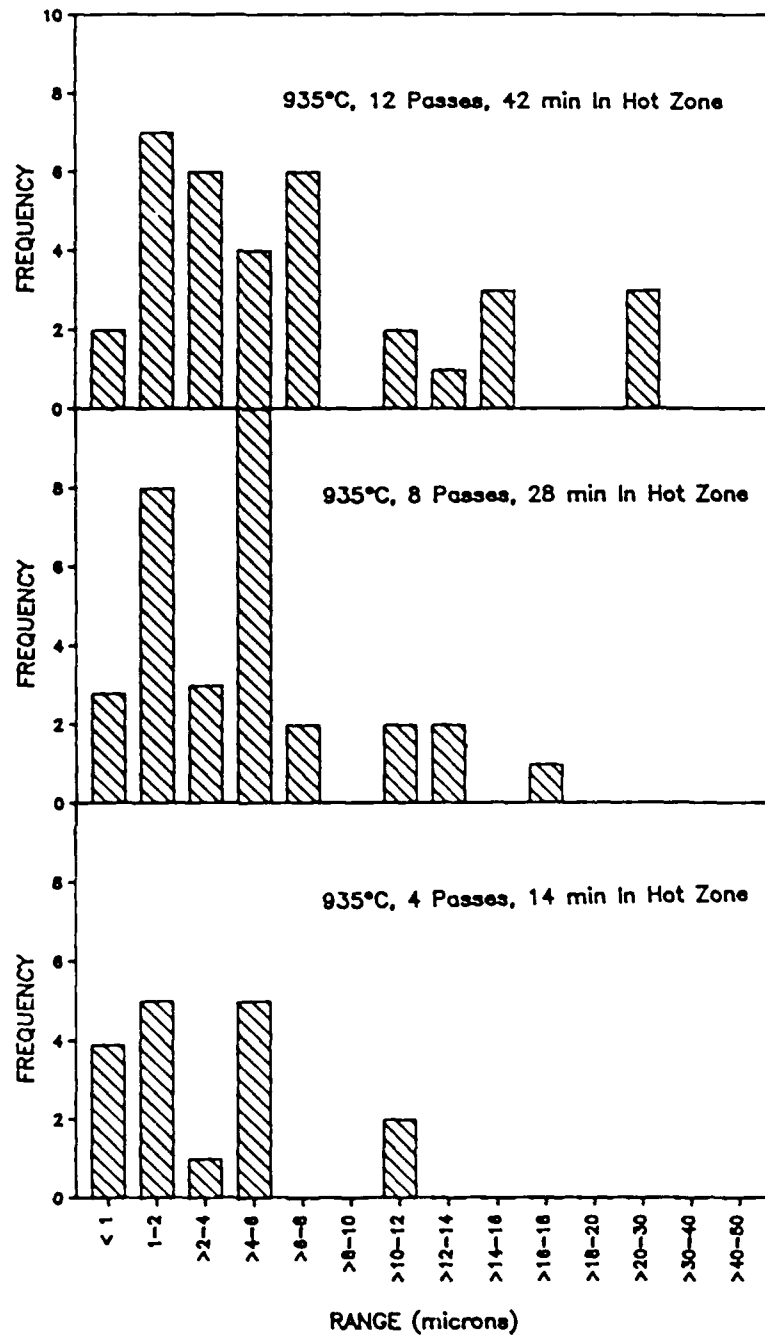


Figure 2.3.10

Grain Length Distributions for  $\text{YBa}_2\text{Cu}_3\text{O}_{7-\delta}$  Filaments Zone Sintered at  $935^\circ\text{C}$  for 4, 8, and 12 Passes. Each Pass Corresponds to 3.5 Minutes at Temperature.

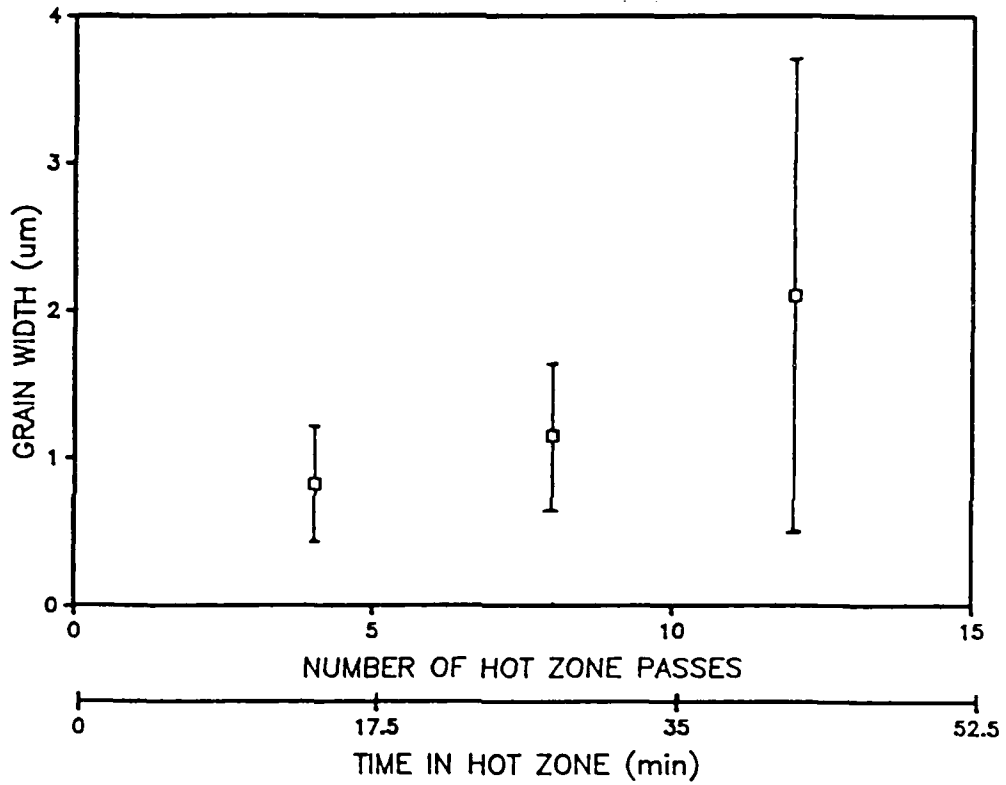


Figure 2.3.11A Average Grain Width versus Number of Zone Passes and Time at Temperature for  $\text{YBa}_2\text{Cu}_3\text{O}_{7-d}$  Filaments Sintered at  $935^\circ\text{C}$ .

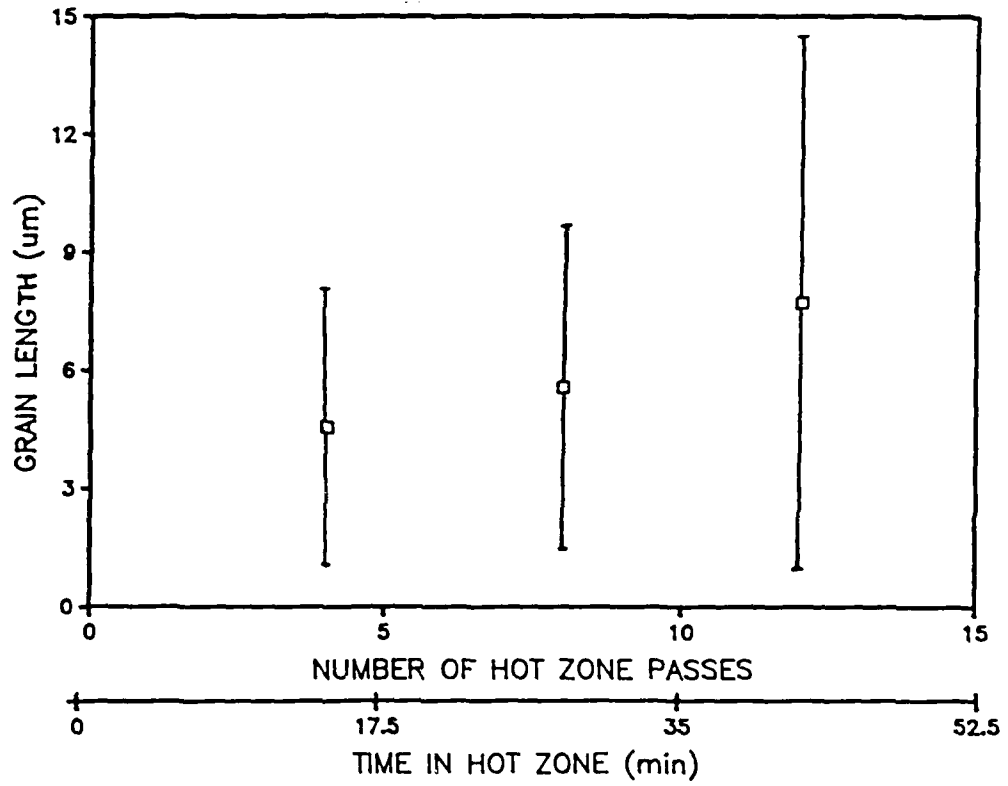


Figure 2.3.11B Average Grain Length versus Number of Passes for  $\text{YBa}_2\text{Cu}_3\text{O}_{7-\delta}$  Filaments Sintered at  $935^\circ\text{C}$ .

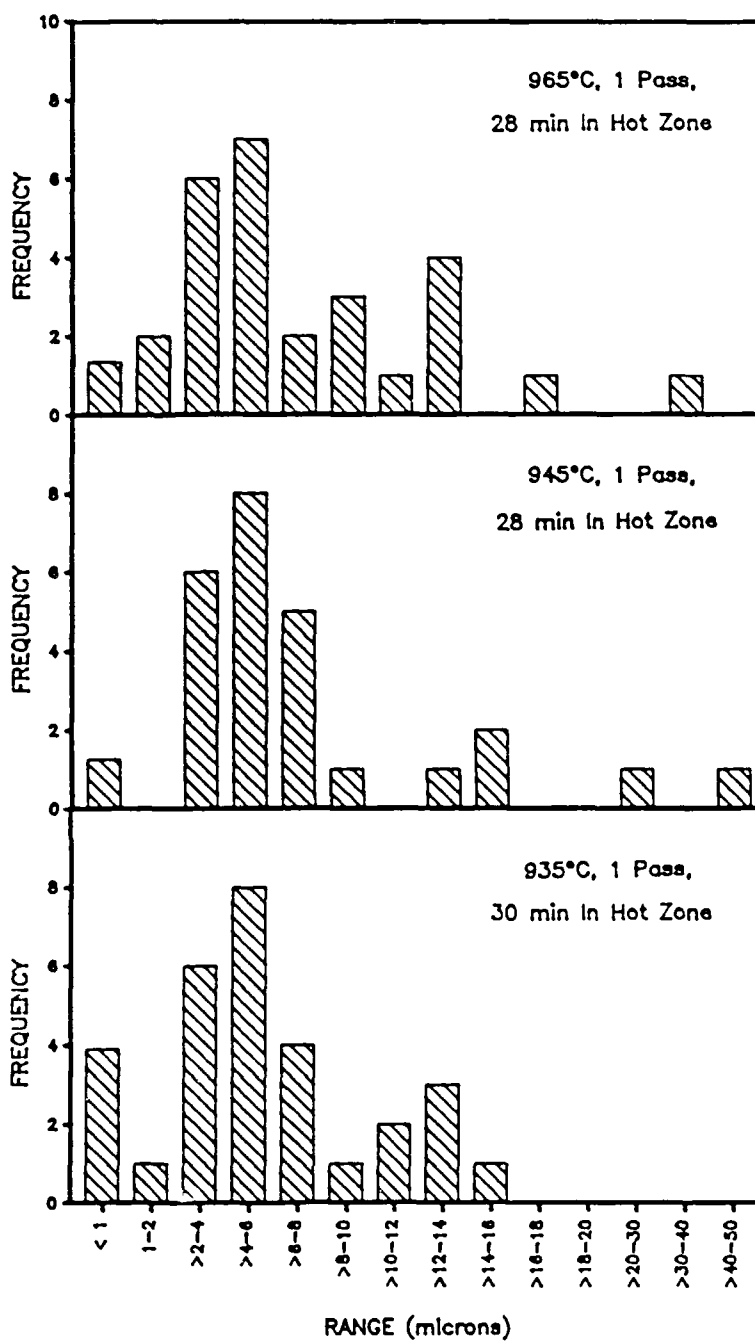


Figure 2.3.12

Grain Size Distributions in Isothermally Sintered  $\text{YBa}_2\text{Cu}_3\text{O}_{7-\delta}$  Filaments.

the eight pass histogram of Figure 2.3.10. In this case, the isothermal and zone sintered specimens are roughly similar.

The entire database of 17 specimens can be used to construct a graph of critical current density versus grain size. Figure 2.3.13 displays such a graph for average grain length of each specimen plotted with its  $J_c$ . The results are highly scattered, but on first glance seem to show a trend of lower  $J_c$  for larger grains. Note, however, that the largest grain size/lowest  $J_c$  combinations are for the isothermally sintered specimens 01153D, E, and F. If these three points are excluded, the trend becomes much weaker. Considering the variability in  $J_c$  and the width of the grain size distributions, it is too early to reach any definite conclusions on the influence of microstructure on weak-link critical current densities. Collecting data of  $J_c$  statistics and microstructural statistics is continuing, and will expand the database to address this important issue.

Finally, the data of Table 2.3.7 can be used to relate critical current density to zone sintering conditions. Figure 2.3.14 displays the data for the 935°C series, showing  $J_c$  as a function of number of zone passes. There is no trend in these data that is visible against the scatter. This contrasts with previous results that indicated a strong effect where there was a clear maximum in  $J_c$  with repeated zone passes over a range of four temperatures. Note, however, that there are two important differences between this data set and the previous data. In the present case, the sled speed is constant, so repeated zone passes increase the total time at temperature. The previous results had constant time at temperature, with the speed changing so that it compared two slow passes with ten rapid passes. Also, the older data had only a single specimen for each condition. This introduces the possibility that the previous "trend" was a fortuitous selection from scattered data.

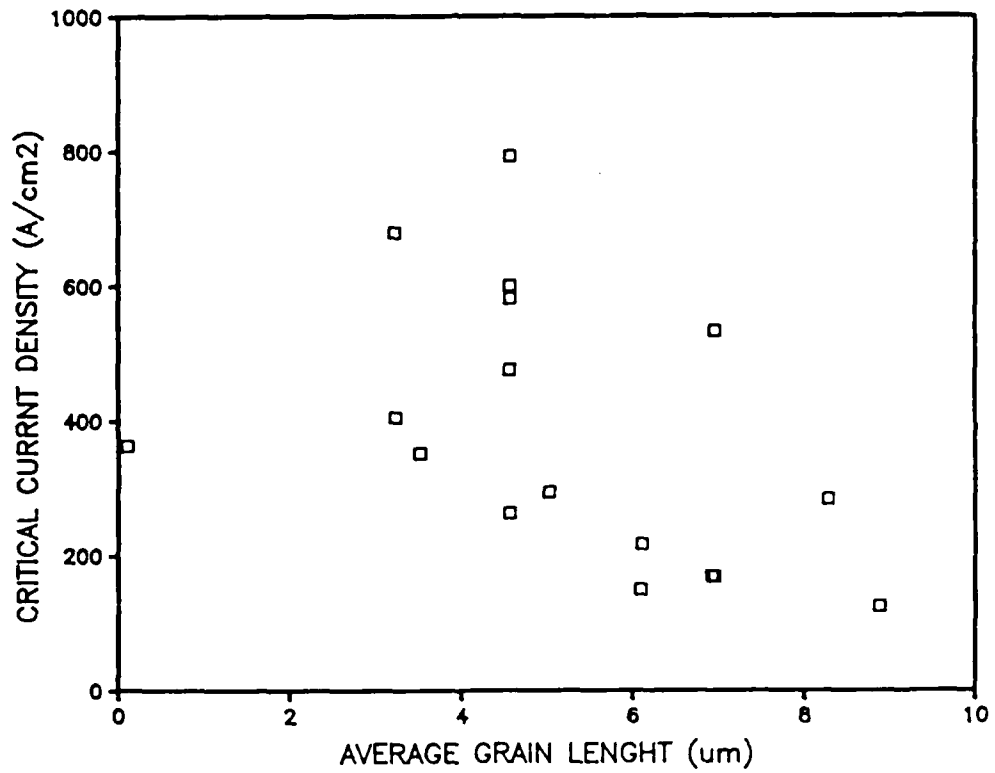


Figure 2.3.13

Critical Current Density versus Average Grain Length for  $\text{YBa}_2\text{Cu}_3\text{O}_{7-\delta}$  Filaments Sintered Under a Variety of Conditions.

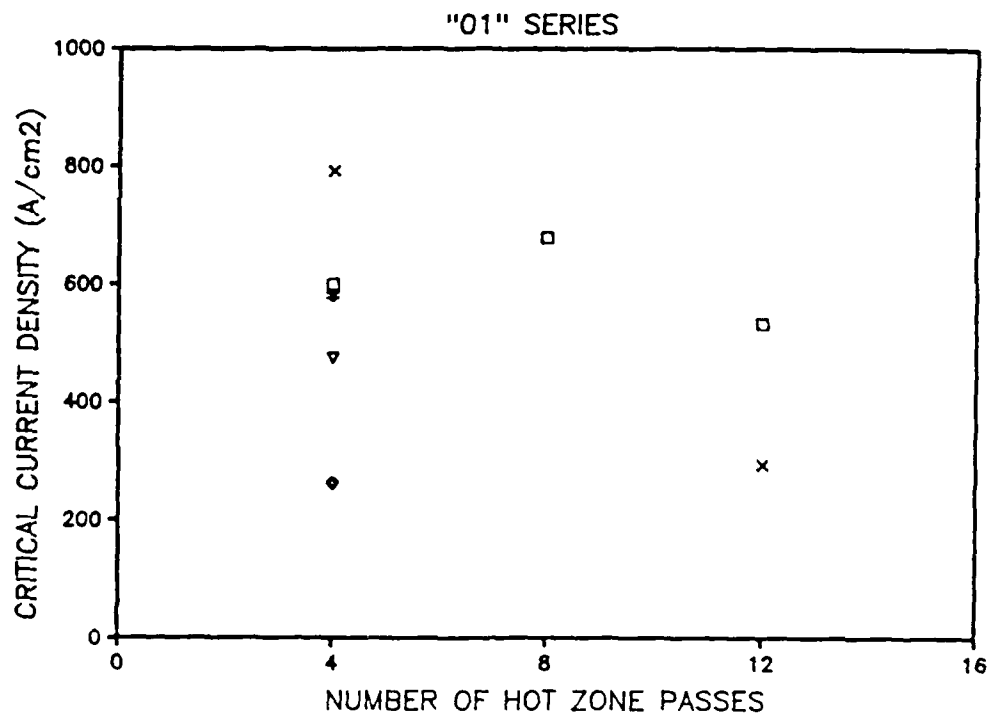


Figure 2.3.14

Critical Current Density versus Number of Repeated Passes for  $\text{YBa}_2\text{Cu}_3\text{O}_{7-\delta}$  Filaments Zone Sintered at  $935^\circ\text{C}$ .

### 2.3.6 Continuous laboratory scale sintering furnace

An appropriate laboratory furnace for sintering ceramic fiber in a continuous mode has been identified. The unit selected is an infrared belt furnace, manufactured by Radiant Technology Corporation (RTC A-306X). This furnace is capable of very rapid heating and cooling rates to precise temperatures with zone controlled atmospheres (limited to contamination of 5 ppm), so that an inert gas can be used in the binder burnout section, an air atmosphere in the sintering zone, followed by an oxygen-rich atmosphere for annealing during cooling. A belt type furnace is appropriate for fiber sintering. The fibers can be supported by and carried on the belt through the operation without applying tension to the delicate filaments. This unit has adjustable belt speeds such that the total time of the heat treatment can be easily controlled. Current work at CPSS has emphasized multiple zone sintering which requires a furnace with a number of independently controlled zones. This particular model provides three zones.

The RTC A306-X radiant furnace uses quartz lamps as the heat source. As the name implies, the primary mode of heat transfer is radiation. With the view factors appropriate for radiation to a fine filament in a wide radiant cavity, the fibers should be heated very rapidly and uniformly. Directional recrystallization requires much sharper thermal gradients than can be achieved in a conventional tube furnace. The radiant furnace should be capable of intense gradients, due to the line-of-sight nature of radiant heat transfer. Additionally, sharp gradients can be generated by including appropriate baffles to cast shadows on the moving filaments.

Delivery of this unit is expected toward the end of the next Quarter. Zone sintering and oxygen annealing development will be transferred to this furnace at that time. A green fiber payout spool will be fitted at the entrance to permit continuous sintering. At the exit the continuous sintered filament will be collected in half-meter lengths for evaluation and

use in the development of the cladding module. When the cladding module is ready, it will be fitted at the exit to complete the lab scale continuous sintering and cladding facility. This facility is expected to be adequate for manufacturing small quantities of experimental ribbon conductor, and will be a test bed for development of the pilot scale facility in the following year.

## 2.4 Filament Cladding and Wire Fabrication

### 2.4.1 Introduction

A key step in the CPSS process for the production of HTSC wire is the cladding operation. This process step must be able to accept the array of fragile ceramic filaments at the point of exit from the sintering furnace and clad them with the appropriate metal stabilizer without damaging the continuity of the sintered filaments. The output of the cladding operation must be a strong, easily handled ribbon that can either be directly spooled, or drawn through a secondary finishing operation before spooling.

Cladding is a challenging step from a mechanical standpoint. Prior to sintering, the green fiber is tractable and readily drawn through guides and spooling equipment. Downstream of the cladding operation, it is anticipated that the ribbon will also be tractable. However, between the sintering furnace and the cladding facility the bare filaments are so fragile that they must be carried rather than pulled through any device. The objective of this task is to develop a metal cladding process, demonstrate feasibility by metallizing short filaments without degrading the superconducting properties, and fabricate an appropriate cladding module.

Several different metal cladding methods are being investigated both at CPSS and in collaboration with other groups. Each of these methods is capable of continuous operation, and include a conceptual design of the cladding module. The major emphasis of work performed at CPSS has been focused on a process in which a filament array is bonded between two copper

strips by a solder reflow operation. Considering the different methods being evaluated, this is potentially the easiest process to scale up to a continuous operation. It is rapid, involves only one step, minimizes exposure and handling of the bare filaments, and may require only a simple set of rollers to implement the actual assembly. Also, it is compatible with the compressive pre-stress ideas outlined in Section 1. One problem with this process is that it would appear to limit the conductor designs to large values of the metal/superconductor stabilizer ratio.

Another method being evaluated involves electrodeposition of copper or aluminum on the  $\text{YBa}_2\text{Cu}_3\text{O}_{7-\delta}$  filaments. This work is being pursued in collaboration with Dr. David Lashmore of the National Institute for Standards and Technology. Dr. Lashmore is an expert on nonaqueous electrodeposition who has developed a reel-to-reel plating cell capable of continuously plating on graphite fibers, under highly controlled conditions. Incorporation of a nonaqueous electrodeposition cladding module, based on Dr. Lashmore's fiber plating cell, is currently being considered. Another possibility involves the work being explored in collaboration with Professor Stanley Bruckenstein, Goodyear Professor of Chemistry at the State University of New York (SUNY) - Buffalo, who has developed a method to electroplate copper onto  $\text{YBa}_2\text{Cu}_3\text{O}_{7-\delta}$  from more conventional aqueous baths as part of a DARPA-sponsored program. Success of this process could make possible a cladding module that would incorporate use of commercial wire plating equipment.

#### 2.4.2 Outline of the reflow bonding process

A new process for encasing the superconducting filaments in metal was developed during this Quarter. This process seems to be capable of directly producing a variation of the flexible ribbon conductor (FRC) using a simple solder reflow step. The anticipated product of this process is shown in Figure 2.4.1. The key is to treat the surface of the  $\text{YBa}_2\text{Cu}_3\text{O}_{7-\delta}$  fiber so

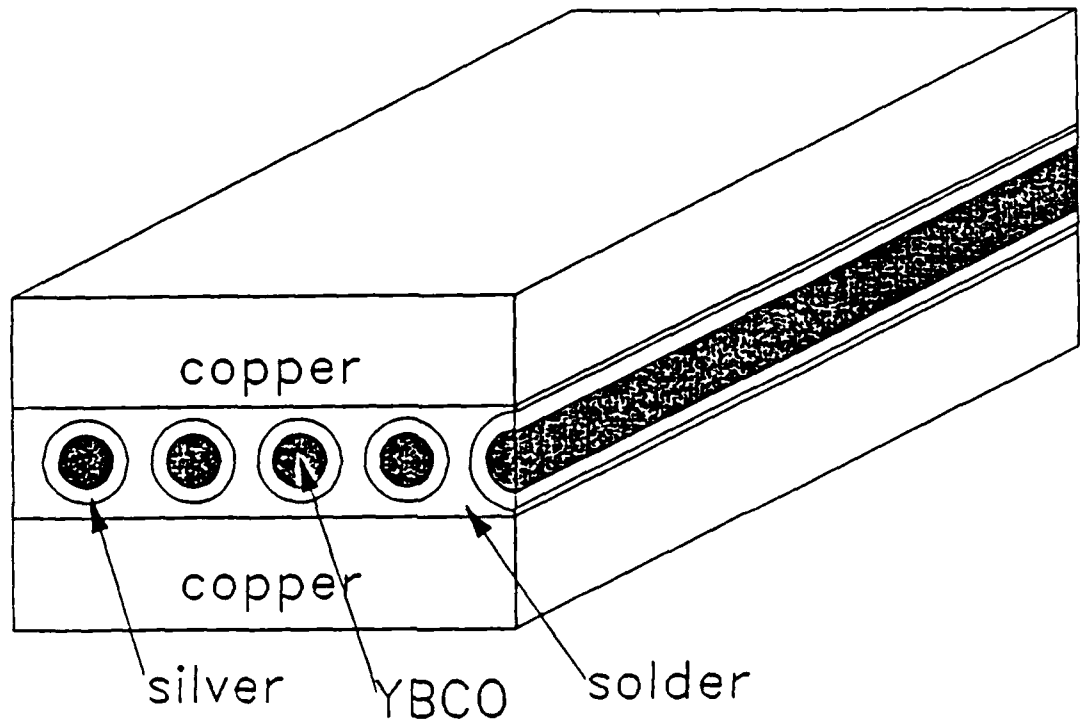


Figure 2.4.1

Flexible Ribbon Conductor Fabricated by Solder Reflow Bonding to Copper Strips.

that it can be wet by solder and bonded to a copper strip, which acts as the primary stabilizer. This surface treatment consists of a silver alloy metallization. It is preferable to have a very thin or even porous silver coating, sufficient to render the filament able to be wet by solder, but not so thick as to present a diffusion barrier during the oxygen intercalation anneal. To avoid handling the fragile sintered filaments, it is preferable to produce silver-coated green fiber and subsequently sinter under conditions that densify the  $\text{YBa}_2\text{Cu}_3\text{O}_{7-\delta}$  ceramic without melting the silver alloy. This has been demonstrated.

The reflow bonding process requires four steps to produce the final ribbon conductor:

1. The green fiber is metallized with silver
2. The fiber is sintered and annealed to get orthorhombic  $\text{YBa}_2\text{Cu}_3\text{O}_{7-\delta}$
3. The array of silver coated superconducting filaments are placed between two solder clad copper strips (on the solder faces)
4. The solder is reflowed by application of heat so the solder flows around the filaments, bonding the filaments and joining the copper strips

This cladding process has a number of advantages: it is a simple process, it can be carried out continuously, it is not likely to degrade any superconducting properties, and it can be scaled up to commercial production. Solder clad copper strips (sometimes referred to as pre-tinned copper strips) are commercially available from several vendors. The ribbon conductor can be produced in any desirable width and thickness in continuous lengths. Also, by a judicious choice of solder which melts at high temperature, a compressive state of stress can be induced around the filaments.

Direct wetting of solder to a ceramic surface is not possible without an intermediate layer. The choice of silver as the intermediate layer is especially appropriate for  $\text{YBa}_2\text{Cu}_3\text{O}_{7-\delta}$ . Silver and gold are the only metals

known not to react with  $\text{YBa}_2\text{Cu}_3\text{O}_{7-\delta}$  during the sintering process. Further, it has been observed recently that the addition of silver to stoichiometric  $\text{YBa}_2\text{Cu}_3\text{O}_{7-\delta}$  may in fact improve the properties of the superconductor.

#### 2.4.3 Preliminary experiments on silver metallization

Experiments were undertaken to test if silver can be cofired with  $\text{YBa}_2\text{Cu}_3\text{O}_{7-\delta}$ , and to observe the morphology of the sintered coating. Several methods of silver application were examined using both green and sintered  $\text{YBa}_2\text{Cu}_3\text{O}_{7-\delta}$  fibers. The fibers were passed through the furnace hot zone (maximum temperature set at  $955^\circ\text{C}$ ) two times after the coating had been applied. The sintered fiber sample, refired after silver application, had a uniform and adherent coating. Figure 2.4.2 shows a fracture surface of this filament. The ductile fracture of silver and the brittle fracture of the ceramic  $\text{YBa}_2\text{Cu}_3\text{O}_{7-\delta}$  can be clearly seen. No delamination of the coating from the surface was observed. A silver coating applied to a green fiber also gave encouraging results.

These preliminary experiments show that it is possible to cofire a silver coated green fiber and get an adherent silver coating. To demonstrate the feasibility of the entire process, effort was concentrated in four key areas:

1. Development of the silver source
2. Development of application equipment to apply the silver source to the green fiber
3. Adjustment of the firing schedule for cofiring of  $\text{Ag}/\text{YBa}_2\text{Cu}_3\text{O}_{7-\delta}$
4. Composite formation by the reflow process



Figure 2.4.2 Fracture Surface of  $\text{YBa}_2\text{Cu}_3\text{O}_{7-\delta}$  Filament with Silver Coating Sintered at  $955^\circ\text{C}$ .

#### 2.4.4 Binder burnout, sintering, and annealing

Preliminary experiments were carried out to determine if any of the heat treatments used for unclad fiber needed to be changed for use with coated fiber. The established binder burnout treatment was found to work well for coated fibers of comparable diameter. It was noticed that in contrast to the unclad fibers, silver coated fibers do not combust when exposed to rapid rates of heating in air. These initial experiments indicate that binder burnout seems to be better in air than in nitrogen for coated samples.

Zone sintering experiments using coated fibers were performed with the same temperature and speed setting (peak temperature 955°C, 5.5 cm/min, 8 passes) used for uncoated fibers. The silver coating was found to be solid after the first few passes, but molten after 4 passes. This was surprising, since the melting point of silver (961.9°C) is above the peak temperature, and the silver did not melt immediately. This is probably the result of dissolution of oxygen in the silver, which results in the formation of the Ag-Ag<sub>2</sub>O eutectic at 931°C<sup>19</sup>. The silver coating did not melt when the filaments were sintered at 950°C in nitrogen. However, the filaments did not sinter well in nitrogen and did not exhibit the Meissner effect. To avoid melting the silver, filaments were subsequently zone sintered using a lower temperature (925°C). For this experiment the number of passes through the hot zone was increased to 12 to compensate for the lower temperature. Under these conditions, the silver coating did not melt but did adhere to the fiber. After a typical oxygen anneal, the silver treated filament was superconducting with a critical current density of 60 A/cm<sup>2</sup>. The fracture surface of this filament (Figure 2.4.3) shows that it was not as dense as filaments sintered at 950°C.

---

<sup>19</sup> T.B. Mussalski, ed., Binary Alloy Phase Diagram, 1, ASM, Metals Park, OH (1986) p. 49

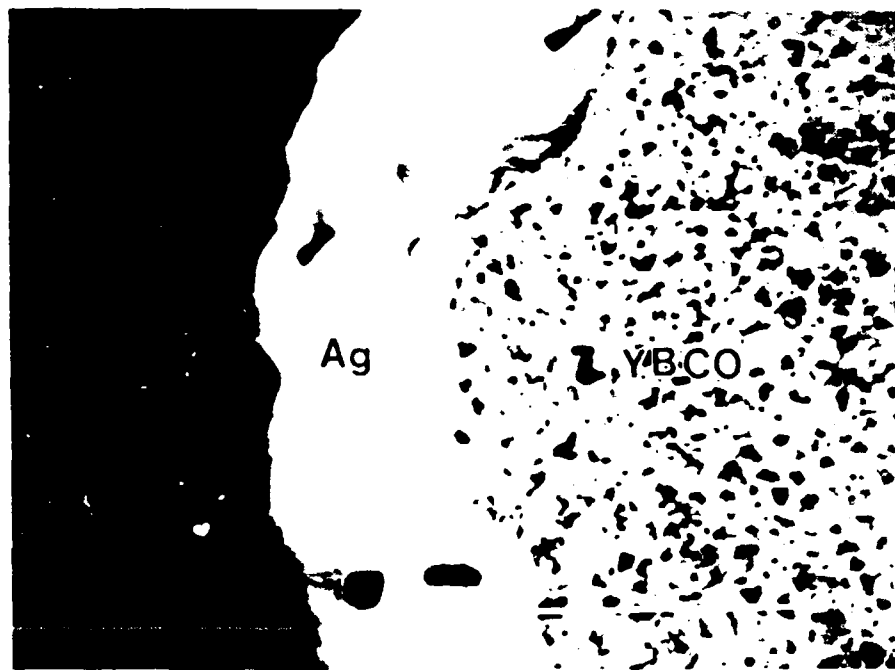


Figure 2.4.3 Cross-Section of Silver Coated Filament Zone Sintered at 925°C.

Since the use of pure silver puts a limit on the maximum sintering temperature, some experiments were carried out to examine the feasibility of using a silver-palladium alloy in the coating. Silver and palladium form a continuous solid solution. Increasing the palladium content increases the solidus and liquidus of the alloy towards the melting point of palladium. A chemically coprecipitated 85/15 Ag-Pd powder<sup>20</sup> (86.19% Ag, 12.24% Pd) with an average particle size of 1.95  $\mu\text{m}$  was examined. To test the adherence of the coating and reactivity of palladium with  $\text{YBa}_2\text{Cu}_3\text{O}_{7-\delta}$ , the powder was pressed into a sintered  $\text{YBa}_2\text{Cu}_3\text{O}_{7-\delta}$  pellet and heat treated at 960°C for 15 min. The interface is shown in Figure 2.4.4, along with a scan of Ag-L $\alpha$  and Pd-L $\alpha$  (these two lines cannot be resolved) intensities determined by energy dispersive spectroscopy (EDS). The change in concentration is very sharp suggesting that no compounds had formed containing silver or palladium. EDS spectra taken 5  $\mu\text{m}$  from the interface (Figure 2.4.5) show that some Ag-Pd has diffused into  $\text{YBa}_2\text{Cu}_3\text{O}_{7-\delta}$ , but no yttrium, barium or copper has diffused into Ag-Pd alloy. X-ray analysis was also performed on a composite sample. A pellet was cold pressed using a composition of 50 vol% Ag-Pd/ 50 vol%  $\text{YBa}_2\text{Cu}_3\text{O}_{7-\delta}$ . The pellet was sintered at 960°C for 0.5 h in air. The x-ray diffraction pattern (Figure 2.4.6) indicates only the presence of Ag-Pd solid solution and  $\text{YBa}_2\text{Cu}_3\text{O}_{7-\delta}$ . From this experiment, it appears that there is no reaction between Ag-Pd and  $\text{YBa}_2\text{Cu}_3\text{O}_{7-\delta}$ .

$\text{YBa}_2\text{Cu}_3\text{O}_{7-\delta}$  green fibers coated with Ag-Pd were zone sintered using a peak temperature of 955°C. Some local melting of Ag-Pd was observed, which is to be expected since this is a physically mixed material and not a true alloy. The sintered filament was superconducting, but had a critical current density of only 3 A/cm<sup>2</sup>. The reasons for this low value are not apparent at this time, and the experiment is being repeated.

---

<sup>20</sup> Handy and Harmon, Inc., East Providence, RI

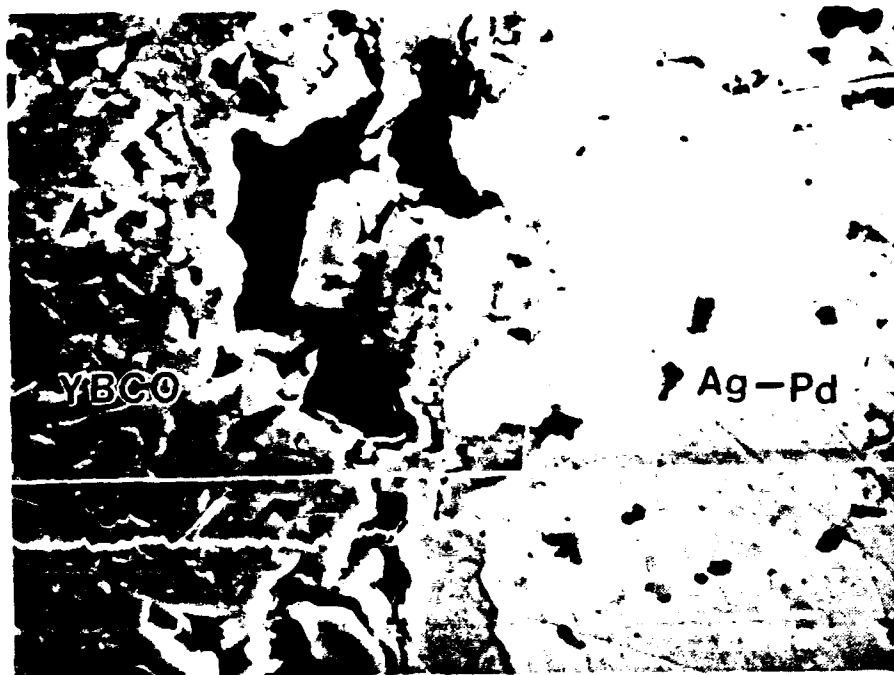


Figure 2.4.4 Ag-Pd and  $\text{YBa}_2\text{Cu}_3\text{O}_{7-\delta}$  Interface.

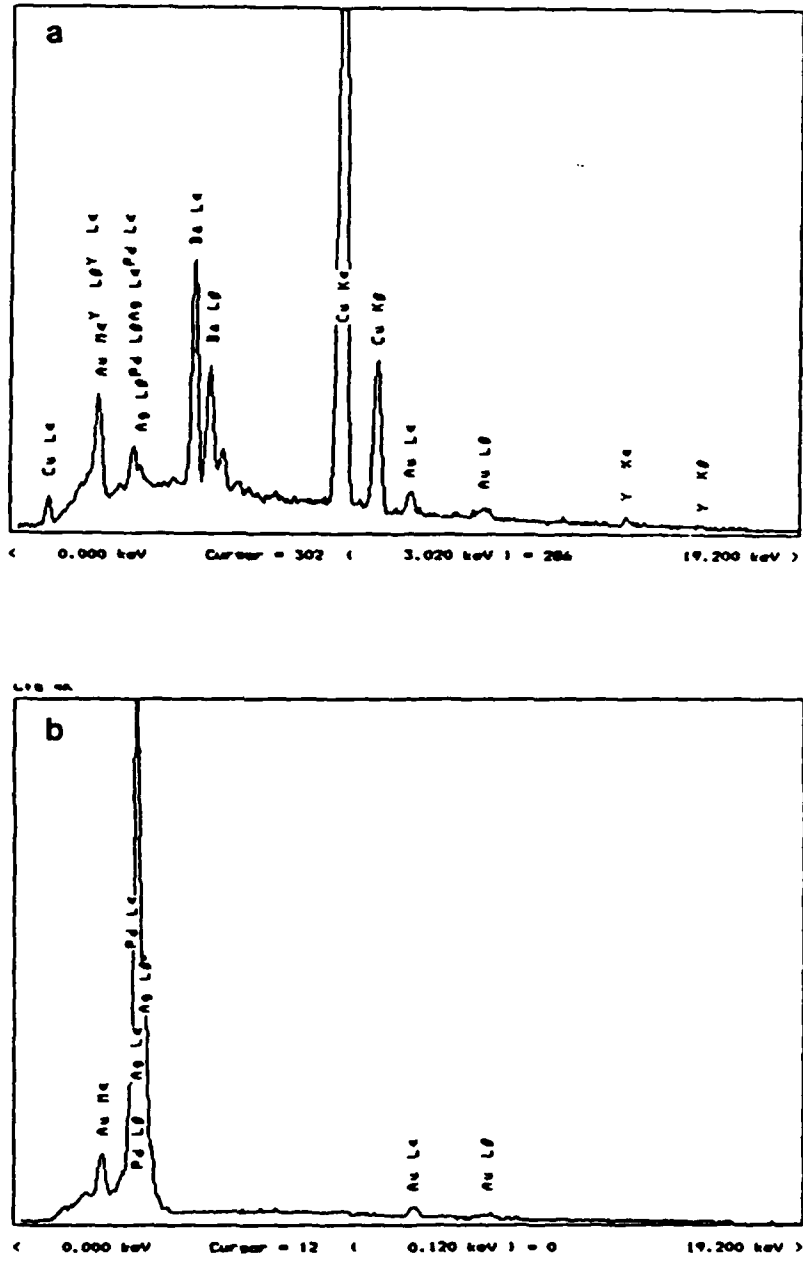


Figure 2.4.5      EDS Spectra from A)  $YBa_2Cu_3O_{7-\delta}$  and B) Ag-Pd.

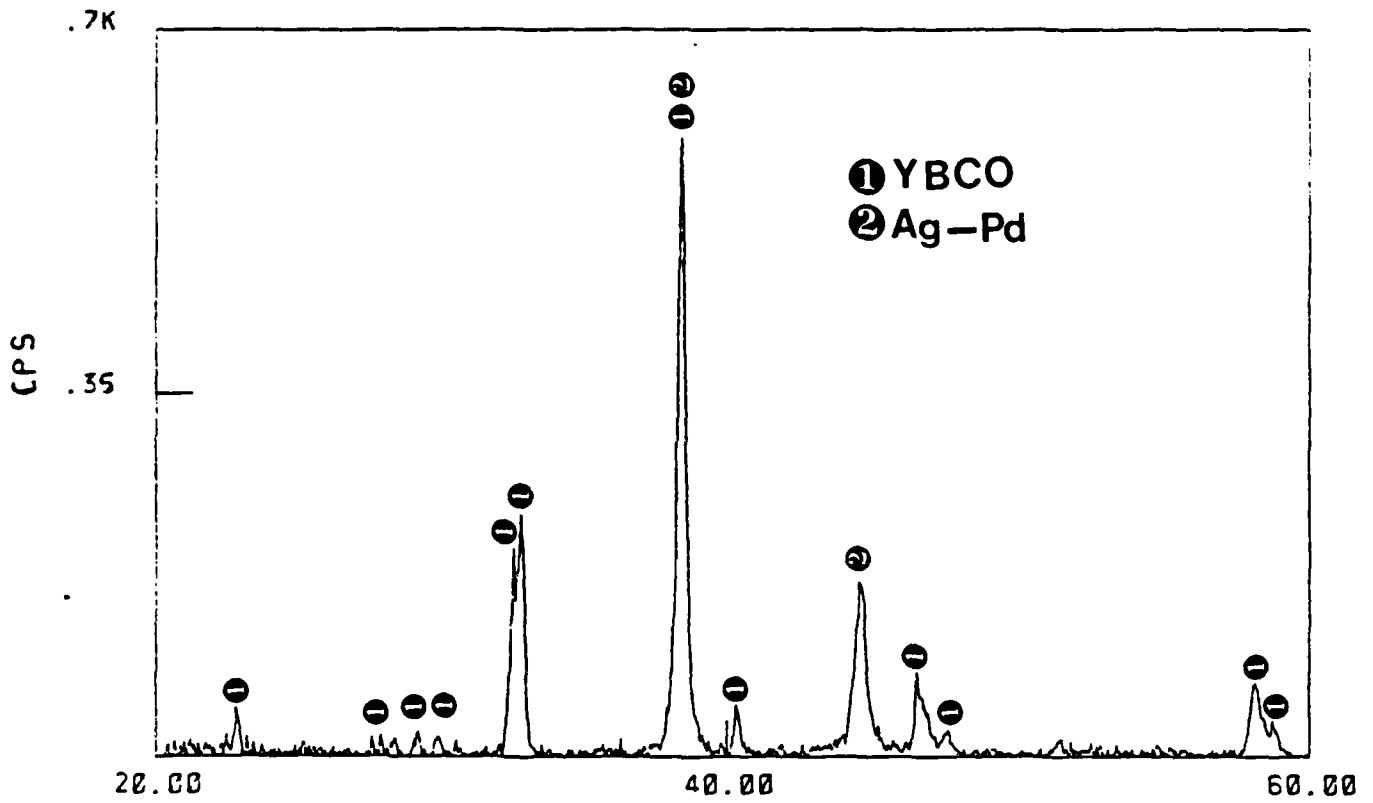


Figure 2.4.6 X-ray Diffraction Scan of Ag-Pd  $\text{YBa}_2\text{Cu}_3\text{O}_{7-\delta}$  Composite.

The oxygen anneal schedule for clad filaments was 30 min at 525°C similar to that used for unclad filaments. As shown in Figure 2.4.7, the silver coating was porous, aiding in diffusion of oxygen to  $\text{YBa}_2\text{Cu}_3\text{O}_{7-x}$  such that similar rapid annealing is possible.

#### 2.4.7 Fabrication of ribbon conductors

The construction of ribbon conductors involves sandwiching the silver treated  $\text{YBa}_2\text{Cu}_3\text{O}_{7-x}$  filaments between pre-tinned copper strips and reflowing the solder to bond the filaments to the copper. Lead-tin solders should be appropriate for cryogenic applications. High-Pb solders are used in conventional low temperature superconductors because of their superconducting as well as their mechanical properties. Low temperature strength studies of lead-tin alloys<sup>21</sup> indicate that the face centered cubic (fcc) structure of the lead phase remains ductile to cryogenic temperatures, while the body-centered cubic (bcc) tin phase loses ductility below 163 K. The exact temperature at which any particular alloy becomes brittle depends on the lead-tin ratio. A 50/50 lead-tin alloy, for example, becomes brittle below 123 K, while its ultimate tensile strength increases to 18,500 psi from 6000 psi at room temperature. Solders with a higher lead content become brittle only at successively lower temperatures. Lead-tin alloys with more than 80% lead remain ductile down to temperatures near absolute zero. Since the ribbon conductor will be used at 77 K, it is necessary to choose a solder that will remain ductile at that temperature. In this program, efforts have been centered around a Pb-Sn solder containing 95% lead, which has a solidus at 310°C and liquidus at 314°C. Another solder with 97.5% Pb, 1% Sn and 1.5% Ag is also under consideration. This solder has a eutectic temperature of 309°C.

---

<sup>21</sup> Jaffee, Minarcik, and Gonser, Met. Progr., December 1948, pp. 843-845; Kalish and Dunkerley, Trans AIME, 180, pp. 637-659, 1949. Cited in Solders and Soldering, H.H. Manko, McGraw-Hill Book Co., New York, 1979.



Figure 2.4.7 Morphology of Silver Coating.

Because it contains some silver, it is known to bond well to silver without leaching it from the substrate.

A solder with a high melting temperature has been chosen purposely. As the solder surrounding the  $\text{YBa}_2\text{Cu}_3\text{O}_{7-\delta}$  filament is cooling to room temperature (and then to 77 K for actual use) considerable compressive stresses will build up at the filament surface due to the higher thermal expansion coefficient of solder (29 ppm/°C) relative to the ceramic (11.5 ppm/°C). This thermal expansion mismatch is desirable since it places the ceramic filament in compression, creating an additional reinforcement by the principle of compressive pre-stress. In the first approximation, the magnitude of this pre-stress is proportional to  $(\alpha_{\text{solder}} - \alpha_{\text{YBCO}})E_{\text{YBCO}} T$ . Therefore, higher T provides higher compressive pre-stress.

Most of the commercially available clad metal strips must be custom ordered. To avoid the expense and time involved in custom ordering of the desired specially clad thin gage copper, initial experimentation was performed using small lengths of thick solder clad copper strips that were available from stock at Polymetallurgical Corporation in North Attleboro, MA. The thickness of the copper was 300  $\mu\text{m}$ , with a 95Pb-5Sn solder cladding 30  $\mu\text{m}$  thick. Since most of the silver treated filaments were of the large diameter (250 to 300  $\mu\text{m}$ ) used for sintering experiments, the available thickness of solder was insufficient. Extra 95/5 solder foil (125  $\mu\text{m}$  thick) was purchased from Arconium Alloys to make up the difference.

Reflow was attempted without the use of flux. Flux must be avoided in the presence of  $\text{YBa}_2\text{Cu}_3\text{O}_{7-\delta}$  since it is by intention, corrosive to oxides. It was quickly discovered that reflow in air (utilizing a slow heating rate) results in considerable blackening of the solder. Using an  $\text{N}_2$  atmosphere, the reflow was better but not satisfactory. The most successful experiment involved reflow in an atmosphere of 96%  $\text{N}_2$  + 4%  $\text{H}_2$ . An overheat temperature of 50°C was necessary to melt the solder.

Using resistance soldering to heat the composite (at very rapid rates of  $\approx 50^\circ\text{C/s}$ ) it was possible to reflow the solder in air without oxidation. However, control of the reflow operation was difficult in these crude benchtop experiments.

Small test specimens were fabricated by placing short lengths of surrogate filaments between the soldered faces of two pre-tinned strips. The solder was reflowed by heating the assembly in a furnace at  $400^\circ\text{C}$  for 15 min in a 96%  $\text{N}_2$  + 4%  $\text{H}_2$  atmosphere. Figure 2.4.8 shows the cross-section of a composite made using silver coated graphite as the surrogate filament. Composites were also made using Ni-Cr wire. These experiments demonstrate the feasibility of making composites with metallized filaments. Composites made with superconducting filaments were also prepared. Figure 2.4.9 shows an optical micrograph of the cross-section of one such composite. It can be observed that the solder flow was not uniform. Since there were no barriers to confine the molten solder, some of it flowed out of the composite, leaving behind cavities. This problem should be easily solved by using a copper channel instead of a strip as shown in Figure 2.4.10.

Some oxidation of tin near the solder-solder interface and solder-silver interface was observed. The EDS spectra from the bulk of the reflowed solder and from the solder-solder interface showed that tin has disappeared from the interface, possibly due to oxidation. This slight oxidation can be avoided by use of cleaner gas and rapid heating rates.

In the near future, scaling up of this process into a continuous operation will be accomplished using steel wires ( $50\ \mu\text{m}$  diameter) as a surrogate filament. Handy & Harman of East Providence, RI will fabricate a  $100\ \mu\text{m}$  thick, 5 mm wide pre-tinned copper strip with a  $50\ \mu\text{m}$  thick solder layer. A schematic of the planned setup is shown in Figure 2.4.11. Using the steel wire surrogate, development of both the mechanical aspects of the materials handling and coiling, and the appropriate reflow conditions can be

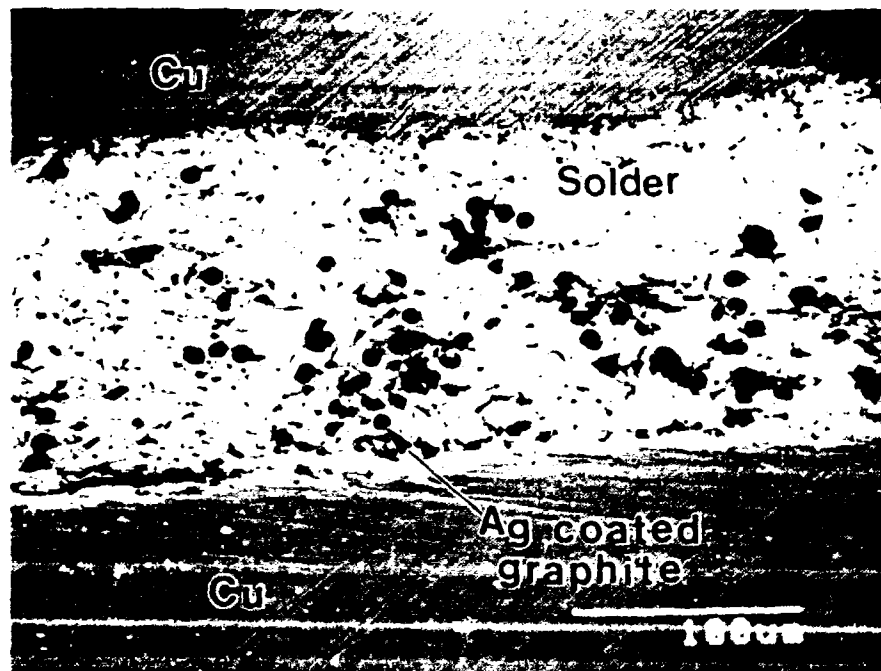


Figure 2.4.8 Composite Conductor with Surrogate Filaments.

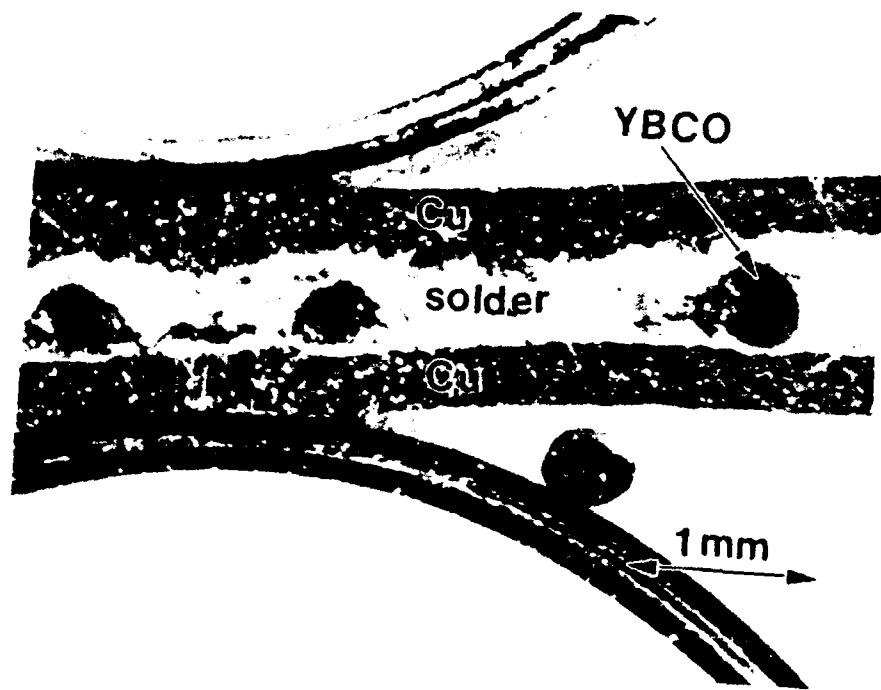


Figure 2.4.9 Cross-section of Composite Conductor with  $\text{YBa}_2\text{Cu}_3\text{O}_{7-\delta}$ .

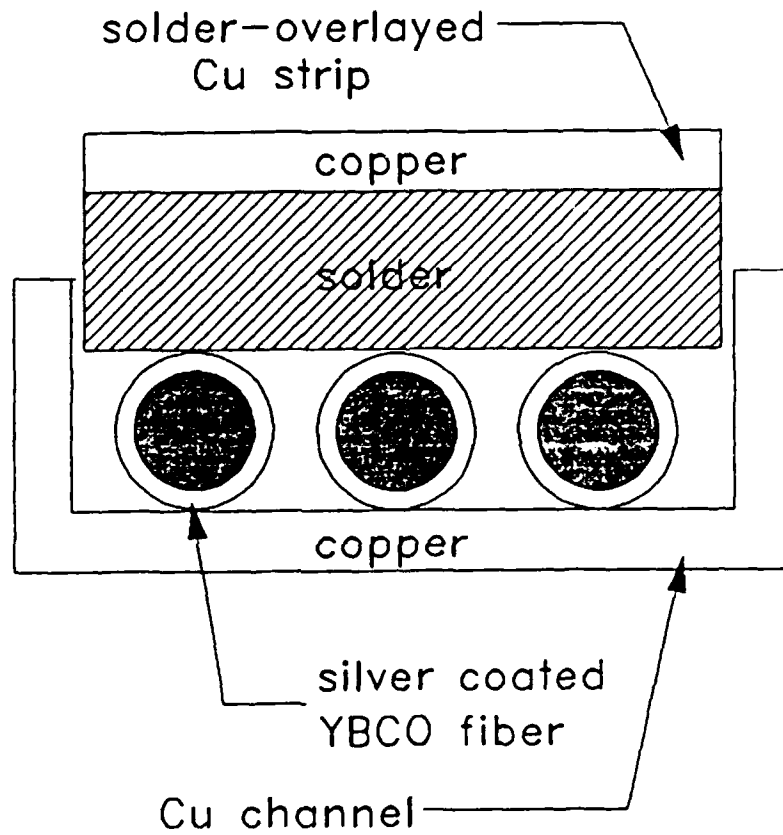


Figure 2.4.10 Assembly of Composite using Copper Channel.

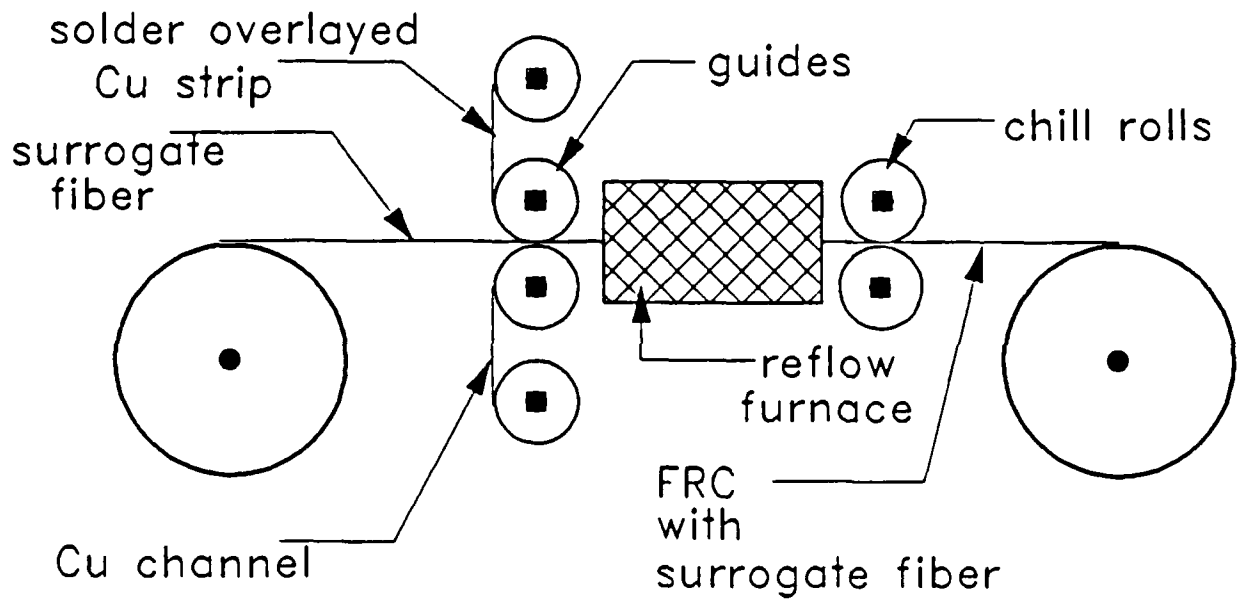


Figure 2.4.11 Set-up For Continuous Production of FRC with Surrogate Filament.

determined. This will form the prototype of a reflow cladding module. Initially, this module will be used to produce short specimens of  $\text{YBa}_2\text{Cu}_3\text{O}_{7-\delta}$  ribbon conductor for electrical evaluation, and later can be joined with the continuous belt sintering furnace to form a complete laboratory scale ribbon conductor facility.

#### 2.4.8 Metal cladding by electrodeposition

Activities in electrodeposition are at present underway in collaboration with outside experts. Dr. Lashmore is doing preliminary experiments with filaments supplied by CPSS. He is attempting to deposit aluminum from molten salts onto the filaments. He will also try to deposit copper from non-aqueous solutions (e.g., acetonitrile) of copper salts. If these preliminary experiments are successful CPSS will undertake a joint program with him to develop one of these methods into a continuous plating cell, modified from Dr. Lashmore's present cell to accept  $\text{YBa}_2\text{Cu}_3\text{O}_{7-\delta}$  filaments. This cell would serve as the plating module attached to the continuous sintering furnace.

Professor S. Bruckenstein at SUNY-Buffalo has been able to electroplate copper onto  $\text{YBa}_2\text{Cu}_3\text{O}_{7-\delta}$  from an aqueous solution. Prof. Bruckenstein is a DARPA awardee himself and has agreed to experiment with CPSS filaments. He will attempt to deposit copper on the filaments from the aqueous solutions. If the experiments are successful, they will open up a whole host of possibilities. Electroplating of copper from aqueous solutions is a known art and all the required engineering is commercially available. Even though  $\text{YBa}_2\text{Cu}_3\text{O}_{7-\delta}$  degrades in water, anodically polarized  $\text{YBa}_2\text{Cu}_3\text{O}_{7-\delta}$  in an alkaline pH is quite stable<sup>22</sup>. This suggests a possibility of passivating the surface of  $\text{YBa}_2\text{Cu}_3\text{O}_{7-\delta}$  before actual electroplating begins. A plating

---

<sup>22</sup> H. Bachtler, W.J. Lorenz, W. Schindler and G. Saemann-Ischenko, J. Electrochem. Soc., 135 (9) pp. 2284-2287

module could be obtained by modifying standard commercial wire plating equipment.

## 2.5 Electrical and Magnetic Characterization

### 2.5.1 Introduction

This section describes the methods and reasoning involved in the various electrical and magnetic measurements performed on  $\text{YBa}_2\text{Cu}_3\text{O}_{7-\delta}$  filament. The issues addressed as part of this work include weak link behavior, self field effects, selection of an appropriate criterion for  $J_c$ , flux creep at 77 K, and pulsed versus DC current sources for  $J_c$  measurements. Actual data will not be presented here except where necessary to illustrate a measurement technique or the effect of one of the above issues. Most of the  $J_c$  data have been presented in Sections 2.3 and 2.4. Preliminary information on the variability of  $J_c$  measurements and its consequences will be discussed.

### 2.5.2 Specimen preparation

Electrical measurements are made on "bare" (unclad) sintered filaments utilizing silver epoxy electrodes bonded to sputtered silver pads. The conductive epoxy attaches the filament to a printed circuit board, onto which the lead wires are soldered. The quality of the specimen mounting, as indicated by room temperature contact resistance, depends on the care with which the specimen is handled and mounted.

After sintering, fibers are placed in labeled plastic boxes that are stored in a desiccator. Samples are prepared for electrical testing by sputtering silver pads onto the bare filaments through a mask, attaching leads to the pads with silver epoxy and curing the epoxy overnight in air at 80°C. The four point contact includes two large current leads, covering several millimeters on each end of the filament, and two smaller voltage contacts. The center to center spacing of the silver pads used for voltage contacts is

4.1 mm. If room temperature contact resistance is excessive the specimen is rejected, and another filament from the same sample box is mounted. In most cases the second specimen is satisfactory.

### 2.5.3 Critical temperature

At present the critical temperature ( $T_c$ ) measurement is performed by immersing the fiber in a liquid nitrogen bath until temperature equilibrates and then monitoring the voltage output from a type K thermocouple (0.005" diameter wires) and from the filament as the filament warms on removal from the bath. The thermocouple voltage is fed directly into one channel of a two channel chart recorder and the filament voltage is passed through a Keithley 181 nanovoltmeter with the analog output from the voltmeter being fed into the other channel of the chart recorder. The excitation current is a DC 10 mA signal from a Keithley 228 voltage/current source. Figure 2.5.1 shows the intended instrumentation layout for future critical temperature measurements. These measurements will be carried out in a Janis liquid nitrogen cryostat with a variable temperature sample chamber, controlled and monitored by a Lake Shore Cryotronics model 805 temperature controller. Temperature will be monitored by a calibrated silicon diode, resulting in improved reliability and resolution (0.1 K) over the current thermocouple based system. In order to eliminate thermal voltages from the acquired data, the Keithley 228 current source will be programmed to produce a 5 Hz square wave of amplitude 10 milliamp. Voltage will be monitored by a Keithley 196 digital multimeter (resolution is 100 nanovolts and measurement speed is 125 ms). Both the temperature and voltage will be fed as digital data to a Keithley 570 data acquisition system. Using this system and the present sample geometry, the detection limit for resistivity will be  $10^{-8}$  to  $10^{-9}$   $\Omega$ -cm. This rather modest detection limit is both adequate and an improvement over the present system (detection limit approximately  $10^{-5}$   $\Omega$ -cm), that uses a more

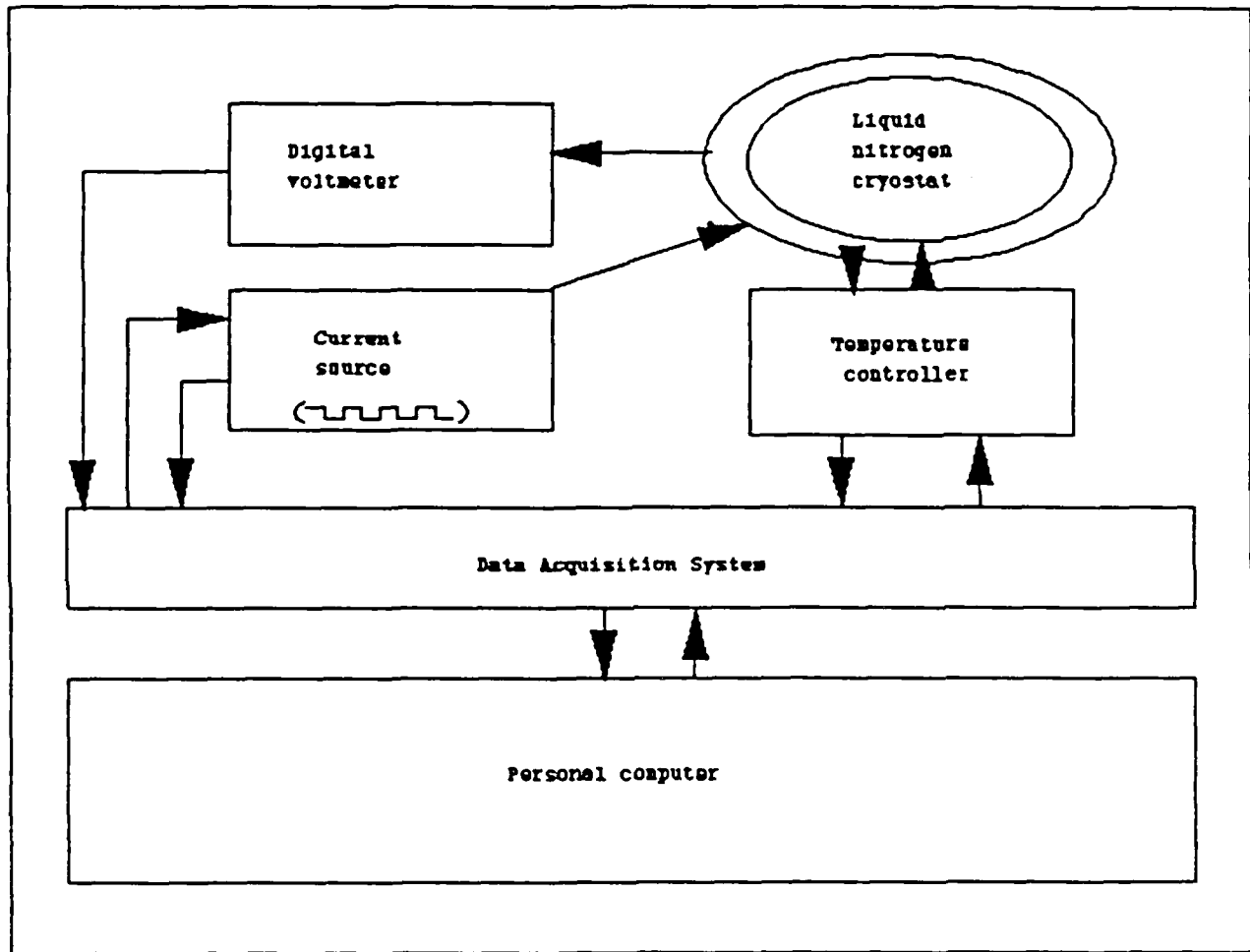


Figure 2.5.1

Proposed Instrumentation for Resistive Measurement of Critical Temperature of Superconducting Fibers.

sensitive voltmeter but can not take advantage of the sensitivity due to the lack of temperature control. These improvements, expected to be implemented during the next Quarter, will provide enhanced speed, reproducibility, reliability, and resolution to the resistive measurement of critical temperature.

#### 2.5.4 Critical current in zero applied magnetic field

##### 2.5.4.1 The error in previous $J_c$ data

Due to an incompatibility between instrumentation and measuring technique, the critical current densities listed in the final report for DARPA Contract N00014-87-C-0789 were in error. Those values are approximately an order of magnitude too high. The  $J_c$  data in the previous report was gathered by passing a 200 msec current pulse of the appropriate magnitude through the sample and measuring the voltage response with a Keithley 181 digital nanovoltmeter. The voltage was recorded on a chart recorder via the analog output of the voltmeter.  $J_c$  was defined as the current density that resulted in a one millivolt response. The current source and the fiber itself are easily able to respond to pulses of this duration in a stable and repeatable fashion. The error occurred because the settling time of the Keithley 181 nanovoltmeter is several seconds. As a result the voltmeter would average the response of the fiber over a time much longer than 200 ms, giving a reading that was roughly an order of magnitude too low. This problem was exacerbated by the high threshold voltage set as the  $J_c$  criterion and by the fact that the voltage was monitored via a chart recorder that had to wait for the voltmeter to convert its reading back to an analog signal before receiving an input. Table 2.5.1 shows the correct and incorrect data of some fibers as reported previously and as re-tested using the DC measurement described in the following paragraph. It should be noted that the large uncertainties presented in Table 2.5.1 result from choosing 1 milliamp current steps. The

TABLE 2.5.1

TABLE OF  $J_c$  VALUES AS MEASURED USING A 200 ms  
CURRENT PULSE VERSUS USING A STEPPED (DC) CURRENT SOURCE

Specimen	Erroneous Current Density From Pulsed Source (A/cm <sup>2</sup> )	Critical Current Density From DC Source (A/cm <sup>2</sup> )
24994E2	270(±180)	0
28737A2	440(± 40)	0
24994E1	200(± 50)	2(± 1)
28737A1	490(± 60)	2(± 1)
24996F1	180(± 60)	3(± 1)
28732E	900(± 40)	12(± 5)
28737B	490(± 50)	13(± 1)
24996A2	910(± 40)	24(± 5)
24994D2	900(±300)	25(± 5)
28757G2	920(± 70)	26(±10)
24996A1	1050(± 50)	28(± 5)
28758A	1180(± 60)	30(±10)
28757E1	1640(± 30)	32(± 5)
24996C1	1450(± 50)	57(±10)
28758B	1530(± 60)	58(± 5)
28732D2	1580(± 50)	67(± 5)
28732D1	1650(±100)	78(± 5)
24996C2	1340(± 60)	78(±10)
24994B1	2300(±100)	120(±10)
28732B1	2650(± 50)	140(±50)
24994C2	2500(±100)	150(± 5)

current instrumentation permits current steps as small as 0.1 milliamp thus providing smaller uncertainty should that become necessary.

#### 2.5.4.1 Present $J_c$ measuring technique

The revised  $J_c$  measurement technique is accomplished by ramping the source current in 1.0 milliamp steps, 10 seconds long. The 10 second step duration is sufficient time for all instrumentation to respond appropriately. Figure 2.5.2 is a scan of a typical  $J_c$  test which shows that the voltage has reached a steady state long before the onset of the next current step. Since the current requirements for these tests are an order of magnitude lower than was previously believed, joule heating of the fibers due to current passing through highly resistive contacts is not a problem. In addition to changing from a pulse to a DC measurement, the  $I_c$  criterion has been redefined to be the current giving rise to a signal of  $10^{-3}$  microvolt-centimeter, i.e., the voltage response multiplied by the cross-sectional area and divided by the length between voltage leads. Note that this value is the resistivity with the current neglected. Thus one can easily calculate the resistivity at the critical current once the critical current is known. For a typical fiber diameter, this criterion corresponds to a voltage signal of about one microvolt. Note also that a constant  $\mu\text{V-cm}$  criterion yields lower and lower resistivities as the critical current density increases. The CPSS criterion has been set at  $10^{-3} \mu\text{V-cm}$ , which yields a resistivity of  $10^{-8} \Omega\text{-cm}$  for an  $I_c$  of 100 mA and a  $1 \mu\text{V}$  signal.

Actual analysis of the raw data is complicated by several non-idealities in the V-I raw data that make detection of the circa  $1 \mu\text{V}$  signal more difficult. This is illustrated in Figure 2.5.3 which shows the V-I data for two particular filaments. In Figure 2.5.2 the flatness of the steps show that the voltage response has reached steady state. In one case, the raw data does not pass through the origin, but has a DC bias, presumably due to emf

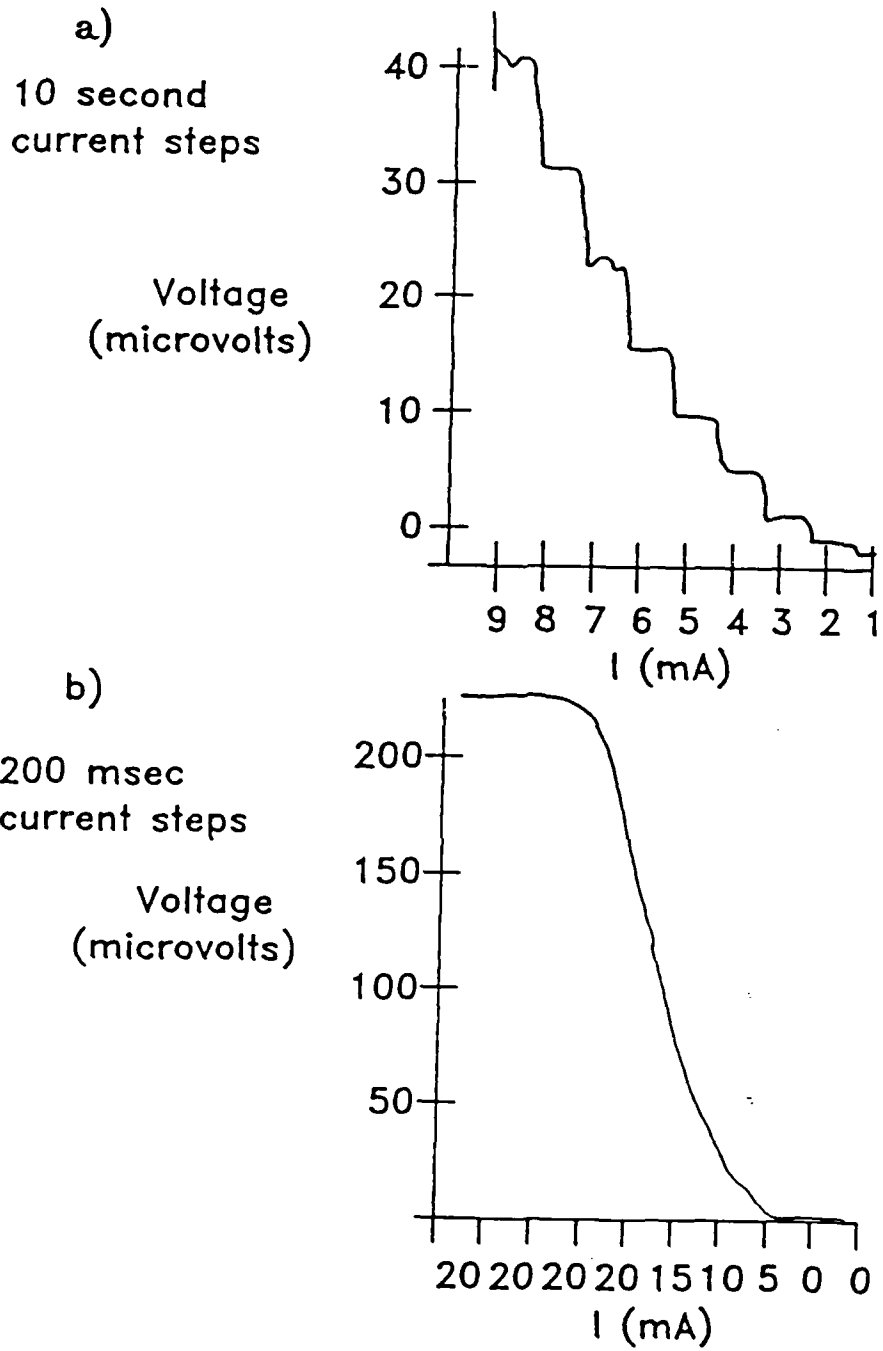


Figure 2.5.2 V-I Data from a Typical  $J_c$  Test.

generated in the leads or elsewhere in the measurement circuit. There is also some drift in voltage in the low current region, which is considered to be an artifact. These errors are removed by constructing a baseline, as shown in Figure 2.5.3. The  $I_c$  is determined by constructing a line parallel to the baseline, offset by the appropriate voltage criterion. Critical currents can be determined with confidence only for specimens with "well behaved" V-I curves, such as shown. Samples with excessive baseline drift or scatter are rejected.

In addition to improvements in defining the  $J_c$  transition and in providing a useable current source, other modifications to the testing procedure are planned. These include the use of the temperature controlled environment in the cryostat and the introduction of the computer controlled data acquisition system mentioned in the previous section. As the development of superconducting wire progresses, it is expected that it will be necessary to describe the departure from the zero resistance state with greater resolution, since the low  $T_c$  industry generally quotes resistivities of  $10^{-12}$  to  $10^{-14}$   $\Omega$ -cm for its products. Assuming a  $J_c$  of  $10^4$  A/cm<sup>2</sup> and a 1  $\mu$ V signal, measurement of resistivities would require a length between voltage leads of 1 to 100 m. This could be accomplished by wrapping the wire into a coil shape before testing (a 100 m wire wrapped into a 5 cm diameter coil would generate 100 gauss when 1 amp ( $J_c=10^4$  A/cm<sup>2</sup>, diameter = 200  $\mu$ m) is passed through it). It is possible to see a resistivity of  $10^{-12}$   $\Omega$ -cm using the present measuring geometry if the voltmeters are used at the limit of their sensitivity ( $10^{-7}$  V) and  $J_c$  is  $10^5$  A/cm<sup>2</sup>.

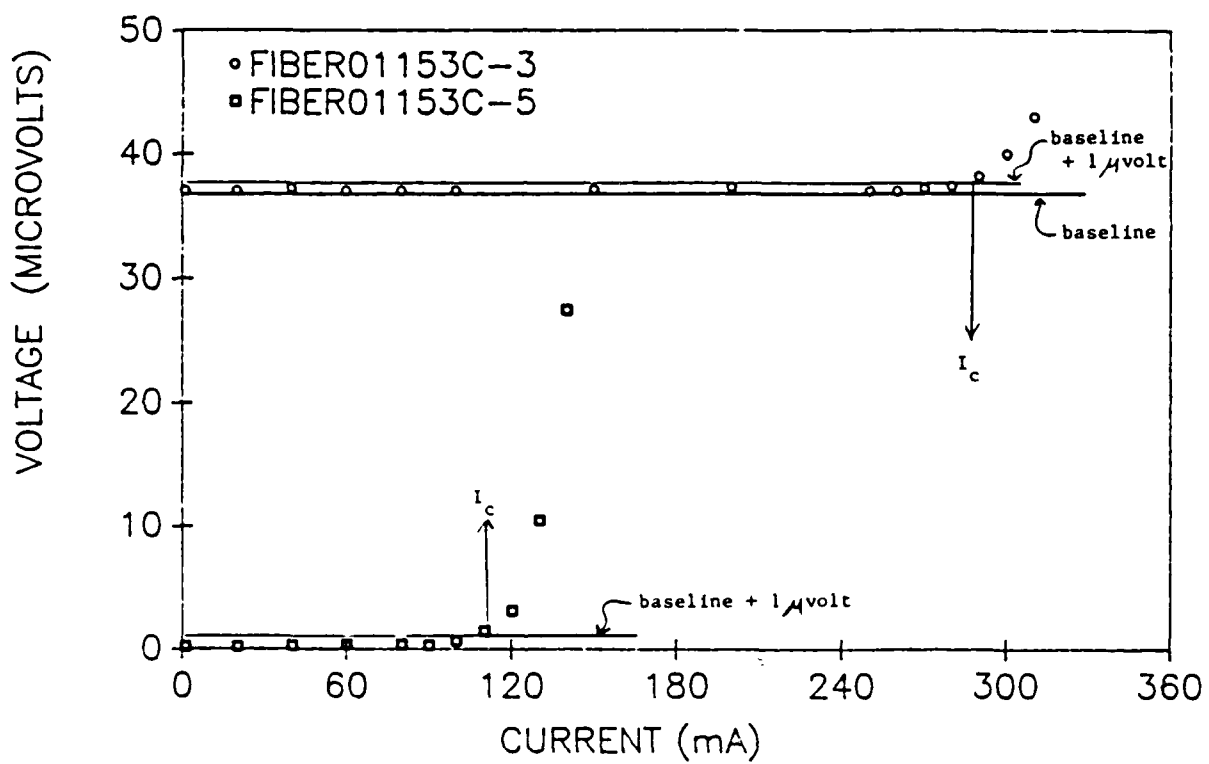


Figure 2.5.3

Voltage-Current Raw Data for Two  $\text{YBa}_2\text{Cu}_3\text{O}_{7-\delta}$  Filaments, Illustrating Method of Determining Critical Current.

#### 2.5.4 Self Field Effects

It has been well established<sup>23</sup> that low  $J_c$   $\text{YBa}_2\text{Cu}_3\text{O}_{7-\delta}$  bulk samples have weak link dominated superconducting transport behavior. Measurements of  $J_c$  in a magnetic field (see the following section) show CPSS materials to be no exception. The sensitivity of a weak link material to magnetic fields raises the possibility of an artifact in critical current determinations, since the flow of the measuring current itself creates a small magnetic field. This magnetic field is the "self field" and depends both on current and geometry. The critical current of a particular weak link (e.g., a grain boundary) depends both on current and magnetic field. The ambiguity that this creates can be illustrated by considering two end member cases. In the strict absence of magnetic field, a weak link can be driven normal if the current approaches a critical value associated with the intrinsic zero field critical current of that weak link. On the other hand, at any sub-critical value, the weak link can be driven normal by applying a magnetic field that exceeds the critical field of that weak link. For the "self field" limited case, the magnetic field generated by the measuring current in the sample exceeds the critical field of the weak link, and a voltage is generated. The "critical current density" calculated from such a test represents a self field limited case, and is lower than the zero field, or intrinsic weak link critical current.

Recent reports (see Stephens<sup>24</sup>) have shown these self field effects in weak link oxide superconductors to be significant. Since the magnitude of the self field is determined in part by the geometry of the sample, measurements of  $J_c$  on these types of samples are not representative of

---

<sup>23</sup> R.L. Peterson and J.W. Ekin, Phys. Rev. B37 (1988) p. 9848

<sup>24</sup> R.B. Stephens, "Critical Current Limitations in Ceramic Oxide Superconductors," General Atomics, PO Box 85608, San Diego, CA 92138-5608, to be published in *Cryogenics*.

the intrinsic current carrying properties of the material. Therefore care must be taken to insure that all weak link materials be tested in a geometry that yields a self field less than the critical field of the weak links. Experiments reported by Stephens, based on calculations by Peterson and Ekin<sup>23</sup>, show that the critical field for the weak links is dependant on the grain size and is in the range of 4 to 25 gauss for grain sizes of 10 to 1  $\mu\text{m}$ , respectively. The self field for a cylindrical fiber can be calculated from

$$H_s = \pi d J / 10$$

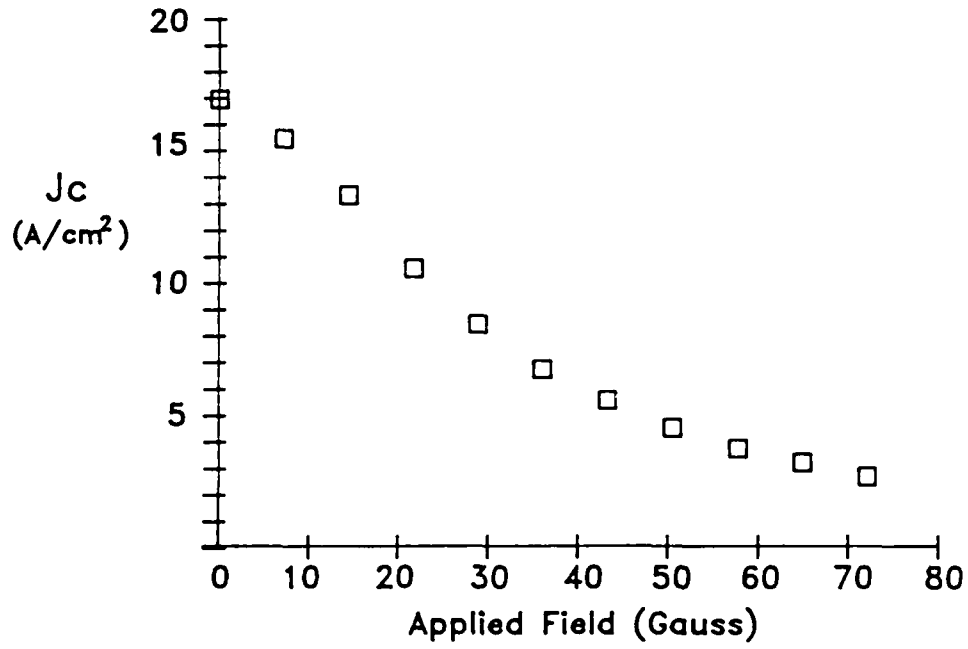
where  $H_s$  the self field in gauss,  $d$  is the fiber diameter in cm and  $J$  is the current density in  $\text{A}/\text{cm}^2$ . Using data from sample 01153-C3 (the highest  $J_c$  sample produced at CPSS to date,  $J_c = 792 \text{ A}/\text{cm}^2$  and  $d = 0.022 \text{ cm}$ ) results in a self field of 5.4 gauss. Any grain boundaries of length greater than about 8  $\mu\text{m}$  will be driven normal by a self field of this magnitude.

There are two complicating factors that affect the distribution of grain boundary lengths in CPSS fibers. The first is the morphology of a typical  $\text{YBa}_2\text{Cu}_3\text{O}_{7-\delta}$  grain. Due to its anisotropic growth rates, these grains tend to grow as plates, where the thickness of the plate is parallel to the c-axis and is about a factor 3 to 5 times less than either the width or breadth of the plates (see Section 2.3 for a more detailed discussion of the filament microstructure). Since the grains in CPSS fibers are randomly oriented at present, this results in a bimodal and possibly trimodal distribution of weak link lengths. In addition to the anisotropic morphology of the individual grains, there is evidence that the fibers undergo an incomplete secondary grain growth so that there may be a bimodal distribution of grain sizes with one mode at about 10  $\mu\text{m}$  and the other mode at one micron or less. This results in another bimodal grain boundary length distribution overlaying the anisotropic morphology driven distribution. For each junction length abundant enough to create a percolative path there will be current sufficient to suppress the measured  $J_c$  due to self field effects. A self

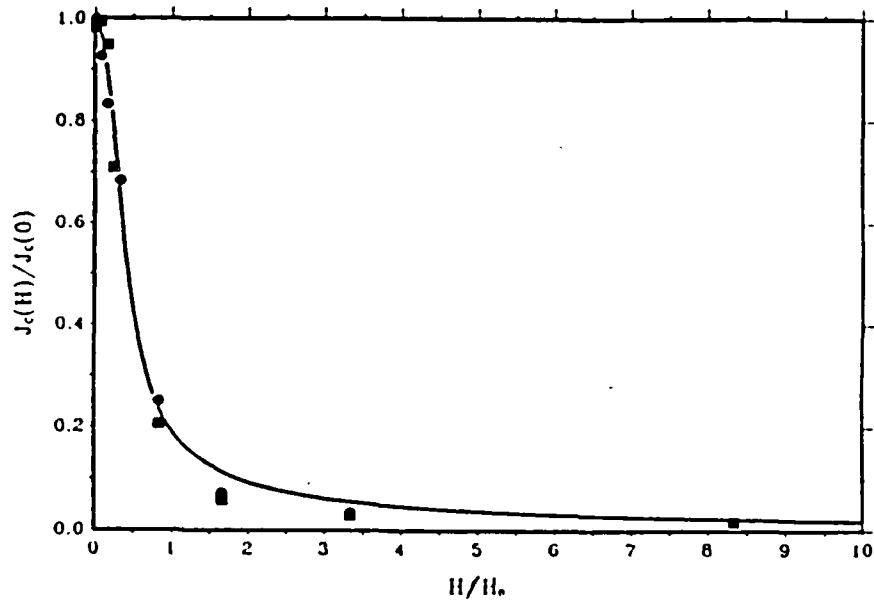
field of 5 gauss would be sufficient to drive grain boundaries with lengths greater than about 8  $\mu\text{m}$  normal, thus shunting the superconducting current to paths containing junctions of smaller length and thereby increasing the effective current density in those paths. Assuming that Josephson junction lengths are set by the length of the longest grain edge participating in the grain boundary, there is microstructural evidence to suggest that higher  $J_c$  values are being affected by self field limitations. Further microstructural analysis needs to be done to characterize the extent of this problem. It should be noted that a properly textured fiber would have the longest grain boundary parallel to the fiber axis and so would not affect current transport.

#### 2.5.5 Critical current density in a magnetic field

As mentioned previously, critical current density measurements have been performed on some CPSS fibers in the presence of a magnetic field. The measurements were carried out at the Francis Bitter National Magnet Laboratory. Figure 2.5.4A is a plot of  $J_c$  versus  $H_{\text{applied}}$  obtained on sample 28764B3. The applied magnetic fields necessary to carry out this experiment were quite low such that the stray field at the lab proved to be significant. Stray field was partially compensated for by passing sufficient current through the cooled sample to render it in mid-transition. It was then placed in the magnet with the fiber axis perpendicular to the magnet axis, and the current through the magnet was adjusted such that the voltage across the sample was minimized. This had the effect of canceling about 14 gauss of stray field oriented normal to the fiber axis. There was presumably a component of stray field perpendicular to both the magnet and fiber axes which did affect the  $J_c$  of this sample. This lends some uncertainty to the absolute value of the applied field in the experiment, but should not disguise the presence of weak links in the fiber. Figure 2.5.4B is reproduced from Peterson and Ekin<sup>23</sup> and contains a calculated curve for the field dependence



a)



b)

Figure 2.5.4

A)  $J_c$  versus  $H_{\text{applied}}$  for a  $YBa_2Cu_3O_{7-\delta}$  Filament,  
 B) Calculated Weak Link  $J_c$  versus  $H_a$  Relationship from  
 Peterson and Ekin.

of the critical current density of weakly linked superconductors. It is clear that the CPSS fiber follows this behavior. This particular fiber had a zero field  $J_c$  of approximately 20 A/cm<sup>2</sup>, a factor of 40 times less than that of the best CPSS fiber. The higher  $J_c$  fibers have not yet been measured in a magnetic field but since they are untextured it is expected that they are weakly linked.

#### 2.5.6 Reproducibility of critical current density data

In addition to the recent attention to the nature of  $J_c$  in weak-linked materials, there have been statistical studies on the reproducibility of experimentally determined values of critical current density. Kimura and co-workers<sup>25</sup> have reported results of round robin tests using a point technique, with a one microvolt/cm voltage criterion. The variation in results was remarkable. Within each laboratory, specimen-to-specimen varied by as much as 40%. Tests were repeated over a 40 day period, with some laboratories observing a dramatic decrease in  $J_c$ , while others observed a modest increase in  $J_c$  with time. Overall, about 100 measurements on dozens of "identical" specimens yielded an average  $J_c$  of 215 A/cm<sup>2</sup>, with a standard deviation of 21 A/cm<sup>2</sup>. The values ranged from a low of 145 to a high of 256 A/cm<sup>2</sup>. It is note-worthy that the laboratory-to-laboratory variation in the average  $J_c$  is similar to the specimen-to-specimen variation within each laboratory. This suggests that details of the measurement technique, while important, are not dominant.

Currently, reproducibility of transport critical current density measurements being performed at CPSS is being more aggressively addressed. In the past, repeated measurements on nominally identical samples had not been

---

<sup>25</sup> Y. Kimura, N. Higuchi, S. Meguro, K. Takahashi, K. Uyeda, T. Ishihara, E. Inukai, and M. Umeda, "Round Robin Tests of  $T_c$  and  $I_c$  on  $YBa_2Cu_3O_{7-\delta}$ ," manuscript submitted to ISS'88, Nagoya, Japan August 1988

emphasized. The data had sometimes suggested good reproducibility, and other times indicated widely scattered results. Repeated  $J_c$  determinations on a particular mounted filament typically exhibit good reproducibility. Two or more nominally identical filaments mounted and measured separately sometimes exhibit widely scattered  $J_c$  values. Unfortunately, it is impossible to demount a particular filament so that it can be re-mounted and measured again, as the filament would be destroyed in an attempt to remove the silver epoxy electrodes. To begin a more serious examination of variability, a group of six filaments was sintered and annealed under identical conditions, electroded, and measured. This group received four zone passes using a peak temperature of 935°C (specimen number 01153C). The critical current data for these samples appear in Table 2.5.2. The individual values ranged from 263 to 792 A/cm<sup>2</sup>, with a mean of 542 A/cm<sup>2</sup> and a standard deviation of 193 A/cm<sup>2</sup>, which suggest considerable scatter<sup>26</sup>. These preliminary findings indicate that specimen-to-specimen variation is significant, similar to that reported by Kimura, et al. Heat treatment experiments are now being performed using larger numbers of fibers, to generate samples consisting of many "identical" filaments. This subject is being vigorously pursued, and will be discussed in the next report.

This series of "identical" filaments provides an opportunity to compare the reproducibility of the voltage-current characteristic of individual specimens. Figure 2.5.5 compares the raw V-I data for the filaments in this series, taken well into the normal region. With the exception of the low current filament, the gross forms of the V-I curves are similar.

---

<sup>26</sup> For the present we interpret the differences between filament as scatter. Note, however, that  $J_c$  seems to decrease systematically as filament diameter increases (except for specimen 01153C-5). It is too early to tell if this is a trend or a coincidence. The database is being searched for similar correlations.

TABLE 2.5.2  
 CRITICAL CURRENT VARIATION  
 FOUR ZONE PASSES AT 935°C

SPECIMEN	$I_c$ (Amp)	FILAMENT DIAMETER ( $\mu\text{m}$ )	CRITICAL CURRENT DENSITY ( $\text{A}/\text{cm}^2$ )
01153C-2	0.29	235	600+/-2
01153C-3	0.29	216	792+/-2
01153C-33	0.29	279	475+/-2
01153C-4	0.29	252	581+/-2
01153C-5	0.11	231	263+/-2
		mean	542
		std. dev.	193

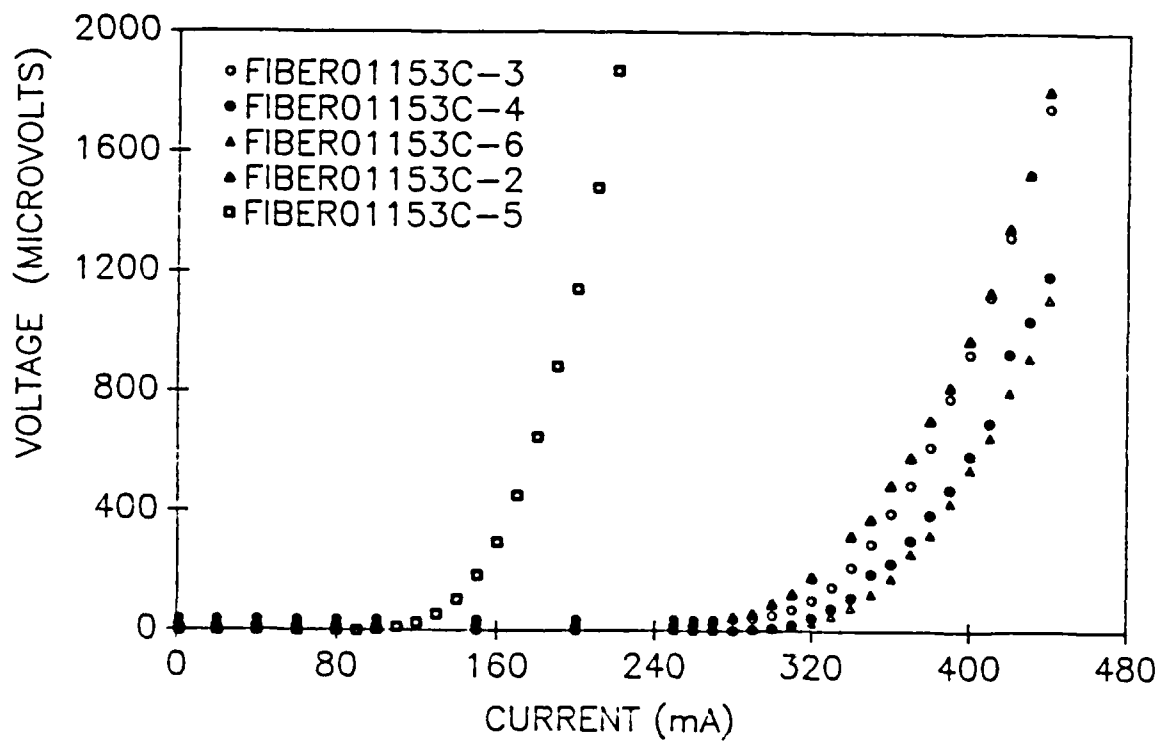


Figure 2.5.5

V-I Data for Five Nominally Identical Filaments.

The significance of variation in critical current density

Preliminary results of this work, and the extensive study by Kimura et al., show that experimental  $J_c$  data is widely scattered for  $\text{YBa}_2\text{Cu}_3\text{O}_{7-\delta}$  in the weak link mode. It is possible that this merely reflects non-reproducibility in the measurement technique. The results may be very sensitive to details of the electroding method or some other area of technique. Currently, a conscious effort is being made to be as consistent as possible, thereby removing any random errors which might be responsible for the scatter. However, it is not too early to suggest the possibility that the variation is not a result of experimental error, but rather reflects a true variation in the property itself. These represent two distinct cases, and demand significantly different experimental protocols. The difference depends on the nature of the weak link critical current density itself.

In one case, the weak link  $J_c$  has a definite value. The value may be dependent upon processing and structure, but it is presumed that for a given structure, there is a particular single value of  $J_c$ . An experimental measurement provides an estimate of this value, distorted perhaps by random and systematic errors. By minimizing these errors, one can obtain more accurate estimates of  $J_c$ . Scatter in experimental values indicates either random measurement errors, or the existence of uncontrolled processing variables that change the structure of individual specimens, and therefore the property. The appropriate action is to conduct all procedures under more carefully controlled conditions, so that the true value of  $J_c$  can be discovered.

On the other hand, the weak link  $J_c$  may be a distributed property, for which there is no definite value. In this case, greater pains taken in processing and measurement may not remove the scatter from the  $J_c$  data. Here, the scatter is not the fault of the experimenter, but is rather the nature of the property itself. An analogy might be drawn to the mechanical strengths of

brittle materials, which are inherently scattered. Strength is a distributed rather than a single valued property because it is governed by the most severe flaw (or mechanical weak link) which obeys extreme value statistics. It is the worst flaw that makes a brittle specimen break, not the typical flaw. Strength distribution reflects the distribution of the worst flaw and as such need not be related in any way to the distribution function for the most populous flaws. The latter is described by central value statistics, while the former defines the extreme value statistics.

It is plausible to consider that a polycrystalline specimen may have transport properties that depend more on the "weakest" weak link boundary than the "typical" weak link boundary. One can envision a polycrystalline specimen as a multiply interconnected network of weak links in series and parallel connections. As current and/or magnetic field increases, the weaker links begin to go normal and shut off. Current then concentrates on the remaining "on" links, forcing some of them to go normal, and so on, in a sort of an avalanche. Thus the behavior of the entire specimen might be governed by a small fraction of "weakest" links; a situation for which extreme value statistics are appropriate. Variability is inherent in such cases.

Clearly, if weak link  $J_c$  is indeed an extreme value problem, the present experimental program, which involves a feedback loop of processing versus  $J_c$ , must be modified. At the least, the cost of this activity would be increased, since one now needs to evaluate a statistically large set of samples for each processing condition. On the other hand, it might be advisable to de-couple the processing from  $J_c$  measurements. This would allow the wire process development to continue without feedback on  $J_c$ , while re-channeling resources to a different HTSC material, such as thallium-2223, which potentially can be prepared as a non-weak linked polycrystal.

## 2.6 Summary

During this first Quarterly period, substantial progress has been made on the composite wire manufacturing task. Although each step in the process is still being carried out discretely, some of the batch processes will be replaced with continuous processes in the near future. By the end of the next Quarter, CPSS expects to be focussing on continuous green fiber spinning, experimenting with a continuous heat treatment, and setting up the prototype of a continuous cladding module.

The conductor design philosophy that guides the approach to fabricating flexible HTSC conductors has been refined. The simple metal clad monofilament concept has been expanded to a multifilament array in the form of a ribbon conductor. Preliminary models have been formulated to predict the allowable bending radius and tensile loads, as related to filament size, cladding thickness, and residual stress state.

A number of commercially available  $\text{YBa}_2\text{Cu}_3\text{O}_{7-\delta}$  powders were evaluated, but no satisfactory source was found. One lot of commercial powder from Rhone-Poulenc proved to be suitable for spinning and also highly sinterable, but it contained excess copper oxide which probably degrades the  $J_c$ . This source has also been unreliable, as follow-on orders were not filled. Much effort went to scaling up in-house powder production of highly phase pure  $\text{YBa}_2\text{Cu}_3\text{O}_{7-\delta}$  powder. Current production rates are adequate to support the development program. An effort is underway to determine the influence of powder characteristics on fiber spinning and sintering, and to optimize the powder production for the needs of the wire manufacturing.

There has been a significant improvement in capability to produce green fiber. In collaboration with AIResCo, a method to melt spin green fiber with high loadings of ceramic powder has been successfully developed. This melt spinning process will probably replace the dry spinning method previously used, since it offers many advantages for manufacturing. The change will be

based upon success with melt spinning barium titanate fibers at solids loadings up to 50 vol%. This fiber has been made in continuous spools of lengths up to 0.25 km, limited only by the small size of experimental batches. The melt spun fiber appears to have favorable binder burnout characteristics. The decision to adopt melt spinning is contingent on successful replacement of the barium titanate surrogate with  $\text{YBa}_2\text{Cu}_3\text{O}_{7-\delta}$  powder. If successful, the continuous spools of  $\text{YBa}_2\text{Cu}_3\text{O}_{7-\delta}$  green fiber will provide the feedstock for developing continuous sintering and annealing processes.

A radiant heat belt furnace has been identified for sintering the continuous fiber arrays. The temperature-time profile for this furnace has been modeled on the results of short fiber heat treatment experiments. The short fiber experiments have also been used for preliminary establishment of the relationship between heat treatment and  $J_c$ . It was found that critical current densities could not be simply correlated to zone sintering conditions, since the relationships are obscured by scatter in the  $J_c$  data. Further observations were made on microstructure development, primarily for the CuO-excess Rhone-Poulenc powder. Preliminary results on rapid oxygen intercalation anneal suggest that filaments may be successfully restored to the superconducting state by a 15 min isothermal anneal at 525°C. In air at the same temperature, anneals must be longer than two hours.

A new cladding concept was developed involving silver-treating the surfaces of  $\text{YBa}_2\text{Cu}_3\text{O}_{7-\delta}$  filaments to promote wetting by solders, and bonding the filaments to copper ribbons by a solder reflow process. This method offers significant advantages over previous electrodeposition concepts. The surface treatment presently involves a thin layer of silver on the  $\text{YBa}_2\text{Cu}_3\text{O}_{7-\delta}$  surface. Most efforts were aimed at developing the silver treatment and cofiring processes. Early ribbon specimens were fabricated with the reflow method using either a few  $\text{YBa}_2\text{Cu}_3\text{O}_{7-\delta}$  filaments or graphite fiber (as a

surrogate). Electrodeposition methods were investigated out-of-house in collaboration with experts in the field.

An improved  $J_c$  measurement technique for the sintered filaments has been developed. Erroneous data from previous work was corrected, and a database of processing conditions versus  $J_c$  is in the process of being constructed. The highest critical current density determined for a  $\text{YBa}_2\text{Cu}_3\text{O}_{7-\delta}$  filament was  $792 \text{ A/cm}^2$ . Examination of the repeatability of  $J_c$  data, to determine if the scatter is due to handling technique or specimen-to-specimen variability has begun. Magnetic field effects were characterized, demonstrating that the  $\text{YBa}_2\text{Cu}_3\text{O}_{7-\delta}$  filaments are limited by weak links. An attempt was made to determine the influence of "self field" on the critical current density data.

## SECTION 3

## HIGH TEMPERATURE SUPERCONDUCTING MOTOR DESIGN AND FABRICATION

This program began before the actual contract was in hand, under authorization from ONR for Ceramics Process Systems to begin "at risk." CPS chose to begin the wire manufacturing task, but delayed the start of the subcontract with Emerson Electric Company until after receipt of the contract. Consequently, there were no research activities at Emerson Motor Division (EMD) during this report period. The Emerson subcontract and the HTSC motor design activities will begin during the Second Quarter of this program. This section presents a brief review of the initial development plans. The detailed work plans were included in Section 1.

In the next Quarter, EMD will begin research on the design, building, and testing of HTSC motors, and related engineering activities. The first activity will be to consider a broad range of applications and design philosophies for these machines, taking into account what is now known about HTSC materials. Although a specific machine has not yet been identified, a small integral horsepower motor (up to 50 hp) is favored. The application study will consider a number of characteristics of the machine, including:

1. Target power density and specific power
2. Load torque
3. Speed characteristics
4. Starting performance
5. Acceleration with load
6. AC loss during high starting currents
7. Mechanical forces on the windings during starting and acceleration

A variety of traditional and novel superconducting motor designs is under consideration. It is essential that the motor design philosophy respect the engineering properties of the (yet to be made) HTSC wire. At present, too many key properties of the HTSC are still unknown. For  $\text{YBa}_2\text{Cu}_3\text{O}_{7-\delta}$  in a weak-link limited mode, the current density drops so rapidly

with magnetic field that it is not possible to determine the optimum design values of current,  $I$ , and air gap flux density,  $B$ , associated with a particular torque value. The AC properties of high temperature superconductors must be characterized to predict behavior in time-varying magnetic fields. Mechanical issues in motor design will be addressed to determine how the wire can be wound, the allowable tension during winding it can withstand, and its susceptibility to mechanical shocks. This requires actual wire samples to be tested, and the testing must be done before machine designs can proceed in detail. Bearing designs will be considered for a machine with room temperature bearings, cryogenic bearings, and superconducting magnetic bearings.

During the next Quarter CPSS and EMD researchers and their consultants will meet to define a set of anticipated materials properties. This database, representing the current best information, will be used to generate design guidelines. Priorities will be defined for characterizing properties, and the database will be continually updated.

Using these guidelines, several design concepts will be evaluated. As wire becomes available, proof-of-principle machines will be built and tested under low stress conditions to evaluate promising designs. Feedback on wire properties will be used to upgrade performance of the conductors. In the third year of the program, functioning models of motors will be built and tested under realistic service conditions.

## SECTION 4

## GENERAL DISCUSSION AND SUMMARY

Work began on the wire manufacturing task during this first Quarterly Period, involving research activities at CPS Superconductor Corporation (CPSS) and Albany International Research Company (AIResCo). Initiation of the HTSC motor design activity at Emerson Motor Division (EMD) was postponed until the second Quarterly Period, due to a delay in obtaining the ONR contract.

Substantial progress has been made in the composite wire manufacturing task. Although each step in the process is currently being carried out discretely, several of the batch processes are about to be replaced with continuous processes. During the next Quarter, continuous green fiber spinning, experimenting with a continuous heat treatment, and setting up the prototype of a continuous cladding module will be the focus of the research activities.

The concepts for design and fabrication of flexible HTSC conductors have been refined. Instead of a simple metal clad monofilament, a multifilament array in the form of a ribbon conductor is now favored by CPSS. Preliminary models for predicting the allowable bending radius and tensile loads have been developed to guide the choice of filament size, cladding thickness, and necessary residual stress state.

A number of commercially available  $\text{YBa}_2\text{Cu}_3\text{O}_{7-\delta}$  powders were evaluated as potential raw material sources, but no satisfactory source could be identified. Much effort went to scaling up in-house production of highly phase pure  $\text{YBa}_2\text{Cu}_3\text{O}_{7-\delta}$  powder, and consequently, current production rates are adequate to supply the development program. The influence of powder characteristics on fiber spinning and sintering is now being studied in an effort to optimize the powder for wire manufacturing.

During this Quarter, most fibers were prepared using Rhone-Poulenc powder. This material was suitable for spinning and was highly sinterable, but contained excess copper oxide.

Research at AIResCo has led to development of a method which can successfully be used to melt spin green fiber with high loadings of ceramic powder. The melt spinning process has many advantages over dry spinning, which will probably be abandoned if the early success with melt spinning barium titanate at solids loadings up to 50 vol% can be duplicated with  $\text{YBa}_2\text{Cu}_3\text{O}_{7-\delta}$ . Melt spun fiber has been made in continuous spools of lengths up to 0.25 km, limited only by the small size of experimental batches. The melt spun fiber appears to have favorable binder burnout characteristics. Continuous spools of  $\text{YBa}_2\text{Cu}_3\text{O}_{7-\delta}$  melt spun green fiber should be prepared early in the next Quarter. This material will be the feedstock for continuous sintering development.

A radiant heat belt furnace has been identified for sintering the continuous fiber arrays. The temperature-time profile for this belt furnace has been modeled on the results of short fiber heat treatment experiments. The short fiber experiments were also aimed at establishing a relationship between heat treatment and  $J_c$ . Critical current densities could not be simply correlated to zone sintering conditions, since the relationships are obscured by scatter in the  $J_c$  data. Further observations were made on microstructure development, primarily for the CuO-excess Rhone-Poulenc powder. Preliminary results on a rapid oxygen intercalation anneal suggest that filaments may be successfully restored to the superconducting state after a 15 min isothermal anneal at 525°C.

A new cladding concept was developed. This method is based upon a technique to treat the surfaces of  $\text{YBa}_2\text{Cu}_3\text{O}_{7-\delta}$  filaments to promote wetting by solders, so that the filaments may be bonded to copper ribbons by a solder reflow process. This method offers significant advantages over previous

electrodeposition concepts, and so was vigorously pursued. The surface treatment presently being used involves treating the  $Y_2Cu_3O_{7-\delta}$  with a thin layer of silver, and cofiring the  $YBa_2Cu_3O_{7-\delta}$  with the silver. Early ribbon specimens were fabricated with the reflow method using  $YBa_2Cu_3O_{7-\delta}$  filaments (or graphite fiber as a surrogate). Electrodeposition methods were investigated out-of-house in collaboration with experts in the field.

An improved  $J_c$  measurement technique for the sintered filaments was established using DC current increased in a stepwise fashion. Erroneous data from previous work was corrected, and a database of processing conditions versus  $J_c$  was constructed. The highest critical current density determined for a CPSS  $YBa_2Cu_3O_{7-\delta}$  filament was  $792 \text{ A/cm}^2$ . CPSS has begun to examine the repeatability of  $J_c$  data, to determine if the scatter is due to handling technique or specimen-to-specimen variability. Magnetic field effects were characterized, demonstrating that the  $YBa_2Cu_3O_{7-\delta}$  filaments are limited by weak links. An attempt was made to determine the influence of "self field" on the critical current density data.

## APPENDIX 1

SUMMARY OF FINAL REPORT OF ONR CONTRACT NUMBER N00014-87-C-0789

COMPOSITE CERAMIC SUPERCONDUCTING FILAMENTS FOR  
SUPERCONDUCTING CABLE

12 July 1988

J. W. Halloran, et al.

Ceramics Process Systems Corporation

Cambridge, MA 02139

This program established the feasibility of manufacturing composite HTSC filaments for use in superconducting cable based on a design consisting of copper-clad  $\text{YBa}_2\text{Cu}_3\text{O}_{7-\delta}$  fibers. Processes were developed to prepare sinterable  $\text{YBa}_2\text{Cu}_3\text{O}_{7-\delta}$  ceramic powders, to render the material in the form of flexible fine diameter green fibers by dry spinning, and to rapidly sinter the fibers producing superconducting filaments with transport critical current densities<sup>27</sup> around 150 A/cm<sup>2</sup>. Feasibility of cladding sintered fibers with copper by electrodeposition has been demonstrated.

Highly sinterable, phase-pure  $\text{YBa}_2\text{Cu}_3\text{O}_{7-\delta}$  powders have been produced with a solid state synthesis process using copper oxide, yttrium oxide, and barium carbonate as raw materials. The raw materials are finely milled, to promote solid state reactivity, and are subsequently granulated, to preserve random mixing. Problems with the decomposition of barium carbonate are avoided by promoting uniform air flow through the bed of granulated raw material.

---

<sup>27</sup> The critical current density values reported in this Appendix are the correct values, redetermined as described in this Quarterly Report. The values reported in the original Final Report were in error.

The calcined powder can be used (without milling) to prepare pellets that are sintered to 96% density at 995°C in 15 h. Milling the  $\text{YBa}_2\text{Cu}_3\text{O}_{7-\delta}$  powder to a particle size of 0.8  $\mu\text{m}$  increases the sinterability so that pellets can reach 95% density after 1 h at 910°C. Additions of 5 wt% excess copper oxide as a sintering aid permit 97% dense pellets to be prepared at 925°C after 15 h, using unmilled powder. The sinterability is significantly enhanced when the material is prepared in the form of fine fibers, rather than pellets. These fine fibers can be rapidly sintered, reaching high density in only a few minutes.

A process was developed to prepare flexible "green" fibers by dry spinning a "dope" containing  $\text{YBa}_2\text{Cu}_3\text{O}_{7-\delta}$  powder in a suspension of polymers, solvents, and processing aids. The dope is extruded through a spinnerette into a drying chamber. At the spinnerette tip the fiber diameter is attenuated into a fine fiber, with diameters controllable between 20 and 400  $\mu\text{m}$ . The linear velocity of the fiber exiting the drying column varies between 3 to 5 m/s.

A variety of spin dope formulations were developed for barium titanate (an inexpensive surrogate used in place of  $\text{YBa}_2\text{Cu}_3\text{O}_{7-\delta}$ ) and  $\text{YBa}_2\text{Cu}_3\text{O}_{7-\delta}$  powders (obtained from various sources, such as Rhone-Poulenc). The latter included  $\text{YBa}_2\text{Cu}_3\text{O}_{7-\delta}$  powder prepared at CPSS, with particle size ranging from relatively coarse (0.7  $\text{m}^2/\text{gm}$  surface area) to very fine (12.5  $\text{m}^2/\text{gm}$ ), and chemistries ranging from stoichiometric to copper-rich or yttrium-rich. The spin dope consisted of a suspension of powder in a mixture of several acrylic polymers, toluene, methylethylketone, and xylene, with the addition of a plasticizer, cross-linking agent, and dispersant. The "green" fiber was a flexible monofilament containing 49-55 vol% (85-87 wt%) ceramic powder in the polymeric matrix.

A laboratory scale dry spinning column was constructed to prepare experimental fibers. The dope delivery system consisted of a syringe, with

delivery rate metered either mechanically or pneumatically. A plastic syringe tip or hypodermic needle served as the spinnerette, through which the dope was injected into the drying column. The column was not long enough to completely dry the fiber to the non-tacky state necessary for collection on a spooler. Accordingly, semi-continuous one meter lengths of fiber were collected during spinning. This apparatus was continually modified and improved during the course of this program.

The "spinnability" of the formulations was evaluated as a function of powder loading, polymer molecular weight, solvent content, content of cross-linker, dispersant, and plasticizer, as well as spinning conditions. These were empirically determined by the quality of the "spinnability," and correlated with the viscoelastic response of the dope as revealed by its dynamic mechanical spectrum.

To date, green fiber with a texture (preferred particle alignment) has not been produced. Such texture is expected as the extensive elongation of the fiber during spinning should orient platy-shaped particles. An attempt at magnetic alignment of particles was not successful.

The dry spinning process was sufficient to routinely prepare  $\text{YBa}_2\text{Cu}_3\text{O}_{7-\delta}$  fibers to support the sintering and electrical property development activity. Development of this process continues beyond this program. Currently, Albany International Research Corporation (AIResCo) of Dedham, Massachusetts is under contract with CPS to further develop the fiber spinning process at the pilot plant level.

A multiple zone sintering process was developed to rapidly densify the  $\text{YBa}_2\text{Cu}_3\text{O}_{7-\delta}$  fibers. This process involves repeated heating and cooling between the peak temperature and a lower temperature (approximately  $600^\circ\text{C}$ ). Total time at temperature varied from 1.3 to 11.7 min, with the most detailed work done at 5.6 min. Sintering of continuous fiber in a multiple zone furnace was simulated using a simple tube furnace. Short fiber lengths were

supported on a low thermal mass sled which was moved through the hot zone at controlled speeds. The brief duration of the sintering treatment avoids reactions between the  $\text{YBa}_2\text{Cu}_3\text{O}_{7-\delta}$  and the supporting setter materials. Typically high purity alumina substrates were used, without noticeable reaction. A variety of other setter materials, including Mg-partially stabilized zirconia, chromel wire, alumina fiber board, and alumina-silica-boria fabrics have also been used with no noticeable reaction with the  $\text{YBa}_2\text{Cu}_3\text{O}_{7-\delta}$  fiber.

Sintered fiber microstructures were examined for a variety of zone sintering conditions, involving variation of peak temperature, number of zone passes, and total time at temperature, and for several types of fibers made from CPS powder (as-calcined, milled, or CuO-doped) and Rhone-Poulenc powder. Quantitative stereological methods were used to characterize grain size distribution, aspect ratio, and grain orientation in sintered fibers. Although the multiple zone sintering process was intended to induce a  $\langle 010 \rangle$  texture by causing directional recrystallization, the sintered fibers proved to have essentially random grain orientation. There was, however, a significant effect of multiple zone sintering on critical current.

A technique was developed to measure transport critical current on small sintered fibers at liquid nitrogen temperature. Critical current density varied from about  $10 \text{ A/cm}^2$  to  $150 \text{ A/cm}^2$ , depending on zone sintering conditions. In one particular experiment where total sintering time was constant, while the number of zone passes was varied (by changing the speed through the hot zone) the critical current was found to be very sensitive to number of zone passes, displaying a maximum as much as a factor of five times larger than the lower values. The number of passes required for optimum  $J_c$  increased with temperature.

At present, the reason for the apparent strong influence of multiple zone sintering on the critical current density is not understood. A

careful examination of the microstructure of high and low  $J_c$  specimens showed no significant differences at the level of resolution of optical and scanning electron microscopy. More detailed characterization is underway.

Two concepts were developed for cladding the sintered fibers with copper or some other strong, conductive metal. These were electrodeposition and a mechanical cladding method. The latter would use indium-clad copper foil; cladding would be accomplished by roll compacting the fibers between two foils, creating a pressure bond between the  $YBa_2Cu_3O_{7-\delta}$  and the indium. Vendors for the In-clad foil were identified, and a variety of experiments were pursued to evaluate the feasibility of the process. At present, the bonding of indium to  $YBa_2Cu_3O_{7-\delta}$  surfaces has proved to be non-reproducible.

The feasibility of electrodeposition was investigated in more detail. Aqueous electroplating damaged the superconductor, as expected. Preliminary results suggest that  $YBa_2Cu_3O_{7-\delta}$  is compatible with molten salt electrolytes such as  $KCl-NaCl$ ,  $CuCl-KCl$ , and  $KNO_3-NaNO_3$ . The latter was examined as a possible electrolyte for anodically charging the  $YBa_2Cu_3O_{7-\delta}$  with oxygen to adjust stoichiometry electrochemically. Copper deposition from  $CuCl-KCl$  was attempted with encouraging results. Electrodeposition cladding methods are currently being pursued in collaboration with consultants and outside experts.

ATTACHMENT I  
REPORT SUMMARY

COMPOSITE CERAMIC SUPERCONDUCTING WIRES FOR ELECTRIC MOTOR APPLICATIONS

First Quarterly Report on  
Contract Number N00014-88-C-0512

September 30, 1988

John W. Halloran, et al., Ceramics Process Systems Corporation,  
Cambridge, MA 02139

Work began on the wire manufacturing task during this first Quarterly Period, involving research activities at CPS Superconductor Corporation and Albany International Research Company. The start of the HTSC motor design activity at Emerson Motor Division was postponed until the second Quarterly Period, due to a delay in obtaining the ONR contract.

Substantial progress has been made in the composite wire manufacturing task. Although each step in the process is still being carried out discretely and insolation, we are ready to begin replacing some of the batch processes with continuous processes. By the end of the next quarter, we expect to focussing on continuous green fiber spinning, experimenting with a continuous heat treatment, and setting up the prototype of a continuous cladding module.

The concepts for design and fabrication of flexible HTSC conductors have been refined. Instead of a simple metal clad monofilament we now favor a multifilament array in the form of a ribbon conductor. Preliminary models for predicting the allowable bending radius and tensile loads have been developed to guide the choice of filament size, cladding thickness, and residual stress state.

A number of commercially available  $\text{YBa}_2\text{Cu}_3\text{O}_7$  powders were evaluated as raw material, but no satisfactory source has been found. During this Quarter, most of the fibers were prepared from a Rhone-Poulenc powder. This material was suitable for spinning and highly sinterable, but contained excess copper oxide. Much effort went to scaling up in-house powder production of highly phase pure  $\text{YBa}_2\text{Cu}_3\text{O}_7$  powder to production rates adequate to supply the development program. The influence of powder characteristics on fiber spinning and sintering is now being studied to optimize the powder for the wire manufacturing.

Research at AIREsCo has led to a method to melt spin green fiber with high loadings of ceramic powder. This melt spinning process has many advantages over the dry spinning process, which will probably be abandoned if the early success with melt spinning barium titanate at solids loadings up to 50 volume percent can be duplicated with  $\text{YBa}_2\text{Cu}_3\text{O}_7$ . Melt spun fiber has been made in continuous spools with lengths up to 0.25 kilometers, limited only by the small experimental batches. This melt spun fiber appears to have favorable binder burnout characteristics. We anticipate preparing continuous spools of  $\text{YBa}_2\text{Cu}_3\text{O}_7$  melt spun green fiber early in the next quarter. This material is the feedstock for the continuous sintering development.

A radiant heated belt furnace had been identified for sintering the continuous fiber arrays. The temperature-time profile for this belt furnace has been modeled on the results of the short fiber heat treatment experiments. The short fiber experiments continued, aimed at establishing a relationship between heat treatment and  $J_c$ . Critical current densities could not be simply correlated to zone sintering conditions, since the relationships are obscured by scatter in the  $J_c$  data. Further observations were made on microstructure development, primarily for the CuO-excess Rhone-Poulenc powder. Preliminary results on a rapid oxygen intercalation anneal suggests that filaments may be successfully restored to the superconducting state by a 15 minute isothermal anneal at 525°C in oxygen.

A new cladding concept was developed. This method is based upon a technique to treat the surfaces of  $\text{YBa}_2\text{Cu}_3\text{O}_7$  filaments to promote wetting by solders, so that the filaments may be bonded to copper ribbons by a solder reflow process. This method offers significant advantages over previous electrodeposition concepts, so was vigorously developed. The surface treatment presently involves a thin layer of silver. Early ribbon coupon specimens were fabricated with the reflow method using a few  $\text{YBa}_2\text{Cu}_3\text{O}_7$  filaments or graphite fiber as a surrogate. Electrodeposition methods were investigated out-of-house in collaboration with experts in the field.

An improved  $J_c$  measurement technique for the sintered filaments was established using DC current increased in a stepwise fashion. Erroneous data from previous work was corrected, and a data base of processing conditions and  $J_c$  was constructed. The highest critical current density determined for a  $\text{YBa}_2\text{Cu}_3\text{O}_7$  filament was 792A/cm<sup>2</sup>. We have begun to examine the repeatability of  $J_c$  data, to determine if the scatter is due to technique or specimen-to-specimen variability. Magnetic field effects were characterized, demonstrating that the  $\text{YBa}_2\text{Cu}_3\text{O}_7$  filaments are limited by weak links. An attempt was made to determine the influence "self field" on the critical current density data.

ATTACHMENT II

ARPA ORDER NUMBER: 9525

PROGRAM CODE NUMBER: 7737

CONTRACTOR: Ceramics Process Systems Corporation  
840 Memorial Drive  
Cambridge, MA 02139

CONTRACT NUMBER: N00014-88-C-0512

CONTRACT EFFECTIVE DATE: 30 JUNE 1988

CONTRACT EXPIRATION DATE: 31 MARCH 1991

SHORT TITLE OF WORK: High Temperature Superconducting Wire and Motor

PRINCIPAL INVESTIGATOR: John W. Halloran  
(617) 354-2020

This is the First Quarterly Report of a program to produce practical HTSC wires, and build a HTSC electric motor using this wire. The HTSC ceramic wire will be a flexible composite of many fine ceramic filaments clad with copper or aluminum. The three basic elements of this method are: 1) spinning polymer-containing "green" fibers; 2) sintering the fibers to make bare superconducting ceramic filaments; and 3) cladding the filaments with copper. Albany International Research Corporation (AIResCo) is working with CPS to improve the green fiber spinning process and bring it to pilot scale production. Emerson Motor Division (EMD) of Emerson Electric Company, will evaluate the composite wire and in define a set of realistic property requirements for practical HTSC motors. The second task, to design and build HTSC motors, will be undertaken by Emerson Motor Division. This report covers development activities during the period July through September 1988, on the wire development task at CPS and AIResCo. The start of the Emerson subcontract was deferred until October 1, 1988.

During this Quarter, most of the fibers were prepared from a Rhone-Poulenc powder. This material was suitable for spinning and highly sinterable, but contained excess copper oxide. Much effort went to scaling up in-house powder production of highly phase pure  $YBa_2Cu_3O_7$  powder to production rates adequate to supply the development program. The influence of powder characteristics on fiber spinning and sintering is now being studied to optimize the powder for the wire manufacturing.

Research at AIResCo has led to a method to melt spin green fiber. Melt spun fiber containing up to 50 volume percent powder has been made in continuous spools with lengths up to 0.25 kilometer, limited only by the small experimental batches. This melt spun fiber appears to have favorable binder burnout characteristics. We anticipate preparing continuous spools of  $YBa_2Cu_3O_7$  melt spun green fiber early in the next quarter to be the feedstock for the continuous sintering development.

Sintering and annealing experiments were conducted to establish a relationship between heat treatment and  $J_c$ , but critical current densities could not be simply correlated to zone sintering conditions because of scatter in the  $J_c$  data. Further observations were made on microstructure development, primarily for the CuO-excess Rhone-Poulenc powder. Preliminary results on a rapid oxygen intercalation anneal suggests that filaments may be successfully restored to the superconducting state by a 15 minute isothermal anneal at 525°C in oxygen.

A new cladding concept was developed, based upon a technique to treat the surfaces of  $YBa_2Cu_3O_7$  filaments so that they can be bonded to copper ribbons by a solder reflow process. The surface treatment presently involves a thin layer of silver. Early ribbon coupon specimens were fabricated with the reflow method using a few  $YBa_2Cu_3O_7$  filaments or graphite fiber as a surrogate.

A data base of processing conditions and  $J_c$  was constructed. The highest critical current density determined for a  $YBa_2Cu_3O_7$  filament was 792A/cm<sup>2</sup>. We have begun to examine the repeatability of  $J_c$  data, magnetic field effects, and self field critical current density data.

ATTACHMENT III

ARPA ORDER NUMBER: 9525

PROGRAM CODE NUMBER: 7737

CONTRACTOR: Ceramic Process Systems Corporation  
840 Memorial Drive  
Cambridge, MA 02139

CONTRACT NUMBER: N00014-88-C-0512

CONTRACT AMOUNT: \$ 5,509,387.00

EFFECTIVE DATE OF CONTRACT: 30 JUNE 1988

EXPIRATION DATE OF CONTRACT: 31 MARCH 1991

PRINCIPAL INVESTIGATOR: John W. Halloran

TELEPHONE NUMBER: (617) 354-2020

SHORT TITLE OF WORK: High Temperature Superconducting Wire and Motor

REPORTING PERIOD: 30 JUNE 1988 through 30 SEPTEMBER 1988

DESCRIPTION OF PROGRESS

The HTSC ceramic wire will be a flexible composite of many fine ceramic filaments clad with copper. The three basic elements of this method are: 1) spinning polymer-containing "green" fibers; 2) sintering the fibers to make bare superconducting ceramic filaments; and 3) cladding the filaments with copper. Albany International Research Corporation (AIResCo) is working with CPS to improve the green fiber spinning process and bring it to pilot scale production. Emerson Motor Division (EMD) of Emerson Electric Company, will evaluate the composite wire and in define a set of realistic property requirements for practical HTSC motors. The second task, to design and build HTSC motors, will be undertaken by Emerson Motor Division starting October 1, 1988.

Melt spun fiber containing up to 50 volume percent powder has been made in continuous spools with lengths up to 0.25 kilometers. We anticipate preparing continuous spools of  $\text{YBa}_2\text{Cu}_3\text{O}_7$  melt spun green fiber early in the next quarter to be the feedstock for the continuous sintering development. Sintering and annealing experiments were conducted to establish a relationship between heat treatment and  $J_c$ , and characterize microstructure development. Preliminary results on a rapid oxygen intercalation anneal suggests that superconducting state can be restored by a 15 minute isothermal anneal at  $525^\circ\text{C}$  in oxygen. A new cladding concept was developed, based upon a technique to treat the surfaces of  $\text{YBa}_2\text{Cu}_3\text{O}_7$  filaments so that they can be bonded to copper ribbons by a solder reflow process. Early ribbon coupon specimens were fabricated with the reflow method using a few  $\text{YBa}_2\text{Cu}_3\text{O}_7$  filaments or graphite fiber as a surrogate. The highest critical current density determined for a  $\text{YBa}_2\text{Cu}_3\text{O}_7$  filament was  $792\text{A}/\text{cm}^2$ . We have begun to examine the repeatability of  $J_c$  data, magnetic field effects, and self field critical current density data.

SUMMARY OF SUBSTANTIVE INFORMATION DERIVED FROM SPECIAL EVENTS

Project members attended the September 13-15, 1988 DARPA/ONR High Temperature Superconductivity Program contractors meeting, and were briefed on current developments.

CHANGE IN KEY PERSONNEL

No change

PROBLEMS ENCOUNTERED AND/OR ANTICIPATED

None

ACTION REQUIRED BY THE GOVERNMENT

None

FISCAL STATUS

1) <u>Amount currently received on contract:</u>	\$	0.00
2) <u>Expenditures and commitments to date:</u>	\$	473,034.00
3) <u>Funds required to complete work:</u>	\$	5,509,387.00